

Alpha Spectroscopy

Appendix A

Nuclear Binding Energy

Source: “Kenneth S. Krane, Introductory Nuclear Physics (from Chap 3)”

3.3 NUCLEAR BINDING ENERGY

The mass energy $m_N c^2$ of a certain nuclide is its atomic mass energy $m_A c^2$ less the total mass energy of Z electrons and the total *electronic binding energy*:

$$m_N c^2 = m_A c^2 - Z m_e c^2 + \sum_{i=1}^Z B_i \quad (3.23)$$

where B_i is the binding energy of the i th electron. Electronic binding energies are of order 10–100 keV in heavy atoms, while atomic mass energies are of order $A \times 1000$ MeV; thus to a precision of about 1 part in 10^6 we can neglect the last term of Equation 3.23. (Even this 10^{-6} precision does not affect measurements in nuclear physics because we usually work with *differences* in mass energies, such as in determining decay or reaction energies; the effects of electron binding energies tend to cancel in these differences.)

The *binding energy* B of a nucleus is the difference in mass energy between a nucleus ${}_Z^A X_N$ and its constituent Z protons and N neutrons:

$$B = \{ Z m_p + N m_n - [m({}^A X) - m_e] \} c^2 \quad (3.24)$$

where we have dropped the subscript from m_A —from now on, unless we indicate otherwise, we shall always be dealing with *atomic* masses.

Grouping the Z proton and electron masses into Z neutral hydrogen atoms, we can rewrite Equation 3.24 as

$$B = [Z m({}^1 H) + N m_n - m({}^A X)] c^2 \quad (3.25)$$

With the masses generally given in atomic mass units, it is convenient to include the unit conversion factor in c^2 , thus: $c^2 = 931.50$ MeV/u.

We occasionally find atomic mass tables in which, rather than $m({}^A X)$, what is given is the *mass defect* $\Delta = (m - A)c^2$. Given the mass defect, it is possible to use Equation 3.25 to deduce the atomic mass.

Other useful and interesting properties that are often tabulated are the neutron and proton separation energies. The *neutron separation energy* S_n is the amount of energy that is needed to remove a neutron from a nucleus ${}_Z^A X_N$, equal to the difference in binding energies between ${}_Z^A X_N$ and ${}^{A-1} {}_{Z-1} X_{N-1}$:

$$\begin{aligned} S_n &= B({}^A_Z X_N) - B({}^{A-1} {}_{Z-1} X_{N-1}) \\ &= [m({}^{A-1} {}_{Z-1} X_{N-1}) - m({}^A_Z X_N) + m_n] c^2 \end{aligned} \quad (3.26)$$

In a similar way we can define the *proton separation energy* S_p as the energy needed to remove a proton:

$$\begin{aligned} S_p &= B({}^A_Z X_N) - B({}^{A-1} {}_{Z-1} X_N) \\ &= [m({}^{A-1} {}_{Z-1} X_N) - m({}^A_Z X_N) + m({}^1 H)] c^2 \end{aligned} \quad (3.27)$$

The hydrogen mass appears in this equation instead of the proton mass, since we are always working with *atomic* masses; you can see immediately how the Z electron masses cancel from Equations 3.26 and 3.27.

The neutron and proton separation energies are analogous to the ionization energies in atomic physics—they tell us about the binding of the outermost or

Table 3.1 Some Mass Defects and Separation Energies

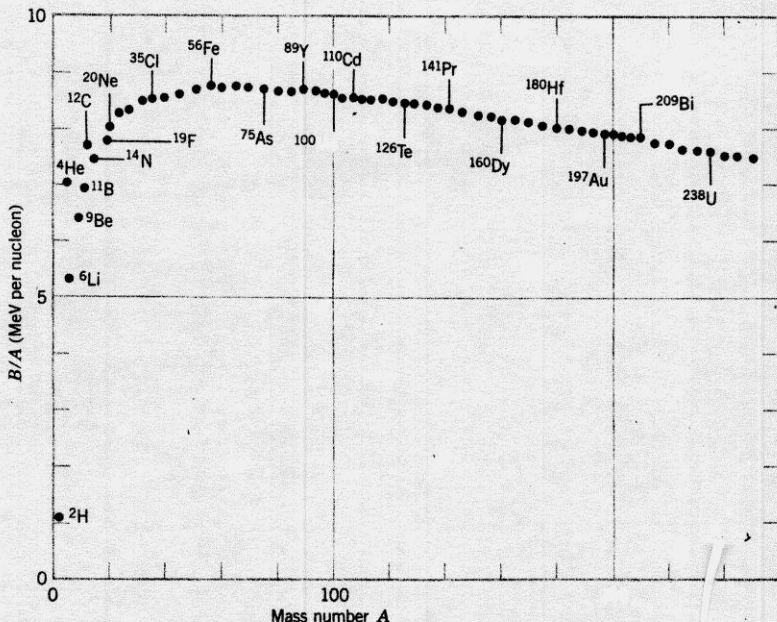
Nuclide	Δ (MeV)	S_n (MeV)	S_p (MeV)
^{16}O	-4.737	15.66	12.13
^{17}O	-0.810	4.14	13.78
^{17}F	+1.952	16.81	0.60
^{40}Ca	-34.847	15.64	8.33
^{41}Ca	-35.138	8.36	8.89
^{41}Sc	-28.644	16.19	1.09
^{208}Pb	-21.759	7.37	8.01
^{209}Pb	-17.624	3.94	8.15
^{209}Bi	-18.268	7.46	3.80

valence nucleons. Just like the atomic ionization energies, the separation energies show evidence for nuclear shell structure that is similar to atomic shell structure. We therefore delay discussion of the systematics of separation energies until we discuss nuclear models in Chapter 5. Table 3.1 gives some representative values of mass defects and separation energies.

As with many other nuclear properties that we will discuss, we gain valuable clues to nuclear structure from a *systematic* study of nuclear binding energy. Since the binding energy increases more or less linearly with A , it is general practice to show the average binding energy per nucleon, B/A , as a function of A . Figure 3.16 shows the variation of B/A with nucleon number. Several remarkable features are immediately apparent. First of all, the curve is relatively constant except for the very light nuclei. The average binding energy of most nuclei is, to within 10%, about 8 MeV per nucleon. Second, we note that the curve reaches a peak near $A = 60$, where the nuclei are most tightly bound. This suggests we can "gain" (that is, release) energy in two ways—below $A = 60$, by assembling lighter nuclei into heavier nuclei, or above $A = 60$, by breaking heavier nuclei into lighter nuclei. In either case we "climb the curve of binding energy" and liberate nuclear energy; the first method is known as *nuclear fusion* and the second as *nuclear fission*. These important subjects are discussed in Chapters 13 and 14.

Attempting to understand this curve of binding energy leads us to the *semiempirical mass formula*, in which we try to use a few general parameters to characterize the variation of B with A .

The most obvious term to include in estimating B/A is the constant term, since to lowest order $B \propto A$. The contribution to the binding energy from this "volume" term is thus $B = a_v A$ where a_v is a constant to be determined, which should be of order 8 MeV. This linear dependence of B on A is in fact somewhat surprising, and gives us our first insight into the properties of the nuclear force. If every nucleon attracted all of the others, then the binding energy would be proportional to $A(A - 1)$, or roughly to A^2 . Since B varies linearly with A , this suggests that each nucleon attracts only its closest neighbors, and *not* all of the other nucleons. From electron scattering we learned that the nuclear density is roughly constant, and thus each nucleon has about the same number of neigh-

**3.16** The binding energy per nucleon.

bors; each nucleon thus contributes roughly the same amount to the binding energy.

An exception to the above statement is a nucleus on the nuclear surface, which is surrounded by fewer neighbors and is less tightly bound than those in the central region. Surface nucleons do not contribute to B quite as much as those in the center, and the $B = a_v A$ overestimates B by giving full weight to the surface nucleons. We must therefore subtract from B a term proportional to the nuclear surface area. The surface area of the nucleus is proportional to R^2 or to $A^{2/3}$, since $R \propto A^{1/3}$. Thus the surface nucleons contribute to the binding energy a term of the form $-a_s A^{2/3}$.

Our binding energy formula must also include the Coulomb repulsion of the protons, which likewise tends to make the nucleus less tightly bound. Since each proton repels all of the others, this term is proportional to $Z(Z - 1)$, and we may do an exact calculation, assuming a uniformly charged sphere, to obtain $-\frac{1}{3}(e^2/4\pi\epsilon_0 R_0)Z(Z - 1)/A^{1/3}$ where the negative sign implies a reduction in binding energy. The constants evaluate to 0.72 MeV with $R_0 = 1.2$ fm; we can allow this constant to be adjustable by replacing it with a general Coulomb constant a_c .

We also note, from our study of the distribution of stable and radioactive isotopes (see 1.1), that stable nuclei have $Z \approx A/2$. (The explanation for this comes from our discussion of the shell model in Chapter 5.) If our binding energy formula is to be realistic in describing the stable nuclei that

actually observed, it must take this effect into account. (Otherwise it would allow stable isotopes of hydrogen with hundreds of neutrons!) This term is very important for light nuclei, for which $Z \approx A/2$ is more strictly observed. For heavy nuclei, this term becomes less important, because the rapid increase in the Coulomb repulsion term requires additional neutrons for nuclear stability. A possible form for this term, called the symmetry term because it tends to make the nucleus symmetric in protons and neutrons, is $-a_{\text{sym}}(A - 2Z)^2/A$ which has the correct form of favoring nuclei with $Z = A/2$ and reducing in importance for large A .

Finally, we must include another term that accounts for the tendency of like nucleons to couple pairwise to especially stable configurations. When we have an odd number of nucleons (odd Z and even N , or even Z and odd N), this term does not contribute. However, when both Z and N are odd, we gain binding energy by converting one of the odd protons into a neutron (or vice versa) so that it can now form a pair with its formerly odd partner. We find evidence for this pairing force similarly by looking at the stable nuclei—there are only four nuclei with odd N and Z (^2H , ^1B , ^{14}N), but 167 with even N and Z . The pairing energy δ is usually expressed as a_p or an even, $-a_p A^{-3/4}$ for Z and N odd, and zero for A odd.

Combining these five terms we get the complete binding energy:

$$B = a_v A - a_s A^{2/3} - a_c Z(Z-1) A^{-1/3} - a_{\text{sym}} \frac{(A-2Z)^2}{A} + \delta \quad (3.28)$$

and using this expression for B we have the semiempirical mass formula:

$$M(Z, A) = Zm(^1\text{H}) + Nm_n - B(Z, A)/c^2 \quad (3.29)$$

The constants must be adjusted to give the best agreement with the experimental curve of Figure 3.16. A particular choice of $a_v = 15.5$ MeV, $a_s = 16.8$ MeV, $a_c = 0.72$ MeV, $a_{\text{sym}} = 23$ MeV, $a_p = 34$ MeV, gives the result shown in Figure 3.17, which reproduces the observed behavior of B rather well.

The importance of the semiempirical mass formula is not that it allows us to predict any new or exotic phenomena of nuclear physics. Rather, it should be regarded as a first attempt to apply nuclear models to understand the systematic behavior of a nuclear property, in this case the binding energy. It includes several different varieties of nuclear models: the liquid-drop model, which treats some of the gross collective features of nuclei in a way similar to the calculation of the properties of a droplet of liquid (indeed, the first three terms of Equation 3.28 would also appear in a calculation of the energy of a charged liquid droplet), and the shell model, which deals more with individual nucleons and is responsible for the last two terms of Equation 3.28.

For constant A , Equation 3.29 represents a parabola of M vs. Z . The parabola will be centered about the point where Equation 3.29 reaches a minimum. To compare this result with the behavior of actual nuclei, we must find the minimum, where $\partial M/\partial Z = 0$:

$$Z_{\text{min}} = \frac{[m_n - m(^1\text{H})] + a_c A^{-1/3} + 4a_{\text{sym}}}{2a_c A^{-1/3} + 8a_{\text{sym}} A^{-1}} \quad (3.30)$$

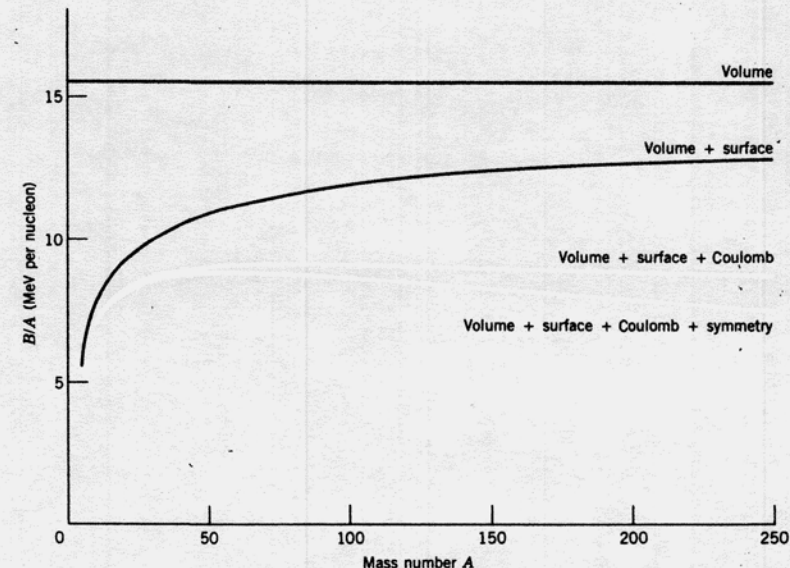


Figure 3.17 The contributions of the various terms in the semiempirical mass formula to the binding energy per nucleon.

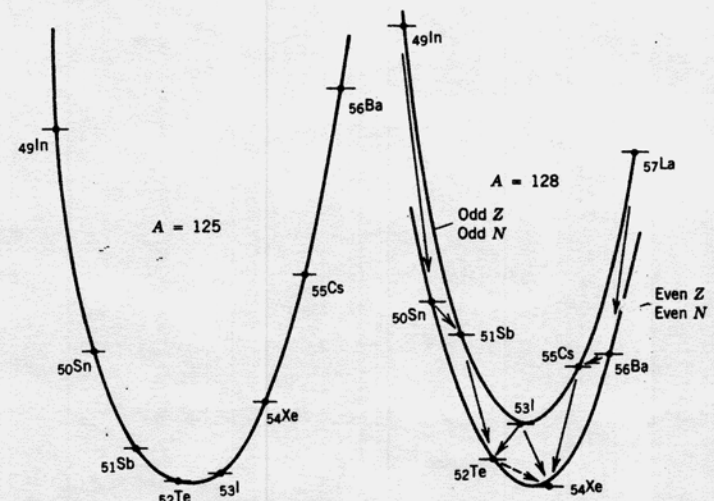


Figure 3.18 Mass chains for $A = 125$ and $A = 128$. For $A = 125$, note how the energy difference between neighboring isotopes increase as we go further from the stable center at the energy minimum. For $A = 128$, note the effect of the pairing term; in particular, ^{128}I can decay in either direction, and it is energetically possible for ^{128}Te to decay directly to ^{128}Xe by the process known as double beta decay.

70 BASIC NUCLEAR STRUCTURE

With $a_c = 0.72$ MeV and $a_{\text{sym}} = 23$ MeV, it follows that the first two terms in the numerator are negligible, and so

$$\boxed{Z_{\min} = \frac{A}{2} \frac{1}{1 + \frac{1}{4} A^{2/3} a_c / a_{\text{sym}}}} \quad (3.31)$$

For small A , $Z_{\min} \approx A/2$ as expected, but for large A , $Z_{\min} < A/2$. For heavy nuclei, Equation 3.31 gives $Z/A \approx 0.41$, consistent with observed values for heavy stable nuclei.

Figure 3.18 shows a typical odd- A decay chain for $A = 125$, leading to the stable nucleus at $Z = 52$. The unstable nuclei approach stability by converting a neutron into a proton or a proton into a neutron by radioactive β decay. Notice how the decay energy (that is, the mass difference between neighboring isobars) increases as we go further from stability. For even A , the pairing term gives two parabolas, displaced by 28. This permits two unusual effects, not seen in odd- A decays: (1) some odd- Z , odd- N nuclei can decay in either direction, converting a neutron to a proton or a proton to a neutron; (2) certain *double β decays* can become energetically possible, in which the decay may change 2 protons to 2 neutrons. Both of these effects are discussed in Chapter 9.

Alpha Spectroscopy

Appendix B

Law of Radioactive Decay

Source: “Kenneth S. Krane, Introductory Nuclear Physics (from Chap 6)”

RADIOACTIVE DECAY

The radioactive decays of naturally occurring minerals containing uranium and thorium are in large part responsible for the birth of the study of nuclear physics. These decays have half-lives that are of the order of the age of the Earth, suggesting that the materials are survivors of an early period in the creation of matter by aggregation of nucleons; the shorter-lived nuclei have long since decayed away, and we observe today the remaining long-lived decays. Were it not for the extremely long half-lives of ^{235}U and ^{238}U , we would today find no uranium in nature and would probably have no nuclear reactors or nuclear weapons.

In addition to this naturally occurring radioactivity, we also have the capability to produce radioactive nuclei in the laboratory through nuclear reactions. This was first done in 1934 by Irene Curie and Pierre Joliot, who used α particles from the natural radioactive decay of polonium to bombard aluminum, thereby producing the isotope ^{30}P , which they observed to decay through positron emission with a half-life of 2.5 min. In their words:

Our latest experiments have shown a very striking fact: when an aluminum foil is irradiated on a polonium preparation, the emission of positrons does not cease immediately when the active preparation is removed. The foil remains radioactive and the emission of radiation decays exponentially as for an ordinary radioelement.

For this work on artificially produced radioactivity the Joliot-Curie team was awarded the 1935 Nobel Prize in Chemistry (following a family tradition—Irene's parents, Pierre and Marie Curie, shared with Becquerel the 1903 Nobel Prize in Physics for their work on the natural radioactivity of the element radium, and Marie Curie became the first person twice honored, when she was awarded the 1911 Nobel Prize in Chemistry).

In this chapter we explore the physical laws governing the production and decay of radioactive materials, which we take to mean those substances whose nuclei spontaneously emit radiations and thereby change the state of the nucleus.

6.1 THE RADIOACTIVE DECAY LAW

Three years following the 1896 discovery of radioactivity it was noted that the decay rate of a pure radioactive substance decreases with time according to an exponential law. It took several more years to realize that radioactivity represents changes in the individual atoms and not a change in the sample as a whole. It took another two years to realize that the decay is statistical in nature, that it is impossible to predict when any given atom will disintegrate, and that this hypothesis leads directly to the exponential law. This lack of predictability of the behavior of single particles does not bother most scientists today, but this early instance of it, before the development of quantum theory, was apparently difficult to accept. Much labor was required of these dedicated investigators to establish what now may seem like evident facts.

If N radioactive nuclei are present at time t and if no new nuclei are introduced into the sample, then the number dN decaying in a time dt is proportional to N , and so

$$\lambda = -\frac{(dN/dt)}{N} \quad (6.1)$$

in which λ is a constant called the *disintegration or decay constant*. The right side of Equation 6.1 is the probability per unit time for the decay of an atom. *That this probability is constant, regardless of the age of the atoms, is the basic assumption of the statistical theory of radioactive decay.* (Human lifetimes do not follow this law!)

Integrating Equation 6.1 leads to the *exponential law of radioactive decay*

$$N(t) = N_0 e^{-\lambda t} \quad (6.2)$$

where N_0 , the constant of integration, gives the original number of nuclei present at $t = 0$. The *half-life* $t_{1/2}$ gives the time necessary for half of the nuclei to decay. Putting $N = N_0/2$ in Equation 6.2 gives

$$t_{1/2} = \frac{0.693}{\lambda} \quad (6.3)$$

It is also useful to consider the *mean lifetime* (sometimes called just the lifetime) τ , which is defined as the average time that a nucleus is likely to survive before it decays. The number that survive to time t is just $N(t)$, and the number that decay between t and $t + dt$ is $|dN/dt| dt$. The mean lifetime is then

$$\tau = \frac{\int_0^\infty t |dN/dt| dt}{\int_0^\infty |dN/dt| dt} \quad (6.4)$$

where the denominator gives the total number of decays. Evaluating the integrals gives

$$\tau = \frac{1}{\lambda} \quad (6.5)$$

Thus the mean lifetime is simply the inverse of the decay constant.

Equation 6.2 allows us to predict the number of undecayed nuclei of a given type remaining after a time t . Unfortunately, the law in that form is of limited usefulness because N is a very difficult quantity to measure. Instead of counting the number of undecayed nuclei in a sample, it is easier to count the number of decays (by observing the emitted radiations) that occur between the times t_1 and t_2 . If we deduce a change ΔN in the number of nuclei between t and $t + \Delta t$, then

$$|\Delta N| = N(t) - N(t + \Delta t) = N_0 e^{-\lambda t} (1 - e^{-\lambda \Delta t}) \quad (6.6)$$

If the interval Δt during which we count is much smaller than λ^{-1} (and thus, in effect, $\Delta t \ll t_{1/2}$), we can ignore higher order terms in the expansion of the second exponential, and

$$|\Delta N| = \lambda N_0 e^{-\lambda t} \Delta t \quad (6.7)$$

Going over to the differential limit gives

$$\left| \frac{dN}{dt} \right| = \lambda N_0 e^{-\lambda t} \quad (6.8)$$

Defining the *activity* \mathcal{A} to be the rate at which decays occur in the sample,

$$\mathcal{A}(t) = \lambda N(t) = \mathcal{A}_0 e^{-\lambda t} \quad (6.9)$$

The initial activity at $t = 0$ is $\mathcal{A}_0 = \lambda N_0$.

Actually, we could have obtained Equation 6.8 by differentiating Equation 6.2 directly, but we choose this more circuitous path to emphasize an important but often overlooked point: *Measuring the number of counts ΔN in a time interval Δt gives the activity of the sample only if $\Delta t \ll t_{1/2}$.* The number of decays in the interval from t_1 to t_2 is

$$\Delta N = \int_{t_1}^{t_2 + t_1 + \Delta t} \mathcal{A} dt \quad (6.10)$$

which equals $\mathcal{A} \Delta t$ only if $\Delta t \ll t_{1/2}$. (Consider an extreme case—if $t_{1/2} = 1$ s, we observe the same number of counts in 1 min as we do in 1 h.) See Problem 1 at the end of this chapter for more on the relation between \mathcal{A} and ΔN .

The activity of a radioactive sample is exactly the number of decays of the sample per unit time, and decays/s is a convenient unit of measure. Another unit for measuring activity is the *curie* (Ci), which originally indicated the activity of one gram of radium but is now defined simply as

$$1 \text{ Ci} = 3.7 \times 10^{10} \text{ decays/s}$$

Most common radioactive sources of strengths typically used in laboratories have activities in the range of microcuries to millicuries. The SI unit for activity is the becquerel (Bq), equal to one decay per second; however, the curie is so firmly in place as a unit of activity that the becquerel has not yet become the commonly used unit.

Note that the activity tells us only the number of disintegrations per second; it says nothing about the *kind* of radiations emitted or their *energies*. If we want to know about the effects of radiation on a biological system, the activity is not a useful quantity since different radiations may give different effects. In Section 6.8 we discuss some alternative units for measuring radiation that take into account their relative biological effects.

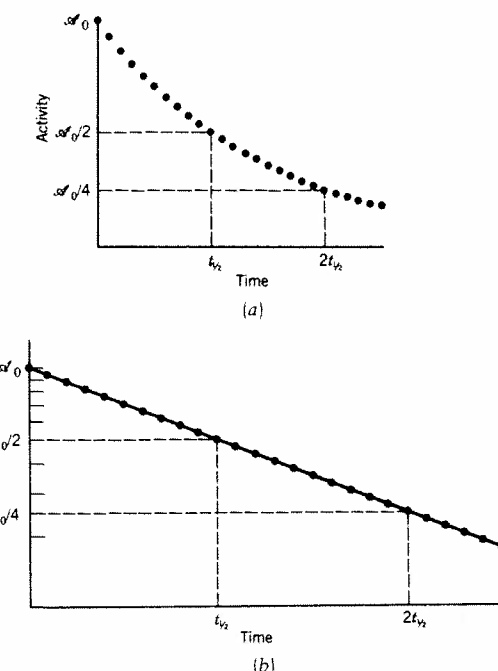


Figure 6.1 The exponential decay of activity. (a) Linear plot. (b) Semilog plot.

Equation 6.9 shows that the activity decays exponentially with time. We can thus measure the activity as a function of time by counting the number of decays in a sequence of short time intervals Δt . Plotting these data on a semilog graph (that is, $\ln \mathcal{A}$ vs t) should give a straight line of slope $-\lambda$. Figure 6.1 is an example of this kind of experiment, from which one can determine the half-life of a radioactive decay.

This method of measurement is useful only for half-lives that are neither too short nor too long. The half-life must be short enough that we can see the sample decaying—for half-lives far greater than a human lifetime, we would not be able to observe any substantial reduction in activity. For such cases, we can use Equation 6.1 directly, by measuring dN/dt (which is just the activity in this simple decay process) and by determining the number of atoms (such as by weighing a sample whose chemical composition is accurately known).

For half-lives that are very short (say, small compared with 1 s), observing the successive disintegration rates is also not useful, for the activity decays to nothing in the time that it would take to switch the counting apparatus on and off. For these cases we use a more precise technique, described in Chapter 7, that permits the routine measurement of half-lives down to nanoseconds (10^{-9} s) and even picoseconds (10^{-12} s).

It is important to keep in mind that the simple exponential law of radioactive decay applies only in a limited set of circumstances—a given initial quantity of a substance decays (by emitting radiation) to a stable end product. Under these circumstances, when radioactive nucleus 1 decays with decay constant λ_1 to stable nucleus 2, the number of nuclei present is

$$N_1 = N_0 e^{-\lambda_1 t} \quad (6.11a)$$

$$N_2 = N_0 (1 - e^{-\lambda_1 t}) \quad (6.11b)$$

Note that the number of nuclei of type 2 starts out at 0 and approaches N_0 as $t \rightarrow \infty$ (all of type 1 eventually end as type 2) and also note that $N_1 + N_2 = N_0$ (the total number of nuclei is constant). If nuclei of type 2 are themselves radioactive, or if nuclei of type 1 are being produced (as a result of a nuclear reaction, for instance) then Equations 6.11 do not apply. We consider these cases in Sections 6.3 and 6.4.

Often it will happen that a given initial nucleus can decay in two or more different ways, ending with two different final nuclei. Let's call these two decay modes a and b. The rate of decay into mode a, $(dN/dt)_a$, is determined by the partial decay constant λ_a , and the rate of decay into mode b, $(dN/dt)_b$, by λ_b :

$$\lambda_a = \frac{-(dN/dt)_a}{N}$$

$$\lambda_b = \frac{-(dN/dt)_b}{N} \quad (6.12)$$

The total decay rate $(dN/dt)_t$ is

$$-\left(\frac{dN}{dt}\right)_t = -\left(\frac{dN}{dt}\right)_a - \left(\frac{dN}{dt}\right)_b = N(\lambda_a + \lambda_b) = N\lambda_t \quad (6.13)$$

where $\lambda_t = \lambda_a + \lambda_b$ is the total decay constant. The nuclei therefore decay according to $N = N_0 e^{-\lambda_t t}$, and the activity $|dN/dt|$ decays with decay constant λ_t . Whether we count the radiation leading to final states a or b, we observe only the total decay constant λ_t ; we never observe an exponential decay of the activity with constants λ_a or λ_b . The relative decay constants λ_a and λ_b determine the probability for the decay to proceed by mode a or b. Thus a fraction λ_a/λ_t of the nuclei decay by mode a and a fraction λ_b/λ_t decay by mode b, so that

$$N_1 = N_0 e^{-\lambda_{1,t} t}$$

$$N_{2,a} = (\lambda_a/\lambda_t) N_0 (1 - e^{-\lambda_{1,t} t}) \quad (6.14)$$

$$N_{2,b} = (\lambda_b/\lambda_t) N_0 (1 - e^{-\lambda_{1,t} t})$$

The separate factors λ_a or λ_b never appear in any exponential term; we cannot "turn off" one decay mode to observe the exponential decay of the other.

Another special case is that of a sample with two or more radionuclei with genetically unrelated decay schemes. Consider a mixture of ^{64}Cu (12.7 h) and ^{61}Cu (3.4 h); such mixtures cannot be chemically separated of course. The activity of a particular mixture is plotted against time on semilog paper in Figure 6.2. At the right end of the curve we assume (because the curve is linear) that only one activity is present; the limiting slope shows a 12.7-h half-life. By (1)

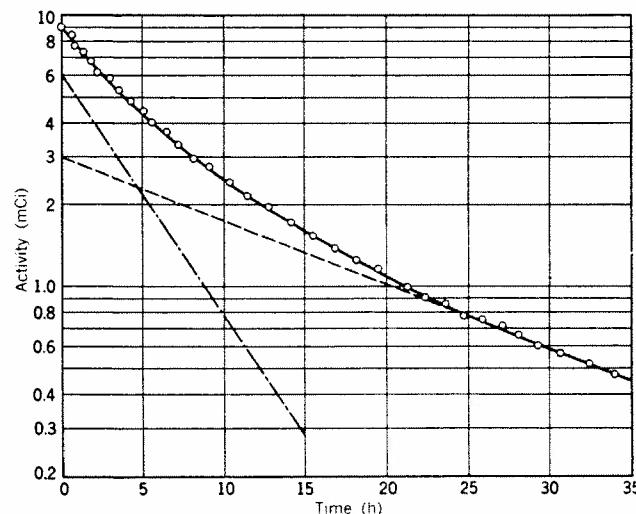


Figure 6.2 Decay curve for a sample containing a mixture of ^{64}Cu (12.7 h) and ^{61}Cu (3.4 h).

extending this limiting slope backward, (2) taking differences between the curve and this straight line at various abscissas, and (3) plotting these differences on the same scale, we get the dot-dashed straight line that represents the 3.4-h half-life. The intercepts of both straight lines on the vertical axis give the initial counting rates for each component. This method can be extended to mixtures with more than two components, if the half-lives are sufficiently different from one another.

6.2 QUANTUM THEORY OF RADIATIVE DECAYS

The energy levels we obtain by solving the Schrödinger equation for various time-independent potentials share one property—they are *stationary states*. A quantum system that is originally in a particular stationary state will remain in that state for all times and will *not* make transitions to (i.e., decay to) other states. We can allow a quantum system to be found sometimes in one state and sometimes in another by making a mixture of two or more states, such as $\psi = c_1\psi_1 + c_2\psi_2$ which has the probability $|c_1|^2$ to be found in state 1 and $|c_2|^2$ to be found in state 2. For time-independent potentials, c_1 and c_2 are independent of time, which does not correspond with observations for decaying states, in which the probability to find one state decays with time. Moreover, on a philosophical level, we should be forced to abandon the notion of pure states with well-defined wave functions, making the interpretation of nuclear structure very difficult indeed.

We therefore adopt the following approach: The potential is assumed to be of the form $V + V'$, where V is the nuclear potential that gives the stationary states and V' is a very weak additional potential that can cause transitions between the

states. For the moment neglecting V' , we solve the Schrödinger equation for the potential V and obtain the static nuclear wave functions. We then use those wave functions to calculate the transition probability between the “stationary states” under the influence of V' . This transition probability is just the decay constant λ , which is given by Fermi’s Golden Rule as discussed in Section 2.8:

$$\lambda = \frac{2\pi}{\hbar} |V'_{fi}|^2 \rho(E_f) \quad (6.15)$$

where

$$V'_{fi} = \int \psi_i^* V \psi_f \, dv \quad (6.16)$$

Given the initial and final wave functions ψ_i and ψ_f , we can evaluate the “matrix element” of V' and thus calculate the transition probability (which can then be compared with its experimental value).

The transition probability is also influenced by the *density of final states* $\rho(E_f)$ —within an energy interval dE_f , the number of final states accessible to the system is $d n_f = \rho(E_f) dE_f$. The transition probability will be large if there is a large number of final states accessible for the decay. There are two contributions to the density of final states because the final state after the decay includes two components—the final nuclear state and the emitted radiation. Let’s consider in turn each of these two components, beginning with the nuclear state.

Solving the Schrödinger equation for the time-independent potential V gives us the stationary states of the nucleus, $\Psi_a(\mathbf{r})$. The time-dependent wave function $\Psi_a(\mathbf{r}, t)$ for the state a is

$$\Psi_a(\mathbf{r}, t) = \psi_a(\mathbf{r}) e^{-iE_a t/\hbar} \quad (6.17)$$

where E_a is the energy of the state. The probability of finding the system in the state a is $|\Psi_a(\mathbf{r}, t)|^2$, which is independent of time for a stationary state. To be consistent with the radioactive decay law, we would like the probability of finding our decaying system in the state a to decrease with time like e^{-t/τ_a} :

$$|\Psi_a(t)|^2 = |\Psi_a(t=0)|^2 e^{-t/\tau_a} \quad (6.18)$$

where $\tau_a = 1/\lambda_a$ is the mean lifetime of the state whose decay constant is λ_a . We should therefore have written Equation 6.17 as

$$\Psi_a(\mathbf{r}, t) = \psi_a(\mathbf{r}) e^{-iE_a t/\hbar} e^{-t/2\tau_a} \quad (6.19)$$

The price we pay for including the *real* exponential term in Ψ_a is the loss of the ability to determine exactly the energy of the state—we no longer have a stationary state. (Recall the energy-time uncertainty relationship, Equation 2.2. If a state lives forever, $\Delta t \rightarrow \infty$ and we can determine its energy exactly, since $\Delta E = 0$. If a state lives on the average for a time τ , we cannot determine its energy except to within an uncertainty of $\Delta E \sim \hbar/\tau$.) We can make this discussion more rigorous by calculating the distribution of energy states (actually the Fourier transform of $e^{-t/2\tau_a}$). The probability to observe the system in the energy interval between E and $E + dE$ in the vicinity of E_a is given by the

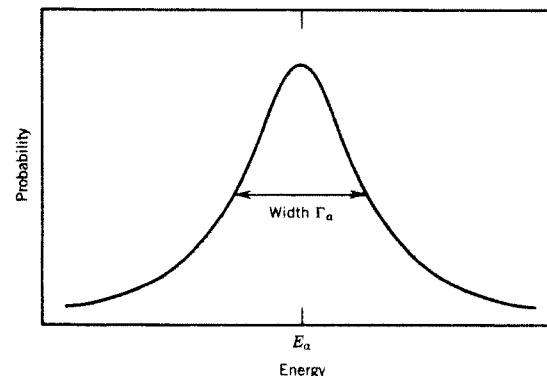


Figure 6.3 Probability to observe the energy of an unstable state of width Γ_a .

square of this distribution:

$$P(E) dE = \frac{dE}{(E - E_a)^2 + \Gamma_a^2/4} \quad (6.20)$$

where $\Gamma_a = \hbar/\tau_a$ is the *width* of the state a . Figure 6.3 shows the function $P(E)$. If we measure the energy of this system, we may no longer find the value E_a (although the average of many measurements gives E_a). The width Γ_a is a measure of our inability to determine precisely the energy of the state (through no fault of our own—nature imposes the limit of uncertainty, not our measuring instruments; as indicated by Figure 6.3, a state with the “exact” energy E_a cannot be observed).

If nuclear states do not have exact energies, can we speak of transitions between distinct levels? We can, because *the widths of the low-lying nuclear levels are small compared with their energy spacing*. Nuclear states typically have lifetimes greater than 10^{-12} s, corresponding to $\Gamma < 10^{-10}$ MeV. The discrete low-lying nuclear states that are populated in ordinary decays (and many nuclear reactions, as well) have typical separations of the order of 10^{-3} MeV and larger. Thus if we were to measure the energy of a final nuclear state after a decay process (by measuring the energy of the emitted radiation, for example), it is very unlikely that the overlap of the energy distributions of two different final states a and b could cause confusion as to the final “stationary” state resulting from the decay (see Figure 6.4).

We therefore conclude that it is reasonable to speak of discrete pseudo-stationary states because their separation is far greater than their width, and we also conclude that such nuclear states do not contribute to the density of final states because there is only one nuclear state that can be reached in a given decay process.

It is thus only the radiation field that contributes to the density of states, and we must consider the properties of the emitted radiations in calculating $\rho(E_f)$. For the present, we will only make some general comments regarding $\rho(E_f)$. If

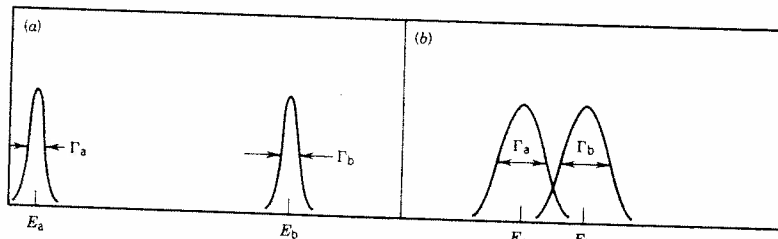


Figure 6.4 When the widths of unstable states are small compared with their separation, as in (a), the states are distinct and observable. In (b), the states a and b overlap and are strongly mixed; these states do not have distinctly observable wave functions.

we observe only the probability to form the nuclear state E_f , then we must consider all possible radiations of energy $E_i - E_f$. Specifically, the radiation can be emitted in any direction and in any state of polarization (if the radiation consists of a particle with spin, the spin may have any possible orientation), assuming of course that we do not observe the direction of the radiation or its polarization. It is this process of counting the number of accessible final states that gives the density of states, which we consider further when we discuss specific radiation types in Chapters 8–10.

In solving the differential equation (6.1) to obtain the radioactive decay law, we assumed the decay probability λ to be (1) small and (2) constant in time, which happen to be the same assumptions made in deriving Fermi's Golden Rule. If V' is independent of time, then λ calculated according to Equation 6.15 will also be independent of time. Under such a condition, the effect of V' on the stationary states a and b of V is

$$\psi_a \rightarrow \psi_a + \frac{V'_{ba}}{E_b - E_a} \psi_b$$

and the system formerly in the state a has a probability proportional to $|V'_{ba}|^2$ to be found in the state b. We observe this as a "decay" from a to b.

To apply Fermi's Golden Rule, the probability for decay must also be small, so that the amplitude of ψ_b in the above expression is small. It is this requirement that gives us a decay process. If the decay probability were large, then there would be enough radiation present to induce the reverse transition b → a through the process of resonant absorption. The system would then oscillate between the states a and b, in analogy with a classical system of two coupled oscillators.

The final connection between the effective decay probability for an ensemble of a large number of nuclei and the microscopic decay probability computed from the quantum mechanics of a single nucleus requires the assumption that each nucleus of the ensemble emits its radiation independently of all the others. We assume that the decay of a given nucleus is independent of the decay of its neighbors. This assumption then permits us to have confidence that the decay constant we measure in the laboratory can be compared with the result of our quantum mechanical calculation.

6.3 PRODUCTION AND DECAY OF RADIOACTIVITY

It quite frequently happens that a basic condition imposed in deriving the exponential law, that no new nuclei are introduced into the sample, is not valid. In solving Equation 6.1 we obtained a fixed number N_0 of nuclei present at $t = 0$. In many applications, however, we produce activity continuously, such as by a nuclear reaction. In this case, Equation 6.2 is no longer valid and we must consider in more detail the processes that occur in the production and decay of the activity.

Let's assume that we place a target of stable nuclei into a reactor or an accelerator such as a cyclotron. The nuclei of the target will capture a neutron or a charged particle, possibly leading to the production of a radioactive species. The rate R at which this occurs will depend on the number N_0 of target atoms present, on the flux or current I of incident particles, and on the reaction cross section σ (which measures the probability for one incident particle to react with one target nucleus). A typical flux of particles in a reactor or cyclotron might be of the order of $10^{14}/\text{s} \cdot \text{cm}^2$, and typical cross sections are at most of the order of barns (10^{-24} cm^2). Thus the probability to convert a target particle from stable to radioactive is about $10^{-10}/\text{s}$. Even if the reaction is allowed to continue for hours, the absolute number of converted target particles is small (say, less than 10^{-6} of the original number). *We can therefore, to a very good approximation, regard the number of target nuclei as constant*, and under this approximation the rate R is constant. (As we "burn up" target nuclei, N_0 will decrease by a small amount and the rate may therefore similarly decrease with time. Obviously N_0 must go to zero as $t \rightarrow \infty$, but for ordinary reaction times and typical cross sections we ignore this very small effect.) Thus

$$R = N_0 \sigma I \quad (6.21)$$

is taken to be a constant giving the rate at which the radioactive product nuclei are formed.

Let's denote by N_1 the number of radioactive nuclei that are formed as a result of the reaction. These nuclei decay with decay constant λ_1 to the stable nuclei denoted by N_2 . Thus the number of nuclei N_1 present *increases* owing to the production at the rate R and *decreases* owing to the radioactive decay:

$$dN_1 = R dt - \lambda_1 N_1 dt \quad (6.22)$$

and the solution to this equation is easily obtained

$$N_1(t) = \frac{R}{\lambda_1} (1 - e^{-\lambda_1 t}) \quad (6.23)$$

and

$$\mathcal{A}_1(t) = \lambda_1 N_1(t) = R(1 - e^{-\lambda_1 t}) \quad (6.24)$$

If the irradiation time is short compared with one half-life, then we can expand the exponential and keep only the term linear in t :

$$\mathcal{A}_1(t) \equiv R\lambda_1 t \quad t \ll t_{1/2} \quad (6.25)$$

For small times, the activity thus increases at a constant rate. This corresponds to the linear (in time) accumulation of product nuclei, whose number is not yet seriously depleted by radioactive decays.

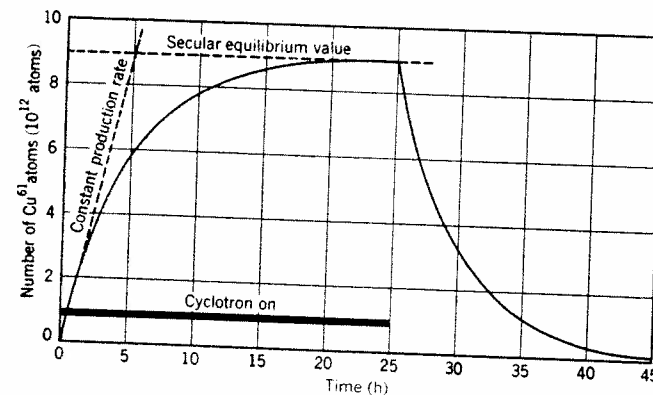


Figure 6.5 A plot of the number of radioactive ^{61}Cu atoms present in a Ni target at various times during and after bombardment with deuterons in a cyclotron.

For times long compared with the half-life the exponential approaches zero and the activity is approximately constant:

$$\mathcal{A}_1(t) \equiv R \quad t \gg t_{1/2} \quad (6.26)$$

In this case new activity is being formed at the same rate at which the older activity decays. This is an example of *secular equilibrium* which we discuss in more detail in the next section.

If we irradiate the sample for a time t_1 and then remove it from the accelerator or reactor, it will decay according to the simple exponential law, since no new activity is being formed. Figure 6.5 shows the activity resulting from the deuteron bombardment of ^{61}Ni to form ^{61}Cu ($t_{1/2} = 3.4$ h).

From Equation 6.24 we see that we produce 75% of the maximum possible activity by irradiating for two half-lives and 87.5% by irradiating for three half-lives. Further irradiation increases the activity by a steadily diminishing amount, so that we gain relatively little additional activity by irradiating for more than 2–3 half-lives. In fact, since the cost of using a reactor or accelerator is usually in direct proportion to the irradiation time, the best value (maximum activity per unit cost) is obtained by remaining close to the linear regime ($t \ll t_{1/2}$).

6.4 GROWTH OF DAUGHTER ACTIVITIES

Another common situation occurs when a radioactive decay results in a product nucleus that is also radioactive. It is thus possible to have series or chains of radioactive decays $1 \rightarrow 2 \rightarrow 3 \rightarrow 4 \dots$, and it has become common to refer to the original nucleus (type 1) as the parent and the succeeding “generations” as daughter (type 2), granddaughter (type 3), and so on.

We assume that we begin with N_0 atoms of the parent at $t = 0$ and that no atoms of the decay products are originally present:

$$\begin{aligned} N_1(t=0) &= N_0 \\ N_2(t=0) &= N_3(t=0) = \dots = 0 \end{aligned} \quad (6.27)$$

The various decay constants are represented by $\lambda_1, \lambda_2, \lambda_3, \dots$. For the present calculation, we will assume that the granddaughter is the stable end-product of the decay. The number of parent nuclei decreases with time according to the usual form

$$dN_1 = -\lambda_1 N_1 dt \quad (6.28)$$

The number of daughter nuclei increases as a result of decays of the parent and decreases as a result of its own decay:

$$dN_2 = \lambda_1 N_1 dt - \lambda_2 N_2 dt \quad (6.29)$$

The number of parent nuclei can be found directly from integrating Equation 6.28:

$$N_1(t) = N_0 e^{-\lambda_1 t} \quad (6.30)$$

To solve Equation 6.29, we try a solution of the form $N_2(t) = A e^{-\lambda_1 t} + B e^{-\lambda_2 t}$ and by substituting into Equation 6.29 and using the initial condition $N_2(0) = 0$ we find

$$N_2(t) = N_0 \frac{\lambda_1}{\lambda_2 - \lambda_1} (e^{-\lambda_1 t} - e^{-\lambda_2 t}) \quad (6.31)$$

$$\mathcal{A}_2(t) \equiv \lambda_2 N_2(t) = N_0 \frac{\lambda_2 \lambda_1}{\lambda_2 - \lambda_1} (e^{-\lambda_1 t} - e^{-\lambda_2 t}) \quad (6.32)$$

Note that Equation 6.31 reduces to Equation 6.11b if nuclei of type 2 are stable ($\lambda_2 \rightarrow 0$). We can also include the results of the previous section as a special case of Equation 6.31. Let's suppose that λ_1 is very small (but not quite zero), so that $N_1 \approx N_0 - N_0 \lambda_1 t$. In a nuclear reaction, the number of target nuclei decreases at the rate R according to $N_0 - Rt$, and thus identifying $N_0 \lambda_1$ with R and neglecting λ_1 in comparison with λ_2 , Equation 6.31 reduces to Equation 6.24 for the activity of type 2.

$$\lambda_1 \ll \lambda_2$$

In this case the parent is so long-lived that it decays at an essentially constant rate; for all practical times $e^{-\lambda_1 t} \approx 1$ and

$$N_2(t) \equiv N_0 \frac{\lambda_1}{\lambda_2} (1 - e^{-\lambda_2 t}) \quad (6.33)$$

which is of the same form as Equation 6.24. Thus the activity \mathcal{A}_2 approaches the limiting value $N_0 \lambda_1$ as was shown in Figure 6.5.

This is another example of *secular equilibrium*, where as t becomes large nuclei of type 2 are decaying at the same rate at which they are formed: $\lambda_2 N_2 = \lambda_1 N_1$. (Note that Equation 6.29 shows immediately that $dN_2/dt = 0$ in this case.) Figure 6.6 shows an example of approximate secular equilibrium.

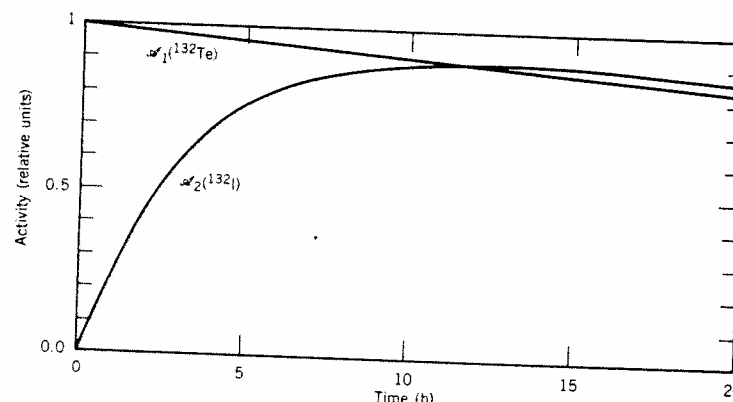


Figure 6.6 In the decay ^{132}Te (78 h) \rightarrow ^{132}I (2.28 h) \rightarrow ^{132}Xe , approximate secular equilibrium is reached at about 12 h.

$$\lambda_1 < \lambda_2$$

From Equations 6.30 and 6.31 we can calculate the ratio of the two activities:

$$\frac{\lambda_2 N_2}{\lambda_1 N_1} = \frac{\lambda_2}{\lambda_2 - \lambda_1} (1 - e^{-(\lambda_2 - \lambda_1)t}) \quad (6.34)$$

As t increases, the exponential term becomes smaller and the ratio α_2/α_1 approaches the limiting constant value $\lambda_2/(\lambda_2 - \lambda_1)$. The activities themselves are not constant, but the nuclei of type 2 decay (in effect) with the decay constant

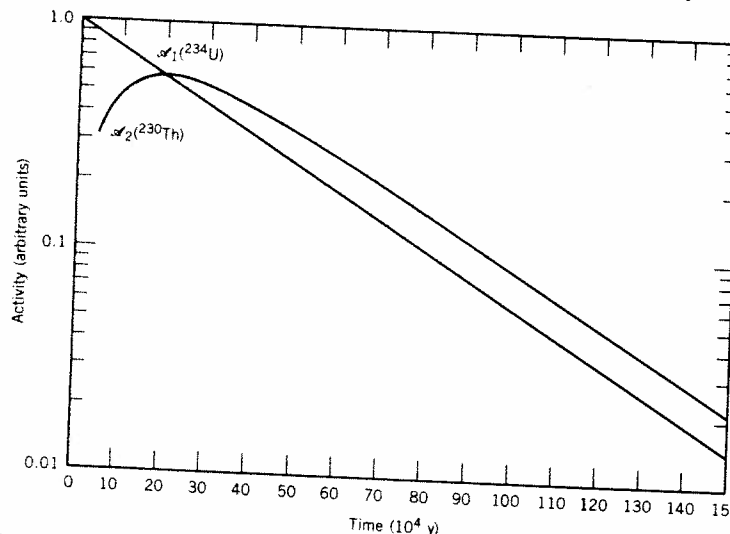


Figure 6.7 An example of equilibrium in the decays of ^{234}U (2.45×10^5 y) to ^{230}Th (8.0×10^4 y). The ratio α_2/α_1 approaches the constant value 1.48.

of type 1. This situation is known as *transient equilibrium* and is illustrated in Figure 6.7.

$$\lambda_1 > \lambda_2$$

In this case the parent decays quickly, and the daughter activity rises to a maximum and then decays with its characteristic decay constant. When this occurs the number of nuclei of type 1 is small and nearly insignificant. If t is so long that $e^{-\lambda_1 t}$ effectively vanishes, then Equation 6.31 becomes

$$N_2(t) \equiv N_0 \frac{\lambda_1}{\lambda_1 - \lambda_2} e^{-\lambda_2 t} \quad (6.35)$$

which reveals that the type 2 nuclei decay approximately according to the exponential law.

Series of Decays

If we now assume that there are several succeeding generations of radioactive nuclei (that is, the granddaughter nuclei type 3 are themselves radioactive, as are types 4, 5, 6, ...), we can then easily generalize Equation 6.29 since each species is populated by the preceding one:

$$dN_i = \lambda_{i-1} N_{i-1} dt - \lambda_i N_i dt \quad (6.36)$$

A general solution, for the case of N_0 nuclei of type 1 and none of the other types initially present, is given by the *Bateman equations*, in which the activity of the n th member of the chain is given in terms of the decay constants of all preceding members:

$$\begin{aligned} \alpha_n &= N_0 \sum_{i=1}^n c_i e^{-\lambda_i t} \\ &= N_0 (c_1 e^{-\lambda_1 t} + c_2 e^{-\lambda_2 t} + \cdots + c_n e^{-\lambda_n t}) \end{aligned} \quad (6.37)$$

where

$$\begin{aligned} c_m &= \frac{\prod_{i=1}^m \lambda_i}{\prod_{i=1}^n (\lambda_i - \lambda_m)} \\ &= \frac{\lambda_1 \lambda_2 \lambda_3 \cdots \lambda_n}{(\lambda_1 - \lambda_m)(\lambda_2 - \lambda_m) \cdots (\lambda_n - \lambda_m)} \end{aligned} \quad (6.38)$$

where the prime on the lower product indicates we omit the term with $i = m$.

It is also possible to have secular equilibrium in this case, with $\lambda_1 N_1 = \lambda_2 N_2 = \cdots = \lambda_n N_n$.

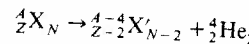
6.5 TYPES OF DECAYS

The three primary decay types, to be discussed in greater detail in Chapters 8, 9, and 10, are α , β , and γ decays. In α - and β -decay processes, an unstable nucleus emits an α or a β particle as it tries to become a more stable nucleus (that is, to

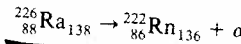
approach the most stable isobar for the resulting mass number). In γ -decay processes, an excited state decays toward the ground state without changing the nuclear species.

α Decay

In this process, a nucleus emits an α particle (which Rutherford and his co-workers showed to be a nucleus of helium, ${}^4_2\text{He}_2$). The ${}^4_2\text{He}$ nucleus is chosen as the agent for this process because it is such a tightly bound system, and thus the kinetic energy released in the decay is maximized. Such decays are favored, as we shall discuss in Chapter 8. The decay process is



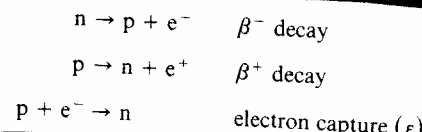
where X and X' represent the chemical symbols of the initial and final nuclei. Notice that the number of protons and the number of neutrons must separately be conserved in the decay process. An example of an α -decay process is



in which the half-life is 1600 years and the α particle appears with a kinetic energy of about 4.8 MeV.

β Decay

Here the nucleus can correct a proton or a neutron excess by directly converting a proton into a neutron or a neutron into a proton. This process can occur in three possible ways, each of which must involve another charged particle to conserve electric charge (the charged particle, originally called a β particle, was later shown to be identical with ordinary electrons).

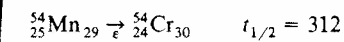
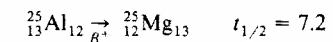
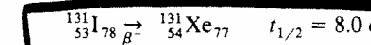


The first process is known as negative β decay or negatron decay and involves the creation and emission of an ordinary electron. The second process is positive β decay or positron decay, in which a positively charged electron is emitted. In the third process, an atomic electron that strays too close to the nucleus is swallowed, allowing the conversion of a proton to a neutron.

In all three processes, yet another particle called a *neutrino* is also emitted, but since the neutrino has no electric charge, its inclusion in the decay process does not affect the identity of the other final particles.

Note that in positive and negative β decay, a particle is created (out of the decay energy, according to $m = E/c^2$). The electron or positron did not exist inside the nucleus before the decay. (Contrast the case of α decay, in which the emitted nucleons were inside the nucleus before the decay.)

Some representative β -decay processes are



In these processes, Z and N each change by one unit, but the total mass number $Z + N$ remains constant.

γ Decay

Radioactive γ emission is analogous to the emission of atomic radiations such as optical or X-ray transitions. An excited state decays to a lower excited state or possibly the ground state by the emission of a photon of γ radiation of energy equal to the difference in energy between the nuclear states (less a usually negligible correction for the "recoil" energy of the emitting nucleus). Gamma emission is observed in all nuclei that have excited bound states ($A > 5$), and usually follows α and β decays since those decays will often lead to excited states in the daughter nucleus.

The half-lives for γ emission are usually quite short, generally less than 10^{-9} s, but occasionally we find half-lives for γ emission that are significantly longer, even hours or days. These transitions are known as *isomeric transitions* and the long-lived excited states are called *isomeric states* or *isomers* (or sometimes *metastable* states). There is no clear criterion for classifying a state as isomeric or not; the distinction was originally taken to be whether or not the half-life was directly measurable, but today we can measure half-lives well below 10^{-9} s. Clearly a state with $t_{1/2} = 10^{-6}$ s is an isomer and one with $t_{1/2} = 10^{-12}$ s is not, but in between the boundary is rather fuzzy. We usually indicate metastable states with a superscript m, thus: ${}^{110}\text{Ag}^m$ or ${}^{110m}\text{Ag}$.

A process that often competes with γ emission is *internal conversion*, in which the nucleus de-excites by transferring its energy directly to an *atomic* electron, which then appears in the laboratory as a free electron. (This is very different from β decay in that no change of Z or N occurs, although the atom becomes ionized in the process.)

Spontaneous Fission

We usually think of fission as occurring under very unnatural and artificial conditions, such as in a nuclear reactor. There are, however, some nuclei that fission spontaneously, as a form of radioactive decay. This process is similar to the neutron-induced fission that occurs in reactors, with the exception that no previous neutron capture is needed to initiate the fission. In the process, a heavy nucleus with an excess of neutrons splits roughly in half into two lighter nuclei; the final nuclei are not rigidly determined, as they are in α or β decay, but are statistically distributed over the entire range of medium-weight nuclei. Examples

of spontaneously fissioning nuclei are ^{256}Fm ($t_{1/2} = 2.6\text{ h}$) and ^{254}Cf ($t_{1/2} = 60.5\text{ days}$).

Nucleon Emission

As we move further and further from the “valley” of stable nuclei, the energy differences between neighboring isobars increases (recall the mass parabolas of constant A of Figure 3.18). Eventually the difference exceeds the nucleon binding energy (about 8 MeV, on the average) and it becomes possible to have radioactive decay by nucleon emission. This type of decay occurs most frequently in fission products, which have a very large neutron excess, and it is responsible for the “delayed” neutrons (that is, delayed by the half-life of the decay) that are used to control nuclear reactors. For example, ^{138}I β^- decays with a half-life of 6.5 s to ^{138}Xe . Most of the β^- decays populate low excited states in ^{138}Xe , but about 5% of the ^{138}I decays populate states in ^{138}Xe at about 6.5 MeV; these states decay by direct neutron emission to ^{137}Xe . Similarly, 0.7% of the ^{73}Kr β^+ decays ($t_{1/2} = 27\text{ s}$) go to states in ^{73}Br at about 5 MeV; these states decay by proton emission to states in ^{72}Se .

Branching Ratios and Partial Half-lives

Figure 6.8 summarizes a variety of different decay processes, and Figure 6.9 shows a small section of the chart of stable and radioactive nuclei (Figure 1.1) with several decay processes indicated. Some nuclei may decay only through a single process, but more often decay schemes are very complicated, involving the emission of α 's, β 's, and γ 's in competing modes. We specify the relative intensities of the competing modes by their *branching ratios*. Thus ^{226}Ra α decays to the ground state of ^{222}Rn with a branching ratio of 94% and to the first excited state with a branching ratio of 6%. Often different decay modes can compete: ^{226}Ac decays by α emission (0.006%), β^- emission (83%), and ϵ (17%); ^{132}Cs decays by β^- emission (2%) and by β^+ and ϵ (98%); the metastable state ^{95m}Nb decays by β^- emission (2.5%) or by an isomeric transition (97.5%). The isomeric transition itself includes a 27% branch by γ emission and a 73% branch by internal conversion.

Frequently, we specify the branching ratio by giving the partial decay constant or partial half-life. For example, we consider the decay of ^{226}Ac ($t_{1/2} = 29\text{ h}$). The total decay constant is

$$\lambda_t = \frac{0.693}{t_{1/2}} = 0.024\text{ h}^{-1} = 6.6 \times 10^{-6}\text{ s}^{-1}$$

The partial decay constants are

$$\lambda_\beta = 0.83\lambda_t = 5.5 \times 10^{-6}\text{ s}^{-1}$$

$$\lambda_\epsilon = 0.17\lambda_t = 1.1 \times 10^{-6}\text{ s}^{-1}$$

$$\lambda_\alpha = 6 \times 10^{-5}\lambda_t = 4 \times 10^{-10}\text{ s}^{-1}$$

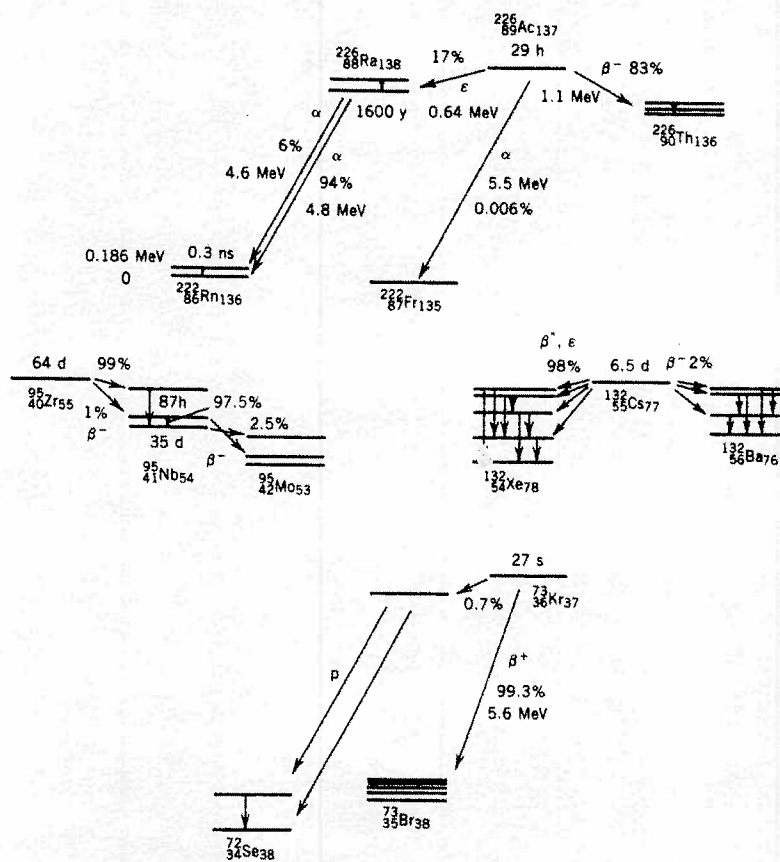


Figure 6.8 A variety of different decay processes.

and the partial half-lives are

$$t_{1/2,\beta} = \frac{0.693}{\lambda_\beta} = 1.3 \times 10^5\text{ s} = 35\text{ h}$$

$$t_{1/2,\epsilon} = \frac{0.693}{\lambda_\epsilon} = 6.1 \times 10^5\text{ s} = 170\text{ h}$$

$$t_{1/2,\alpha} = \frac{0.693}{\lambda_\alpha} = 1.7 \times 10^9\text{ s} = 55\text{ y}$$

The partial half-life is merely a convenient way to represent branching ratios; a glance at the above figures shows that α emission is far less probable than β emission for ^{226}Ac . However, the activity would be observed to decay only with the total half-life. Even if we were to observe the decay of ^{226}Ac by its α emission, the

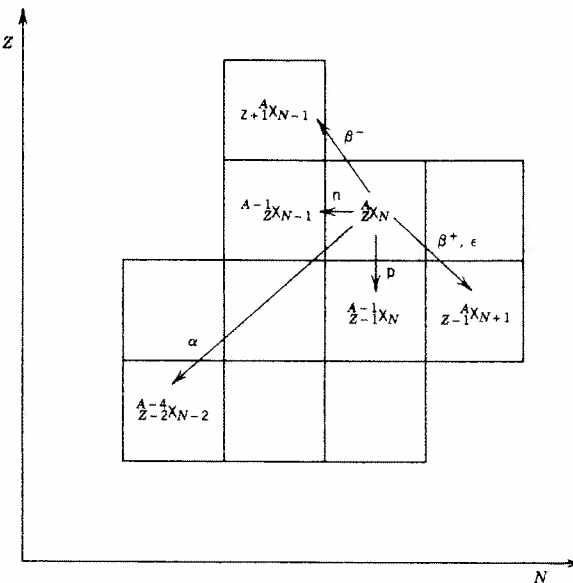


Figure 6.9 The initial nucleus ${}^A_Z X_N$ can reach different final nuclei through a variety of possible decay processes.

activity would decay with time according to a half-life of 29 h. (Imagine if this were not so, and two observers were studying the decay of ${}^{226}\text{Ac}$, one by observing the β 's and the other by observing the α 's. Since the radioactive decay law gives the number of undecayed nuclei, the β observer would conclude that half of the original ${}^{226}\text{Ac}$ nuclei remained after 35 h, while the α observer would have to wait 55 years similarly to observe half of the nuclei undecayed! In reality, half of the nuclei decay every 29 h, no matter what method we use to observe those decays.)

6.6 NATURAL RADIOACTIVITY

The Earth and the other planets of our solar system formed about 4.5×10^9 y ago out of material rich in iron, carbon, oxygen, silicon, and other medium and heavy elements. These elements in turn were created from the hydrogen and helium that resulted from the Big Bang some 15×10^9 y ago. During the 10×10^9 y from the Big Bang until the condensation of the solar system, the hydrogen and helium were "cooked" into heavier elements in stellar interiors, novas, and supernovas; we are made of the recycled debris of these long dead stars. Most of the elements thus formed were radioactive, but have since decayed to stable nuclei. A few of the radioactive elements have half-lives that are long compared with the age of the Earth, and so we can still observe their radioactivity. This radioactivity forms the major portion of our natural radioactive environment, and is also probably responsible for the inner heating of the terrestrial planets.

Table 6.1 Some Characteristics of the Disintegration Series of the Heavy Elements

Name of Series	Type ^a	Final Nucleus (Stable)	Longest-Lived Member	
			Nucleus	Half-Life, (y)
Thorium	$4n$	${}^{208}\text{Pb}$	${}^{232}\text{Th}$	1.41×10^{10}
Neptunium	$4n + 1$	${}^{209}\text{Bi}$	${}^{237}\text{Np}$	2.14×10^6
Uranium	$4n + 2$	${}^{206}\text{Pb}$	${}^{238}\text{U}$	4.47×10^9
Actinium	$4n + 3$	${}^{207}\text{Pb}$	${}^{235}\text{U}$	7.04×10^8

^a n is an integer.

Although there are long-lived natural radioactive elements of other varieties, most of those observed today originate with the very heavy elements, which have no stable isotopes at all. These nuclides decay by α and β emission, decreasing Z and A until a lighter, stable nucleus is finally reached. Alpha decay changes A by four units and β decay does not change A at all, and so therefore we have four independent decay chains with mass numbers $4n$, $4n + 1$, $4n + 2$, and $4n + 3$, where n is an integer. The decay processes will tend to concentrate the nuclei in the longest-lived member of the chain, and if the lifetime of that nuclide is at least of the order of the age of the Earth, we will observe that activity today. The four series are listed in Table 6.1. Notice that the longest-lived member of the neptunium series has far too short a half-life to have survived since the formation of the Earth; this series is not observed in natural material.

Consider, for example, the thorium series illustrated in Figure 6.10. Let us assume that we had created, in a short period of time, a variety of plutonium (Pu) isotopes. The isotopes ${}^{232}\text{Pu}$ and ${}^{236}\text{Pu}$ decay rapidly to 72-y ${}^{232}\text{U}$ and other species of much shorter half-lives. Thus in a time long compared with 72 y (say, 10^3 y), all traces of these isotopes have vanished, leaving only the stable end product ${}^{208}\text{Pb}$. The isotopes ${}^{240}\text{Pu}$ and ${}^{244}\text{Pu}$ decay much more slowly, the former comparatively quickly and the latter very slowly to ${}^{236}\text{U}$, which in turn decays to the longest-lived member of the series, ${}^{232}\text{Th}$. In a time greater than 81×10^6 y but less than 14×10^9 y, the original ${}^{240}\text{Pu}$ and ${}^{244}\text{Pu}$ (and the intermediate ${}^{236}\text{U}$) will all have decayed to ${}^{232}\text{Th}$, the decay of which we still observe today.

These radioactive isotopes are present in material all around us, especially in rocks and minerals that condensed with the Earth 4.5×10^9 y ago. (In fact, their decays provide a reliable technique for determining the time since the condensation of the rocks and thus the age of the Earth; see Section 6.7 and Chapter 19 for discussions of these techniques.) In general the radioactive elements are tightly bound to the minerals and are not hazardous to our health, but all of the natural radioactive series involve the emission of a gaseous radioactive element, radon. This element, if formed deep within rocks, normally has little chance to migrate to the surface and into the air before it decays. However, when rocks are fractured, the radon gas can escape (in fact the presence of radon gas has in recent years been observed as a precursor of earthquakes). There is also the possibility of escape of radon from the surface of minerals, and particularly those that are used in the construction of buildings. Inhalation of this radioactive gas

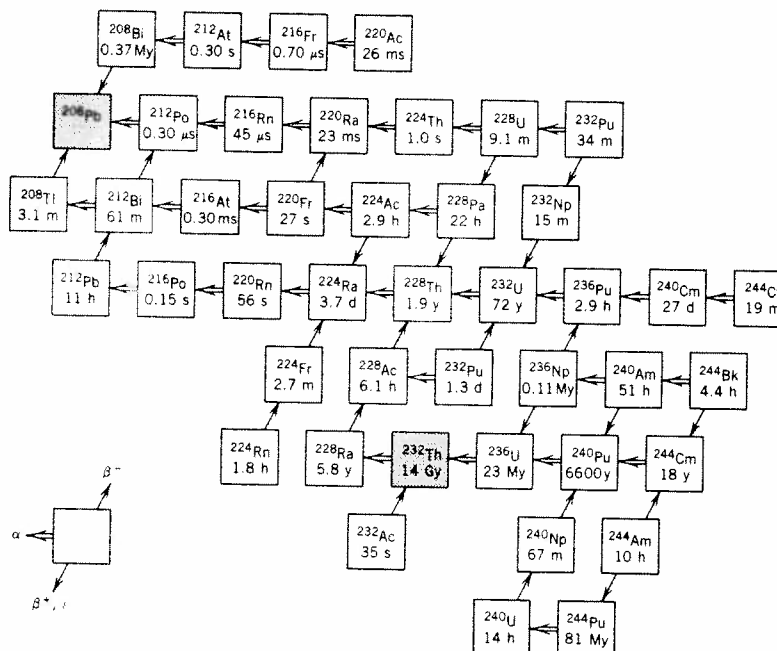


Figure 6.10 The thorium series of naturally occurring radioactive decays. Some half-lives are indicated in My (10^6 y) and Gy (10^9 y). The shaded members are the longest-lived radioactive nuclide in the series (Th, after which the series is named) and the stable end product.

Table 6.2 Some Natural Radioactive Isotopes

Isotope	$t_{1/2}$ (y)
^{40}K	1.28×10^9
^{87}Rb	4.8×10^{10}
^{113}Cd	9×10^{15}
^{115}In	4.4×10^{14}
^{138}La	1.3×10^{11}
^{176}Lu	3.6×10^{10}
^{187}Re	5×10^{10}

could possibly be responsible for many lung cancers, and there is a current suspicion that smoking may accelerate this process by causing the accumulation of these radioactive products in the lungs. It is perhaps ironic that the recent trends toward well insulated and tightly sealed buildings to conserve energy may be responsible for an increased concentration of radon gas, and as of this writing there is active research on the problem, including measurement of radon gas accumulation in buildings.

The heavy element series are not the only sources of naturally occurring radioactive isotopes of half-lives long enough to be present in terrestrial matter. Table 6.2 gives a partial list of others, some of which can also be used for radioactive dating.

There are also other natural sources of radioactivity of relatively short half-lives, which are not remnants of the production of elements before the Earth formed, but instead are being formed continuously today. These elements include ^3H and ^{14}C , which are formed in the upper atmosphere when cosmic rays (high-energy protons) strike atoms of the atmosphere and cause nuclear reactions. The isotope ^{14}C has had important applications in radioactive dating.

6.7 RADIOACTIVE DATING

Although we cannot predict with certainty when an individual nucleus will decay, we can be very certain how long it will take for half of a large number of nuclei to decay. These two statements may seem inconsistent; their connection has to do with the statistical inferences that we can make by studying random processes. If we have a room containing a single gas molecule, we cannot predict with certainty whether it will be found in the left half of the room or the right half. If however we have a room containing a large number N of molecules ($N \sim 10^{24}$), then we expect to find on the average $N/2$ molecules in each half. Furthermore, the fluctuations of the number in each half about the value $N/2$ are of the order of \sqrt{N} ; thus the deviation of the fraction in each half from the value 0.5 is about $\sqrt{N}/N \approx 10^{-12}$. The fraction in each half is thus $0.500000000000 \pm 0.000000000001$. This extreme (and unreasonable) precision comes about because N is large and thus the fractional error $N^{-1/2}$ is small.

A similar situation occurs for radioactive decay. (The laws of counting statistics are discussed in detail in Chapter 7.) If we had at $t = 0$ a collection of a large number N_0 of radioactive nuclei, then after a time equal to one half-life, we should find that the remaining fraction is $\frac{1}{2} \pm N_0^{-1/2}$. Thus despite the apparently random nature of the decay process, the decay of radioactive nuclei gives us a very accurate and entirely reliable clock for recording the passage of time. That is, if we know the decay constant λ , the exponential decrease in activity of a sample can be used to measure time.

The difficulty in using this process occurs when we try to apply it to decays that occur over geological times ($\sim 10^9$ y) because in this case we do not measure the activity as a function of time. Instead, we use the relative number of parent and daughter nuclei observed at time t_1 (now) compared with the relative number at time t_0 (when the “clock” started ticking, usually when the material such as a rock or mineral condensed, trapping the parent nuclei in their present sites). In

principle this process is rather simple. Given the decay of parent isotope P to daughter isotope D, we merely count (by chemical means, for instance) the present numbers of P and D atoms, $N_P(t_1)$ and $N_D(t_1)$:

$$N_D(t_1) + N_P(t_1) = N_P(t_0) \quad (6.39)$$

$$N_P(t_1) = N_P(t_0) e^{-\lambda(t_1 - t_0)} \quad (6.40)$$

$$\Delta t \equiv t_1 - t_0 = \frac{1}{\lambda} \ln \frac{N_P(t_0)}{N_P(t_1)}$$

$$\Delta t = \frac{1}{\lambda} \ln \left(1 + \frac{N_D(t_1)}{N_P(t_1)} \right) \quad (6.41)$$

Given the decay constant (which we can measure in the laboratory) and the present ratio of daughter to parent nuclei, the age of the sample is directly found, with a precision determined by our knowledge of λ and by the counting statistics for N_P and N_D .

Equations 6.39 and 6.40 contain assumptions that must be carefully tested before we can apply Equation 6.41 to determine the age of a sample. Equation 6.39 assumes that $N_D(t_0) = 0$ —no daughter atoms are present at t_0 —and also that the total number of atoms remains constant—no parent or daughter atoms escape from the mineral or solid in which they were originally contained. As we discuss below, we can modify the derivation of Δt to account for the daughter atoms present at t_0 (even though when we analyze the sample today at time t_1 , we cannot tell which daughter atoms were originally present and which resulted from decays during Δt). Equation 6.40 assumes that the variation in N_P comes only from the decay—no new parent atoms are introduced (by a previous decay or by nuclear reactions induced by cosmic rays, for example).

Let's relax the assumption of Equation 6.39 and permit daughter nuclei to be present at $t = t_0$. These daughter nuclei can be formed from the decay of parent nuclei at times before t_0 or from the process that formed the original parent nuclei (a supernova explosion, for example); the means of formation of these original daughter nuclei is of no importance for our calculation. We therefore take

$$N_D(t_1) + N_P(t_1) = N_D(t_0) + N_P(t_0) \quad (6.42)$$

Because we have introduced another unknown, $N_D(t_0)$, we can no longer solve directly for the age Δt . If, however, there is also present in the sample a different isotope of the daughter, D', which is neither radioactive nor formed from the decay of a long-lived parent, we can again find the age of the sample. The population of this stable isotope is represented by $N_{D'}(t_1)$, and if D' is stable then $N_{D'}(t_1) = N_{D'}(t_0)$, in which case

$$\frac{N_D(t_1) + N_P(t_1)}{N_{D'}(t_1)} = \frac{N_D(t_0) + N_P(t_0)}{N_{D'}(t_0)} \quad (6.43)$$

which can be written as

$$\frac{N_D(t_1)}{N_{D'}(t_1)} = \frac{N_P(t_1)}{N_{D'}(t_1)} [e^{\lambda(t_1 - t_0)} - 1] + \frac{N_D(t_0)}{N_{D'}(t_0)} \quad (6.44)$$

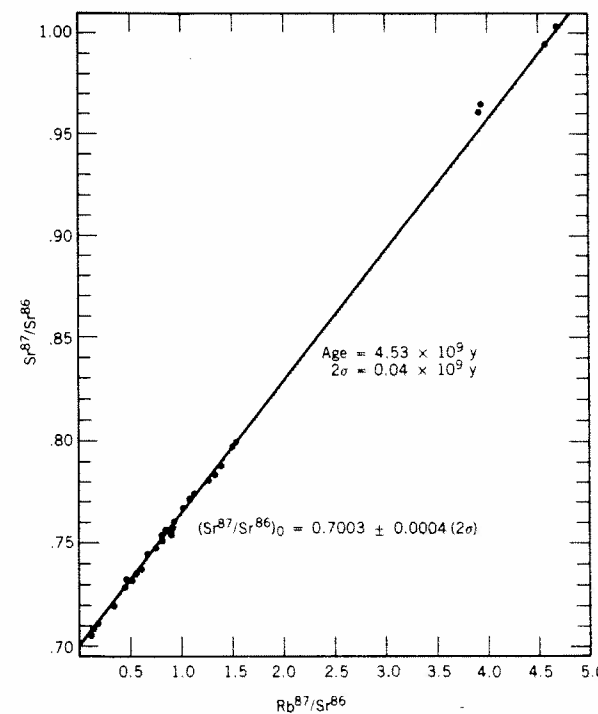


Figure 6.11 The Rb-Sr dating method, allowing for the presence of some initial ^{87}Sr . The linear behavior is consistent with Equation 6.44. From G. W. Wetherill, *Ann. Rev. Nucl. Sci.* **25**, 283 (1975).

The ratios $N_D(t_1)/N_{D'}(t_1)$ and $N_P(t_1)/N_{D'}(t_1)$ can be measured in the laboratory, but that still leaves two unknowns in Equation 6.44: the age Δt and the initial isotopic ratio $N_D(t_0)/N_{D'}(t_0)$. Minerals that crystallize from a common origin should show identical ages and identical isotopic ratios $N_D(t_0)/N_{D'}(t_0)$, even though the original $N_P(t_0)$ may be very different (from differing chemical compositions, for example). If these hypotheses are correct, we expect to observe today minerals with various ratios $N_D(t_1)/N_{D'}(t_1)$ and $N_P(t_1)/N_{D'}(t_1)$ corresponding to common values of Δt and $N_D(t_0)/N_{D'}(t_0)$. We can test these assumptions by plotting $y = N_D(t_1)/N_{D'}(t_1)$ against $x = N_P(t_1)/N_{D'}(t_1)$ for a variety of minerals. Equation 6.44 is of the form $y = mx + b$, a straight line with slope $m = e^{\lambda(t_1 - t_0)} - 1$ and intercept $b = N_D(t_0)/N_{D'}(t_0)$. Figure 6.11 is an example of such a procedure for the decay $^{87}\text{Rb} \rightarrow ^{87}\text{Sr}$ ($t_{1/2} = 4.8 \times 10^{10}$ y), in which the comparison is done with stable ^{86}Sr . Even though the present ratio of ^{87}Rb to ^{86}Sr varies by more than an order of magnitude, the data indicate a common age of the Earth, $\Delta t = 4.5 \times 10^9$ y. The good linear fit is especially important, for it justifies our assumptions of no loss of parent or daughter nuclei.

Other similar methods for dating minerals from the Earth, Moon, and meteorites give a common age of 4.5×10^9 y. These methods include the decay

of ^{40}K to ^{40}Ar , the decay of ^{235}U and ^{238}U to ^{207}Pb and ^{206}Pb , and the spontaneous fission of ^{238}U and ^{244}Pu , which are analyzed either by chemical separation of the fission products or by microscopic observation of the tracks left in the minerals by the fission fragments.

For dating more recent samples of organic matter, the ^{14}C dating method is used. The CO_2 that is absorbed by organic matter consists almost entirely of stable ^{12}C (98.89%), with a small mixture of stable ^{13}C (1.11%). Radioactive ^{14}C is being continuously formed in the upper atmosphere as a result of cosmic-ray bombardment of atmospheric nitrogen, and thus all living matter is slightly radioactive owing to its ^{14}C content. Because the production rate of ^{14}C by cosmic rays has been relatively constant for thousands of years, living organic material reaches equilibrium of its carbon with atmospheric carbon, with about 1 atom of ^{14}C for every 10^{12} atoms of ^{12}C . The half-life of ^{14}C is 5730 y, and thus each gram of carbon shows an activity of about 15 decays per minute. When an organism dies, it goes out of equilibrium with atmospheric carbon; it stops acquiring new ^{14}C and its previous content of ^{14}C decreases according to the radioactive decay law. We can therefore determine the age of samples by measuring the *specific activity* (activity per gram) of their carbon content. This method applies as long as we have enough ^{14}C intensity to determine the activity; from matter that has decayed for 10 or more half-lives, the decay is so weak that the ^{14}C method cannot be used. Recent techniques using accelerators as mass spectrometers have the potential to exceed this limit by counting ^{14}C atoms directly; these techniques are discussed in Chapter 20.

The major assumption of this method is the relatively constant production of ^{14}C by cosmic rays over the last 50,000 y or so. We can test this assumption by comparing the ages determined by radiocarbon dating with ages known or determined by independent means (historical records or tree-ring counting, for example). These comparisons show very good agreement and support the assumption of a relatively uniform flux of cosmic rays.

In later millennia, the radiocarbon method may no longer be applicable. During the last 100 years, the burning of fossil fuels has upset the atmospheric balance by diluting the atmosphere with stable carbon (the hydrocarbons of fossil fuels are old enough for all of their ^{14}C to have decayed away). During the 1950s and 1960s, atmospheric testing of nuclear weapons has placed additional ^{14}C in the atmosphere, perhaps doubling the concentration over the equilibrium value from cosmic-ray production alone.

6.8 UNITS FOR MEASURING RADIATION

The activity of a radioactive sample (in curies or in decays per second) does not depend on the type of radiation or on its energy. Thus the activity may be a useful means to compare two different sources of the same decaying isotope (10 mCi of ^{60}Co is stronger than 1 mCi of ^{60}Co), but how can we compare different decays? For instance, how does a 10-mCi source of ^{60}Co compare in strength with 10 mCi of ^{14}C , or how does a 10- μCi γ emitter compare in strength with a 10-mCi α emitter? And just what exactly do we mean by the “strength” of a source of radiation?

One common property of nuclear radiations is their ability to *ionize* (knock electrons from) atoms with which they interact. (For this reason, nuclear radiation is often called *ionizing radiation*.) We begin by considering the passage of X-ray and γ -ray photons through air. The photons interact many times with atoms in the air through a variety of processes (Compton scattering, photoelectric effect, electron-positron pair production), each of which creates a free electron, often of reasonably high energy. These secondary electrons can themselves produce ionization (and additional electrons). The total electric charge Q on the ions produced in a given mass m of air is called the *exposure* X , and we may take γ -ray sources as being of the same strength if they result in the same exposure, even though the energies of the γ rays and the activities of the sources may be quite different. Specifically, the exposure is

$$X = \frac{Q}{m} \quad (6.45)$$

and is measured in the SI units of coulomb per kilogram. More frequently we encounter the *roentgen* unit (R), which is defined as the exposure resulting in an ionization charge of 1 electrostatic unit (the cgs unit of electric charge, in terms of which the electronic charge e is 4.80×10^{-10} electrostatic unit) in 1 cm^3 of air at 0°C and 760 mm pressure (corresponding to a mass of 0.001293 g). Thus

$$1 \text{ R} = \frac{1 \text{ esu}}{0.001293 \text{ g}} = 2.58 \times 10^{-4} \text{ C/kg}$$

Assigning one unit of electric charge to each ion, an exposure of 1 R means that $(2.58 \times 10^{-4} \text{ C/kg})/1.60 \times 10^{-19} \text{ C} = 1.61 \times 10^{15}$ ions are formed per kg of air, or 2.08×10^9 ions per cm^3 . It takes on the average about 34 eV to form an ion in air, and thus an exposure of 1 R results in an energy absorption by the air of $7.08 \times 10^{10} \text{ eV/cm}^3$ or 0.113 erg/cm^3 , or 88 erg/g.

The ionization produced by a γ ray depends on its energy. With about 34 eV needed to produce each ion in air, a 1-MeV γ ray can be expected to produce, on the average, about 30,000 ions. A radioactive source of a given activity will generally produce many different γ rays with different intensities and energies. The exposure resulting from this source will depend on the number of decays and also on the intensities and energies of each of the γ rays, and the exposure rate (exposure per unit time) will depend on the activity of the source. It will also depend on how far we are from the source; if we imagine that we are to measure the ionization produced in 1 cm^3 of air, that ionization will obviously depend on whether we hold that volume of air very close to the radioactive source or very far away. We can therefore write

$$\frac{\Delta X}{\Delta t} = \Gamma \frac{\mathcal{A}}{d^2} \quad (6.46)$$

where $\Delta X/\Delta t$ is the exposure rate, \mathcal{A} is the activity, d is the distance from the source, and Γ is a constant, the *specific γ -ray constant*, which depends on the details of γ -ray emission of each radionuclide (the fraction of γ rays with each particular energy and the ionizing ability of photons of that particular energy). It is customary to take $d = 1 \text{ m}$ as a standard distance for measuring the relation-

Table 6.3 Specific γ -Ray Constants for Various Radioisotopes^a

Nuclide	$t_{1/2}$	γ -Ray Energy (MeV) and Abundance (%)	Γ
^{22}Na	2.6 y	0.511 (181), 1.275 (100)	1.20
^{24}Na	15.02 h	1.369 (100), 2.754 (100)	1.84
^{59}Fe	44.6 d	0.143 (1), 0.192 (3), 1.099 (56), 1.292 (44)	0.60
^{57}Co	270 d	0.014 (9), 0.122 (85), 0.136 (11)	0.059
^{60}Co	5.27 y	1.173 (100), 1.333 (100)	1.28
^{131}I	8.06 d	0.08 (2), 0.284 (6), 0.364 (82), 0.637 (7), 0.723 (2)	0.22
^{137}Cs	30.1 y	0.032 (8), 0.662 (85)	0.32
^{198}Au	2.7 d	0.412 (95), 0.676 (1)	0.23
^{226}Ra and daughters			0.84

^aUnits for Γ are $\text{R} \cdot \text{m}^2/\text{h} \cdot \text{Ci}$. Note the relationship between Γ and the energy and intensity of the γ rays.

ship between exposure rate and activity, and thus Γ has units of $(\text{R}/\text{h})/(\text{Ci}/\text{m}^2)$. Some representative values of Γ are given in Table 6.3.

Materials other than air exposed to ionizing radiation will differ in their rate of energy absorption. It is therefore necessary to have a standard for defining the energy absorption by ionization in different materials. This quantity is called the *absorbed dose* D of the material and measures the energy deposited by ionizing radiation per unit mass of material. The commonly used unit of absorbed dose is the *rad* (*radiation absorbed dose*) equal to an energy absorption of 100 ergs per gram of material. (Thus 1 R = 0.88 rad in air.) The SI unit for absorbed dose is the *gray* (Gy), equal to the absorption of 1 joule per kilogram of material, and so 1 Gy = 100 rad.

To define standards for radiation protection of human beings, it is necessary to have some measure of the biological effects of different kinds of radiations. That is, some radiations may deposit their energy over a very long path, so that relatively little energy is deposited over any small interval (say, of the size of a typical human cell); β and γ rays are examples of such radiations. Other types of radiations, α particles for instance, lose energy more rapidly and deposit essentially all of their energy over a very short path length. The probability of cell damage from 1 rad of α radiation is thus far greater than that from 1 rad of γ radiation. To quantify these differences, we define the *relative biological effectiveness* (RBE), as the ratio of the dose of a certain radiation to the dose of X rays that produces the same biological effect. Values of the RBE range from 1 to about 20 for α radiation. Since the RBE is a relatively difficult quantity to measure, it is customary to work instead with the *quality factor* (QF), which is calculated for a given type (and energy) of radiation according to the energy deposited per unit path length. Radiations that deposit relatively little energy per unit length (β 's and γ 's) have QF near 1, while radiations that deposit more energy per unit length (α 's) have QF ranging up to about 20. Table 6.4 shows some representative values of QF.

Table 6.4 Quality Factors for Absorbed Radiation

Radiation	QF
X rays, β , γ	1
Low-energy p, n (~ keV)	2–5
Energetic p, n (~ MeV)	5–10
α	20

Table 6.5 Quantities and Units for Measuring Radiation

Quantity	Measure of	Traditional Unit	SI Unit
Activity (\mathcal{A})	Decay rate	curie (Ci)	becquerel (Bq)
Exposure (X)	Ionization in air	roentgen (R)	coulomb per kilogram (C/kg)
Absorbed dose (D)	Energy absorption	rad	gray (Gy)
Dose equivalent (DE)	Biological effectiveness	rem	sievert (Sv)

The effect of a certain radiation on a biological system then depends on the absorbed dose D and on the quality factor QF of the radiation. The *dose equivalent* DE is obtained by multiplying these quantities together:

$$\text{DE} = D \cdot \text{QF} \quad (6.47)$$

The dose equivalent is measured in units of *rem* (*roentgen equivalent man*) when the dose D is in rads. When the SI unit of gray is used for D , then the dose equivalent is in *sievert* (Sv). Previously we noted that 1 Gy = 100 rad, and so it follows that 1 Sv = 100 rem.

We therefore see that "strength" of radiation has many different ways of being defined, depending on whether we wish to merely count the rate at which the decays occur (activity) or to measure the effect on living systems (dose equivalent). Table 6.5 summarizes these various measures and the traditional and SI units in which they are expressed.

Standards for radiation exposure of the general public and of radiation workers are specified in rems over a certain period of time (usually per calendar quarter and per year). From natural background sources (cosmic rays and naturally occurring radioactive isotopes, such as the uranium and thorium series and ^{40}K) we receive about 0.1–0.2 rem per year. The International Commission on Radiation Protection (ICRP) has recommended limiting annual whole-body absorbed dose to 0.5 rem per year for the general public and 5 rem per year for those who work with radiation. By way of contrast, the dose absorbed by a particularly sensitive area of the body, the bone marrow, is about 0.05 rem for a typical chest X ray and 0.002 rem for dental X rays. Unfortunately, the physiological effects of radiation exposure are difficult to calculate and to measure, and so the guideline must be to keep the exposure as low as possible. (For this reason, many physicians no longer recommend chest X rays as a part of

the regular annual physical examination, and dentists often place a lead apron over the sensitive areas of a patient's body while taking X-ray pictures of the mouth.) Although the evidence is not conclusive, there is reason to believe that the risk of radiation-induced cancers and genetic damage remains at even very low doses while other effects, such as cataracts and loss of fertility, may show a definite threshold of exposure below which there is no risk at all. Much of our knowledge in this area comes from studies of the survivors of the nuclear weapons exploded over Hiroshima and Nagasaki in World War II, from which we know that there is virtual certainty of death following a short-term dose of 100 rem, but the evidence regarding the linear relationship between dose and risk is less clear. The effects of long-term, low-level doses are still under active debate, with serious consequences for standards of radiation protection and for the health of the general public.

REFERENCES FOR ADDITIONAL READING

The quantum mechanics of decay processes is treated in more detail in M. G. Bowler, *Nuclear Physics* (Oxford: Pergamon, 1973); see especially Sections 3.1 and 3.2.

A more complete treatment of radioactive decay series can be found in R. D. Evans, *The Atomic Nucleus* (New York: McGraw-Hill, 1955), Chapter 15.

Radioactive dating of the solar system has been reviewed by L. T. Aldrich and G. W. Wetherill, *Ann. Rev. Nucl. Sci.* **8**, 257 (1958), and more recently by G. W. Wetherill, *Ann. Rev. Nucl. Sci.* **25**, 283 (1975).

For more information on radioactivity in the atmosphere and in the oceans, see D. Lal and H. E. Suess, *Ann. Rev. Nucl. Sci.* **18**, 407 (1968).

Additional information on radiation exposure can be found in many references on health physics. See, for example, E. Pochin, *Nuclear Radiation: Risks and Benefits* (Oxford: Clarendon, 1983).

PROBLEMS

- Three radioactive sources each have activities of $1.0 \mu\text{Ci}$ at $t = 0$. Their half-lives are, respectively, 1.0 s, 1.0 h, and 1.0 d. (a) How many radioactive nuclei are present at $t = 0$ in each source? (b) How many nuclei of each source decay between $t = 0$ and $t = 1$ s? (c) How many decay between $t = 0$ and $t = 1$ h?
- Naturally occurring samarium includes 15.1% of the radioactive isotope ^{147}Sm , which decays by α emission. One gram of natural Sm gives $89 \pm 5 \alpha$ decays per second. From these data calculate the half-life of the isotope ^{147}Sm and give its uncertainty.
- Among the radioactive products emitted in the 1986 Chernobyl reactor accident were ^{131}I ($t_{1/2} = 8.0$ d) and ^{137}Cs ($t_{1/2} = 30$ y). There are about five times as many ^{137}Cs atoms as ^{131}I atoms produced in fission. (a) Which

isotope contributes the greater activity to the radiation cloud? Assume the reactor had been operating continuously for several days before the radiation was released. (b) How long after the original incident does it take for the two activities to become equal? (c) About 1% of fission events produce ^{131}I , and each fission event releases an energy of about 200 MeV. Given a reactor of the Chernobyl size (1000 MW), calculate the activity in curies of ^{131}I after 24 h of operation.

- Consider a chain of radioactive decays $1 \rightarrow 2 \rightarrow 3$, where nuclei of type 3 are stable. (a) Show that Equation 6.31 is the solution to Equation 6.29. (b) Write a differential equation for the number of nuclei of type 3 and solve the differential equation for $N_3(t)$. (c) Evaluate $N_1(t) + N_2(t) + N_3(t)$ and interpret. (d) Examine N_1 , N_2 , and N_3 at small t , keeping only linear terms. Interpret the results. (e) Find the limits of N_1 , N_2 , and N_3 as $t \rightarrow \infty$ and interpret.
- The human body contains on the average about 18% carbon and 0.2% potassium. Compute the intrinsic activity of the average person from ^{14}C and ^{40}K .
- A radioactive isotope is prepared by a nuclear reaction in a cyclotron. At the conclusion of the irradiation, which lasts a very short time in comparison with the decay half-life, a chemical procedure is used to extract the radioactive isotope. The chemical procedure takes 1 h to perform and is 100% efficient in recovering the activity. After the chemical separation, the sample is counted for a series of 1-min intervals, with the following results ($t = 0$ is taken to be the conclusion of the irradiation):

t (min)	Decays / min	t (min)	Decays / min	t (min)	Decays / min
62.0	592	112.0	290	163.0	125
68.0	527	120.0	242	170.0	110
73.0	510	125.0	215	175.0	109
85.0	431	130.0	208	180.0	100
90.0	380	138.0	187		
97.0	353	144.0	177		
101.0	318	149.0	158		
105.0	310	156.0	142		

- Plot these data on semilog paper and determine the half-life and initial ($t = 0$) activity from your graph. Show the range of uncertainty of each data point, and try to estimate the resulting uncertainty in the half-life. (b) Use an analytic procedure to do a linear least-squares fit of the data (in the form of $\log N$ vs t) and determine the half-life and its uncertainty. Formulas for linear least-squares fits can be found in K. S. Krane and L. Schecter, *J. Phys.* **50**, 82 (1982).
- A sample of a certain element with two naturally occurring isotopes becomes activated by neutron capture. After 1 h in the reactor, it is placed

Alpha Spectroscopy

Appendix C

Alpha Decay

Source: “Kenneth S. Krane, Introductory Nuclear Physics (from Chap 8)”

ALPHA DECAY

Alpha particles were first identified as the least penetrating of the radiations emitted by naturally occurring materials. In 1903, Rutherford measured their charge-to-mass ratio by deflecting α particles from the decay of radium in electric and magnetic fields. Despite the difficulty of these early experiments, Rutherford's result was only about 25% higher than the presently accepted value. In 1909 Rutherford showed that, as suspected, the α particles were in fact helium nuclei; in his experiments the particles entered an evacuated thin-walled chamber by penetrating its walls, and after several days of collecting, atomic spectroscopy revealed the presence of helium gas inside the chamber.

Many heavy nuclei, especially those of the naturally occurring radioactive series, decay through α emission. Only exceedingly rarely does any other spontaneous radioactive process result in the emission of nucleons; we do not, for example, observe deuteron emission as a natural decay process. There must therefore be a special reason that nuclei choose α emission over other possible decay modes. In this chapter we examine this question and study the α decay process in detail. We also show how α spectroscopy can help us to understand nuclear structure.

8.1 WHY α DECAY OCCURS

Alpha emission is a Coulomb repulsion effect. It becomes increasingly important for heavy nuclei because the disruptive Coulomb force increases with size at a faster rate (namely, as Z^2) than does the specific nuclear binding force, which increases approximately as A .

Why is the α particle chosen as the agent for the spontaneous carrying away of positive charge? When we call a process *spontaneous* we mean that some kinetic energy has suddenly appeared in the system for no apparent cause; this energy must come from a decrease in the mass of the system. The α particle, because it is a very stable and tightly bound structure, has a relatively small mass compared with the mass of its separate constituents. It is particularly favored as an emitted particle if we hope to have the disintegration products as light as possible and thus get the largest possible release of kinetic energy.

Table 8.1 Energy Release (Q value) for Various Modes of Decay of ^{232}U ^a

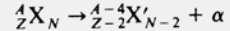
Emitted Particle	Energy Release (MeV)	Emitted Particle	Energy Release (MeV)
n	-7.26	${}^4\text{He}$	+5.41
${}^1\text{H}$	-6.12	${}^5\text{He}$	-2.59
${}^2\text{H}$	-10.70	${}^6\text{He}$	-6.19
${}^3\text{H}$	-10.24	${}^6\text{Li}$	-3.79
${}^3\text{He}$	-9.92	${}^7\text{Li}$	-1.94

^aComputed from known masses.

For a typical α emitter ^{232}U (72 y) we can compute, from the known masses, the energy release for various emitted particles. Table 8.1 summarizes the results. Of the particles considered, spontaneous decay is energetically possible *only* for the α particle. A positive disintegration energy results for some slightly heavier particles than those listed, ${}^8\text{Be}$ or ${}^{12}\text{C}$, for example. We will show, however (Section 8.4), that the partial disintegration constant for emission of such heavy particles is normally vanishingly small compared with that for α emission. Such decays would be so rare that in practice they would almost never be noticed. This suggests that if a nucleus is to be recognized as an alpha emitter it is not enough for α decay to be energetically possible. The disintegration constant must also not be too small or else α emission will occur so rarely that it may not be detected. With present techniques this means that the half-life must be less than about 10^{16} y. Also, β decay, if it has a much higher partial disintegration constant, can mask the α decay. Most nuclei with $A > 190$ (and many with $150 < A < 190$) are energetically unstable against α emission but only about one-half of them can meet these other requirements.

8.2 BASIC α DECAY PROCESS

The spontaneous emission of an α particle can be represented by the following process:



The α particle, as was shown by Rutherford, is a nucleus of ${}^4\text{He}$, consisting of two neutrons and two protons. To understand the decay process, we must study the conservation of energy, linear momentum, and angular momentum.

Let's first consider the conservation of energy in the α decay process. We assume the initial decaying nucleus X to be at rest. Then the energy of the initial system is just the rest energy of X, $m_X c^2$. The final state consists of X' and α , each of which will be in motion (to conserve linear momentum). Thus the final total energy is $m_{X'} c^2 + T_{X'} + m_\alpha c^2 + T_\alpha$, where T represents the kinetic energy of the final particles. Thus conservation of energy gives

$$m_X c^2 = m_{X'} c^2 + T_{X'} + m_\alpha c^2 + T_\alpha \quad (8.1)$$

or

$$(m_X - m_{X'} - m_\alpha) c^2 = T_{X'} + T_\alpha \quad (8.2)$$

The quantity on the left side of Equation 8.2 is the net energy released in the decay, called the Q value:

(8.3)

and the decay will occur spontaneously only if $Q > 0$. (The decay Q values for ^{232}U were listed in Table 8.1.) Q values can be calculated from atomic mass tables because even though Equation 8.3 represents a nuclear process, the electron masses will cancel in the subtraction. When the masses are in atomic mass units (u), expressing c^2 as $931.502 \text{ MeV}/u$ gives Q values directly in MeV.

The Q value is also equal to the total kinetic energy given to the decay fragments:

$$Q = T_{X'} + T_\alpha \quad (8.4)$$

If the original nucleus X is at rest, then its linear momentum is zero, and conservation of linear momentum then requires that X' and α move with equal and opposite momenta in order that the final momentum also be zero:

$$p_\alpha = p_{X'} \quad (8.5)$$

α decays typically release about 5 MeV of energy. Thus for both X' and α , $T \ll mc^2$ and we may safely use nonrelativistic kinematics. Writing $T = p^2/2m$ and using Equations 8.4 and 8.5 gives the kinetic energy of the α particle in terms of the Q value:

$$T_\alpha = \frac{Q}{(1 + m_\alpha/m_{X'})} \quad (8.6)$$

Because the mass ratio is small compared with 1 (recall that X' represents a heavy nucleus), it is usually sufficiently accurate to express this ratio simply as $4/(A - 4)$, which gives, with $A \gg 4$,

$$T_\alpha = Q(1 - 4/A) \quad (8.7)$$

Typically, the α particle carries about 98% of the Q value, with the much heavier nuclear fragment X' carrying only about 2%. (This recoil energy of the heavy fragment is not entirely negligible. For a typical Q value of 5 MeV, the recoiling nucleus has an energy of the order of 100 keV. This energy is far in excess of that which binds atoms in solids, and thus the recoiling nucleus, if it is near the surface of the radioactive source, escapes from the source and can spread to the surroundings. If the α decay is part of a decay chain, then the recoiling daughter nucleus may itself be radioactive, and these recoils can result in the spread of radioactive material. Fortunately, the heavy recoil nuclei have an extremely short range in matter and their spread can be prevented by a thin coating, such as Mylar or lacquer, placed over the radioactive sample.)

The kinetic energy of an α particle can be measured directly with a magnetic spectrometer, and so the Q value of a decay can be determined. This gives us a way to determine atomic masses, such as in a case in which we might know the mass of long-lived X as a result of direct measurement but X' is so short-lived that its mass cannot be determined by direct measurement.

8.3 α DECAY SYSTEMATICS

One feature of α decay is so striking that it was noticed as long ago as 1911, the year that Rutherford "discovered" the nucleus. Geiger and Nuttall noticed that α emitters with large disintegration energies had short half-lives and conversely. The variation is astonishingly rapid as we may see from the limiting cases of ^{232}Th ($1.4 \times 10^{10} \text{ y}$; $Q = 4.08 \text{ MeV}$) and ^{218}Th ($1.0 \times 10^{-7} \text{ s}$; $Q = 9.85 \text{ MeV}$). A factor of 2 in energy means a factor of 10^{24} in half-life! The theoretical explanation of this Geiger-Nuttall rule in 1928 was one of the first triumphs of quantum mechanics.

A plot of $\log t_{1/2}$ against Q in which all α emitters are included shows a considerable scatter about the general Geiger-Nuttall trend. Very smooth curves result, however, if we plot only α emitters with the same Z and if further we select from this group only those with Z and N both even (Figure 8.1). Even-odd, odd-even, and odd-odd nuclei obey the general trend but do not plot into quite such smooth curves; their periods are 2–1000 times longer than those for even-even types with the same Z and Q .

It is interesting that ^{235}U (even Z , odd N) is one of these "extra-long-life" types. If its half-life were 1000 times shorter, this important nucleus would not occur in nature, and we probably would not have nuclear reactors today! We see in Chapter 13 that the same feature that apparently accounts for the long life against α decay, namely the odd neutron, also makes ^{235}U very susceptible to fission by thermal neutrons.

Figure 8.2 shows another important systematic relationship for α emitters. Looking for the moment only at the data for $A > 212$, we see that adding neutrons to a nucleus reduces the disintegration energy, which, because of the

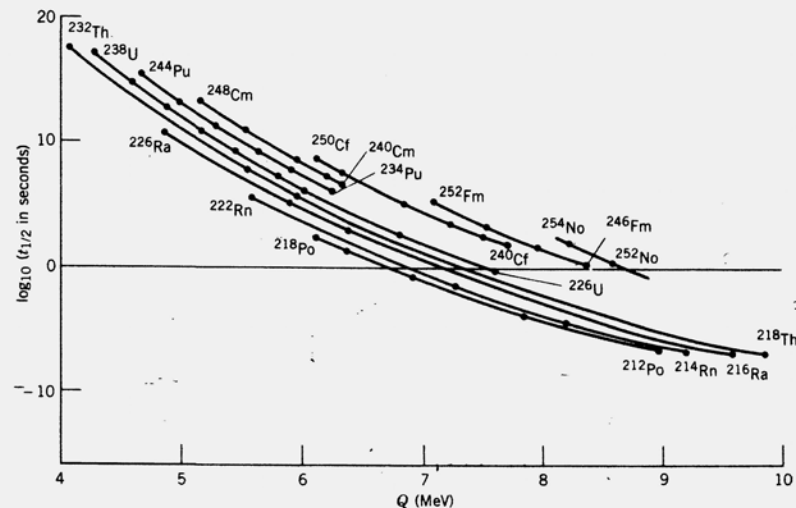


Figure 8.1 The inverse relationship between α -decay half-life and decay energy, called the Geiger-Nuttall rule. Only even- Z , even- N nuclei are shown. The solid lines connect the data points.

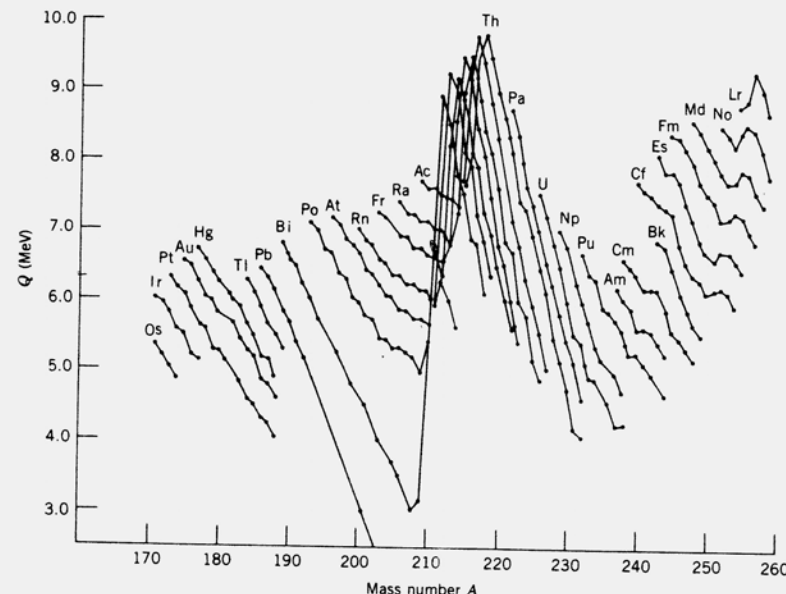


Figure 8.2 Energy released in α decay for various isotopic sequences of heavy nuclei. In contrast to Figure 8.1, both odd- A and even- A isotopes are shown, and a small amount of odd-even staggering can be seen. The effects of the shell closures at $N = 126$ (large dip in data) and $Z = 82$ (larger than average spacing between Po, Bi, and Pb sequences) are apparent.

Geiger-Nuttall rule, increases the half-life. The nucleus becomes more stable. A striking discontinuity near $A = 212$ occurs where $N = 126$ and is another example of nuclear shell structure.

We can compare the systematic dependence of Q on A with the prediction of the semiempirical mass formula, Equation 3.28.

$$Q = B(^4\text{He}) + B(Z - 2, A - 4) - B(Z, A) \quad (8.8)$$

$$\approx 28.3 - 4a_v + \frac{8}{3}a_s A^{-1/3} + 4a_c Z A^{-1/3}(1 - Z/3A) \\ - 4a_{\text{sym}}(1 - 2Z/A)^2 + 3a_p A^{-7/4} \quad (8.9)$$

where the approximation in Equation 8.9 is $Z, A \gg 1$. For ^{226}Th , this formula gives $Q = 6.75$ MeV, not too far from the measured value of 6.45 MeV. What is perhaps more significant is that the general trend of Figure 8.2 is reproduced: for ^{232}Th , Equation 8.9 gives $Q = 5.71$ MeV (to be compared with $Q = 4.08$ MeV), while for ^{220}Th the formula gives $Q = 7.77$ MeV (compared with $Q = 8.95$ MeV). Keep in mind that the parameters of the semiempirical mass formula are chosen to give rough agreement with observed binding energies across the entire range of nuclei. It is important that the formula gives us rough agreement with the decay Q values and that it correctly gives $Q > 0$ for the heavy nuclei. It also

correctly predicts the decrease of Q with increasing A for a sequence of isotopes such as those of thorium, although it gives too small a change of Q with A (the formula gives $\Delta Q = -0.17$ MeV per unit change in A , while for Th the observed average change is $\Delta Q = -0.40$ MeV per unit change in A).

8.4 THEORY OF α EMISSION

The general features of Figure 8.1 can be accounted for by a quantum mechanical theory developed in 1928 almost simultaneously by Gamow and by Gurney and Condon. In this theory an α particle is assumed to move in a spherical region determined by the *daughter* nucleus. The central feature of this *one-body model* is that the α particle is preformed inside the parent nucleus. Actually there is not much reason to believe that α particles do exist separately within heavy nuclei; nevertheless, the theory works quite well, especially for even-even nuclei. This success of the theory does not prove that α particles are preformed, but merely that they behave as if they were.

Figure 8.3 shows a plot, suitable for purposes of the theory, of the potential energy between the α particle and the residual nucleus for various distances between their centers. The horizontal line Q is the disintegration energy. Note that the Coulomb potential is extended inward to a radius a and then arbitrarily cut off. The radius a can be taken as the sum of the radius of the residual nucleus and of the α particle. There are three regions of interest. In the spherical region $r < a$ we are inside the nucleus and speak of a potential well of depth $-V_0$, where V_0 is taken as a positive number. Classically the α particle can move in this region, with a kinetic energy $Q + V_0$ but it cannot escape from it. The annular-shell region $a < r < b$ forms a potential barrier because here the potential energy

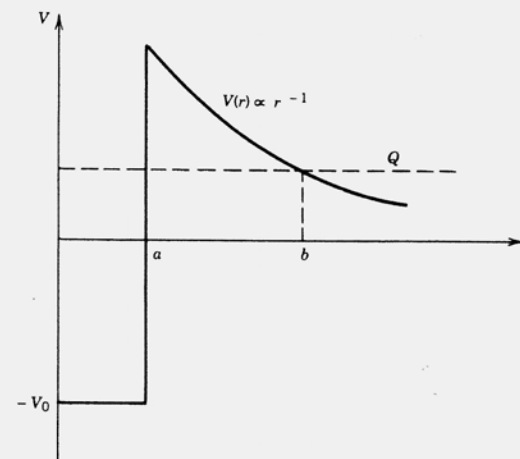


Figure 8.3 Relative potential energy of α -particle, daughter-nucleus system as a function of their separation. Inside the nuclear surface at $r = a$, the potential is represented as a square well; beyond the surface, only the Coulomb repulsion operates. The α particle tunnels through the Coulomb barrier from a to b .

is more than the total available energy Q . Classically the α particle cannot enter this region from either direction, just as a tennis ball dropped from a certain height cannot rebound higher; in each case the kinetic energy would have to be negative. The region $r > b$ is a classically permitted region outside the barrier.

From the classical point of view, an α particle in the spherical potential well would sharply reverse its motion every time it tried to pass beyond $r = a$. Quantum mechanically, however, there is a chance of "leakage" or "tunnelling" through such a barrier. This barrier accounts for the fact that α -unstable nuclei do not decay immediately. The α particle within the nucleus must present itself again and again at the barrier surface until it finally penetrates. In ^{238}U , for example, the leakage probability is so small that the α particle, on the average, must make $\sim 10^{38}$ tries before it escapes ($\sim 10^{21}$ per second for $\sim 10^9$ years)!

The barrier also operates in reverse, in the case of α -particle scattering by nuclei (see Sections 3.1 and 11.6). Alpha particles incident on the barrier from outside the nucleus usually scatter in the Coulomb field if the incident energy is well below the barrier height. Tunnelling through the barrier, so that the nuclear force between the particle and target can cause nuclear reactions, is a relatively improbable process at low energy. The theoretical analysis of nuclear reactions induced by charged particles uses a formalism similar to that of α decay to calculate the barrier penetration probability. Fusion reactions, such as those responsible for the energy released in stars, also are analyzed using the barrier penetration approach (see Section 14.2).

The disintegration constant of an α emitter is given in the one-body theory by

$$\lambda = fP \quad (8.10)$$

where f is the frequency with which the α particle presents itself at the barrier and P is the probability of transmission through the barrier.

Equation 8.10 suggests that our treatment is going to be semiclassical in that our discussion of the situation for $r < a$ is very "billiard-ballish." A rigorous wave-mechanical treatment, however, gives about the same results for this problem. The quantity f is roughly of the order of v/a where v is the relative velocity of the α particle as it rattles about inside the nucleus. We can find v from the kinetic energy of the α particle for $r < a$. Estimating $V_0 \approx 35$ MeV for a typical well depth gives $f \approx 6 \times 10^{21}/\text{s}$ for $Q \approx 5$ MeV. We will see later that we do not need to know f very precisely to check the theory.

The barrier penetration probability P must be obtained from a quantum mechanical calculation similar to the one-dimensional problem discussed in Section 2.3. Let's first use the result of that calculation, Equation 2.39, to estimate the probability P . Of course, the calculation that led to Equation 2.39 was based on a one-dimensional rectangular barrier, which is not directly applicable to the $1/r$ Coulomb potential, but we can at least find a rough order-of-magnitude estimate. The result, Equation 2.39, depends on the width of the barrier and on its height (called V_0 for the rectangular barrier) above the energy E of the particle. The Coulomb barrier of Figure 8.3 has height B at $r = a$, where

$$B = \frac{1}{4\pi\epsilon_0} \frac{zZ'e^2}{a} \quad (8.11)$$

In this expression the α particle has charge ze and the daughter nucleus, which

provides the Coulomb repulsion, has charge $Z'e = (Z - z)e$. The height of the barrier thus varies from $(B - Q)$ above the particle's energy at $r = a$ to zero at $r = b$, and we can take a representative average height to be $\frac{1}{2}(B - Q)$. We can similarly choose a representative average width to be $\frac{1}{2}(b - a)$. The factor k_2 of Equation 2.39 then becomes $\sqrt{(2m/\hbar^2)} \cdot \frac{1}{2}(B - Q)$. For a typical heavy nucleus ($Z = 90$, $a = 7.5$ fm), the barrier height B is about 34 MeV, so the factor k_2 is about 1.6 fm^{-1} . The radius b at which the α particle "leaves" the barrier is found from the equality of the particle's energy and the potential energy:

$$b = \frac{1}{4\pi\epsilon_0} \frac{zZ'e^2}{Q} \quad (8.12)$$

and for a typical case of a heavy nucleus with $Q \approx 6$ MeV, $b \approx 42$ fm. Thus $k_2 \cdot \frac{1}{2}(b - a) \gg 1$ and we can approximate Equation 2.39 as

$$P \approx e^{-2k_2 \cdot (1/2)(b - a)} \quad (8.13)$$

since the factors in front of the exponential are of unit order of magnitude. For the case we are estimating here, $P \sim 2 \times 10^{-25}$ and thus $\lambda \sim 10^{-3}/\text{s}$ and $t_{1/2} \sim 700$ s. A slight change of Q to 5 MeV changes P to 1×10^{-30} and $t_{1/2} \sim 10^8$ s. Even this very crude calculation is able to explain the many orders of magnitude change of $t_{1/2}$ between $Q = 5$ MeV and $Q = 6$ MeV, as illustrated in Figure 8.1.

The exact quantum mechanical calculation is very similar in spirit to the crude estimate above. We can think of the Coulomb barrier as made up of a sequence of infinitesimal rectangular barriers of height $V(r) = zZ'e^2/4\pi\epsilon_0 r$ and width dr . The probability to penetrate each infinitesimal barrier, which extends from r to $r + dr$, is

$$dP = \exp \left\{ -2 dr \sqrt{(2m/\hbar^2)[V(r) - Q]} \right\} \quad (8.14)$$

The probability to penetrate the complete barrier is

$$P = e^{-2G} \quad (8.15)$$

where the *Gamow factor* G is

$$G = \sqrt{\frac{2m}{\hbar^2 Q}} \int_a^b [V(r) - Q]^{1/2} dr \quad (8.16)$$

which can be evaluated as

$$G = \sqrt{\frac{2m}{\hbar^2 Q}} \frac{zZ'e^2}{4\pi\epsilon_0} \left[\arccos \sqrt{x} - \sqrt{x(1-x)} \right] \quad (8.17)$$

where $x = a/b = Q/B$. The quantity in brackets in Equation 8.17 is approximately $\pi/2 - 2x^{1/2}$ when $x \ll 1$, as is the case for most decays of interest. Thus the result of the quantum mechanical calculation for the half-life of α decay is

$$t_{1/2} = 0.693 \frac{a}{c} \sqrt{\frac{mc^2}{2(V_0 + Q)}} \exp \left\{ 2 \sqrt{\frac{2mc^2}{(\hbar c)^2 Q}} \frac{zZ'e^2}{4\pi\epsilon_0} \left(\frac{\pi}{2} - 2\sqrt{\frac{Q}{B}} \right) \right\} \quad (8.18)$$

Table 8.2 Calculated α -Decay Half-lives for Th Isotopes

A	Q (MeV)	$t_{1/2}$ (s)	
		Measured	Calculated
220	8.95	10^{-5}	3.3×10^{-7}
222	8.13	2.8×10^{-3}	6.3×10^{-5}
224	7.31	1.04	3.3×10^{-2}
226	6.45	1854	6.0×10^1
228	5.52	6.0×10^7	2.4×10^6
230	4.77	2.5×10^{12}	1.0×10^{11}
232	4.08	4.4×10^{17}	2.6×10^{16}

The results of this calculation for the even isotopes of Th are shown in Table 8.2. The agreement is not exact, but the calculation is able to reproduce the trend of the half-lives within 1–2 orders of magnitude over a range of more than 20 orders of magnitude. We have neglected several important details in the calculation: we did not consider the initial and final nuclear wave functions (Fermi's Golden Rule, Equation 2.79, must be used to evaluate the decay probability), we did not consider the angular momentum carried by the α particle, and we assumed the nucleus to be spherical with a mean radius of $1.25A^{1/3}$ fm. The latter approximation has a very substantial influence on the calculated half-lives. The nuclei with $A \geq 230$ have strongly deformed shapes, and the calculated half-lives are extremely sensitive to small changes in the assumed mean radius. For instance, changing the mean radius to $1.20A^{1/3}$ (a 4% change in a) changes the half-lives by a factor of 5! In fact, because of this extreme sensitivity, the procedure is often reversed—the measured half-lives are used to deduce the nuclear radius; what actually comes out of the calculation is more like the sum of the radii of the nucleus X' and the α particle, if we assume their charge distributions to have a sharp edge. This result can then be used to obtain an estimate of the nuclear radius; see, for example, L. Marquez, *J. Phys. Lett.* **42**, 181 (1981).

Even though this oversimplified theory is not strictly correct, it gives us a good estimate of the decay half-lives. It also enables us to understand why other decays into light particles are not commonly seen, even though they may be allowed by the Q value. For example, the decay $^{220}\text{Th} \rightarrow ^{12}\text{C} + ^{208}\text{Po}$ would have a Q value of 32.1 MeV, and carrying through the calculation using Equation 8.18 gives $t_{1/2} = 2.3 \times 10^6$ s for the ^{220}Th decay into ^{12}C . This is a factor of 10^{13} longer than the α -decay half-life and thus the decay will not easily be observable.

Recently, just such a decay mode has in fact been observed, the first example of a spontaneous decay process involving emission of a particle heavier than an α . The decay of ^{223}Ra normally proceeds by α emission with a half-life of 11.2 d, but there has now been discovered the decay process $^{223}\text{Ra} \rightarrow ^{14}\text{C} + ^{209}\text{Pb}$. The probability for this process is very small, about 10^{-9} relative to the α decay. To confirm that the emitted particle is ^{14}C requires the $\Delta E \cdot T$ technique discussed in Chapter 7. Figure 8.4 shows a portion of the high-energy end of the tail of the hyperbola expected for observation of carbon. From the mass tables,

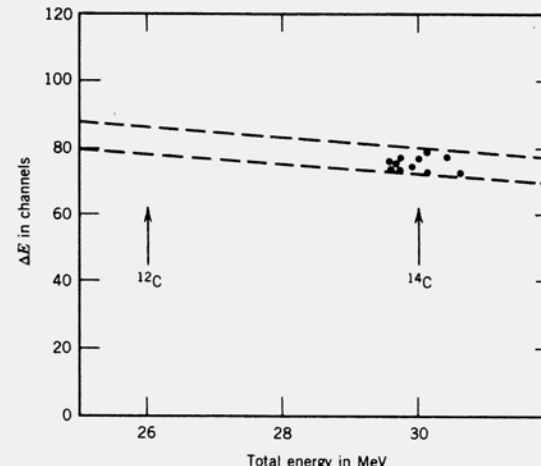


Figure 8.4 A portion of the tail of the $\Delta E \cdot T$ hyperbola showing the observed ^{14}C events from the decay of ^{223}Ra . The dashed lines show the limits expected for carbon. The 11 ^{14}C events result from 6 months of counting. From H. J. Rose and G. A. Jones, *Nature* **307**, 245 (1984). Reprinted by permission, copyright © Macmillan Journals Limited.

the decay Q value is calculated to be 31.8 MeV, which (when corrected for the recoil) gives a ^{14}C kinetic energy of 29.8 MeV. By contrast, the calculated energy for ^{12}C emission would be about 26 MeV. The total of 11 events observed represents about six months of counting with a source of 3.3 μCi of ^{223}Ra in secular equilibrium with 21-y ^{227}Ac , a member of the naturally occurring actinium series beginning with ^{235}U .

Calculating the Gamow factor for ^{14}C emission gives a decay probability of about 10^{-3} relative to α emission; the discrepancy between the calculated and observed (10^{-9}) values results from the assumptions about the preformation of the particle inside the nucleus. You will recall that our theory of α decay is based on the assumption that the α is preformed inside the nucleus. What the experiment tells us is that the probability for forming ^{14}C clusters inside the nucleus is about 10^{-6} relative to the probability to preform α 's.

For a description of the experiment, see H. J. Rose and G. A. Jones, *Nature* **307**, 245 (1984). Emission of ^{14}C from several other nuclei in this region has also been observed, and emission of heavier decay fragments, including ^{24}Ne , has been reported.

Going in the opposite direction, we can use Equation 8.18 with $z = 1$ to evaluate the half-life for proton decay—that is, the spontaneous emission of a proton by an unstable nucleus. In this case the Coulomb barrier will be only half as high as it is for α decay, but these decays are inhibited for a stronger reason: the Q values for proton decay are generally negative and so the decays are absolutely forbidden by energy conservation. Such decays have recently been observed for a few proton-rich unstable nuclei, which are formed in nuclear reactions by bombarding a target with $N \approx Z$ using a projectile having $N \approx Z$.

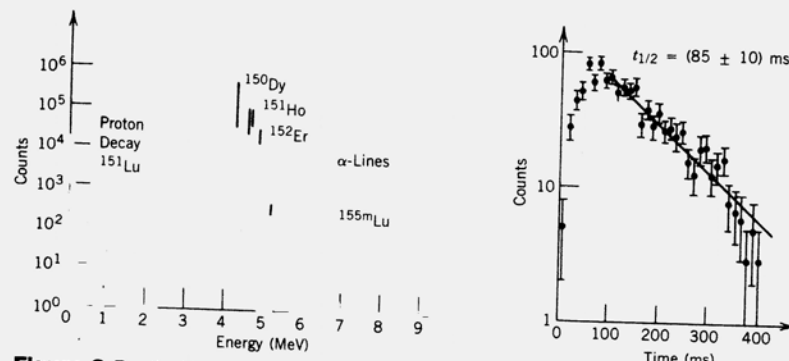


Figure 8.5 (Left) Charged-particle spectrum emitted in the radioactive decays of products of the reaction $^{96}\text{Ru} + ^{58}\text{Ni}$. The peaks above 4 MeV represent α decays; the 1.2-MeV peak is from proton emission. (Right) The decay with time of the proton peak gives a half-life of 85 ms. From S. Hofmann et al., *Z. Phys. A* **305**, 111 (1982).

This creates a heavy nucleus with $N \approx Z$, a very unstable configuration, and proton emission may be energetically possible, as the nucleus tries to relieve itself of its proton excess. The Q value for proton decay can be found by a slight modification of Equation 8.3, which gives exactly the negative of the proton separation energy, Equation 3.27. Proton decay will be energetically possible when the Q value is positive and therefore when the separation energy is negative. A glance at the mass tabulations (see A. H. Wapstra and G. Audi, *Nucl. Phys. A* **432**, 1 (1985)) shows only a few very rare cases in which the proton separation energy is negative, and even these are not directly measured but instead obtained by extrapolations from more stable nuclei.

In an experiment reported by Hofmann *et al.*, *Z. Phys. A* **305**, 111 (1982), a target of ^{96}Ru was bombarded with ^{58}Ni projectiles. Figure 8.5 shows the spectrum of light particles emitted following the reaction. The more energetic peaks are identified as α decays from unstable nuclei in the neighborhood of $A = 150$ produced in the reaction. The peak at 1.239 MeV was identified as a proton using $\Delta E \cdot T$ techniques as described in Chapter 7. Its half-life was measured as 85 ms, as shown in Figure 8.5. The decay was assigned to the isotope ^{151}Lu based on a series of indirect arguments; unfortunately, reactions such as this produce many different products, and it is often a difficult task to identify the source of the observed radiations. This experiment thus provides evidence for the decay $^{151}\text{Lu} \rightarrow ^{150}\text{Yb} + p$.

Study of decays such as this enables us to extend our knowledge of nuclear mass systematics far beyond the previous limits; for instance, at the time of this work ^{151}Lu was three protons further from stability than the previous last known isobar (^{151}Er). Figure 8.6 shows the Q_p values deduced from known masses and theoretical calculation based on systematics. The value for ^{151}Lu lies right on the theoretical calculation, giving confidence to both the identification of the isotope and to the theoretical calculation.

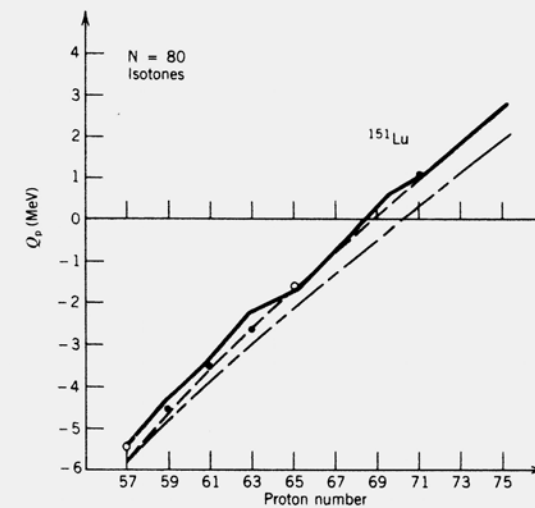


Figure 8.6 Proton-decay energies of $N = 80$ isotones. The solid lines are theoretical calculations based on nuclear mass formulas (somewhat like the semiempirical mass formula). Only for ^{151}Lu is the decay energy positive. From S. Hofmann et al., *Z. Phys. A* **305**, 111 (1982).

Using Equation 8.18 for the half-life gives a value of about $1.7\ \mu\text{s}$, too small by nearly 5 orders of magnitude. For this reason, it has been proposed that the decay is inhibited by differences in the nuclear structure of the initial and final states (or possibly by a large angular momentum change in the decay, examples of which are discussed in the next section).

8.5 AN ULA MO TU A D PARITY IN α DECAY

We have up to this point neglected to discuss the angular momentum carried by the α particle. In a transition from an initial nuclear state of angular momentum I_i to a final state I_f , the angular momentum of the α particle can range between $|I_i + I_f|$ and $|I_i - I_f|$. The nucleus ^4He consists of two protons and two neutrons, all in $1s$ states and all with their spins coupled pairwise to 0. The spin of the α particle is therefore zero, and the total angular momentum carried by an α particle in a decay process is purely orbital in character. We will designate this by ℓ_α . The α particle wave function is then represented by a $Y_{\ell m}$ with $\ell = \ell_\alpha$; thus the parity change associated with α emission is $(-1)^{\ell_\alpha}$, and we have a parity selection rule, indicating which transitions are permitted and which are absolutely forbidden by conservation of parity: if the initial and final parities are the same, then ℓ_α must be even; if the parities are different, then ℓ_α must be odd.

To study the applications of these rules, we must recognize that we have also neglected one very significant feature of α decay—a given initial state can populate many different final states in the daughter nucleus. This property is

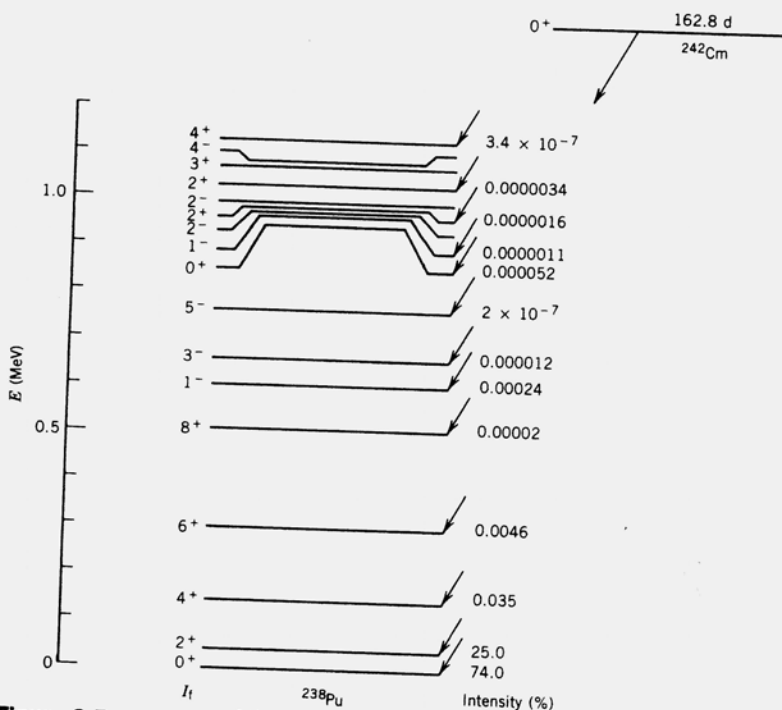


Figure 8.7 α decay of ^{242}Cm to different excited states of ^{238}Pu . The intensity of each α -decay branch is given to the right of the level.

sometimes known as the “fine structure” of α decay, but of course has nothing whatever to do with atomic fine structure. Figure 8.7 shows the α decay of ^{242}Cm . The initial state is spin zero, and thus the angular momentum of the α particle ℓ_α is equal to the angular momentum of the final nuclear state I_f . You can see that many different states of ^{238}Pu are populated. The α decays have different Q values (given by the Q value for decay to the ground state, 6.216 MeV, less the excitation energy of the excited state) and different intensities. The intensity depends on the wave functions of the initial and final states, and also depends on the angular momentum ℓ_α . In Equation 2.60, it was shown how the “centrifugal potential” $\ell(\ell+1)\hbar^2/2mr^2$ must be included in spherical coordinates. This term, which is always positive, has the effect of raising the potential energy for $a < r < b$ and thus increasing the thickness of the barrier which must be penetrated. Consider for example the 0^+ , 2^+ , 4^+ , 6^+ , and 8^+ states of the ground-state rotational band. The decay to the 2^+ state has less intensity than the decay to the ground state for two reasons—the “centrifugal potential” raises the barrier by about 0.5 MeV, and the excitation energy lowers Q by 0.044 MeV. The decay intensity continues to decrease for these same reasons as we go up the band to the 8^+ state. If we use our previous theory for the decay rates, taking

into account the increasing effective B and decreasing Q , we obtain the following estimates for the relative decay branches: 0^+ , 76%; 2^+ , 23%; 4^+ , 1.5%; 6^+ , 0.077%; 8^+ , $8.4 \times 10^{-5}\%$. These results are not in exact agreement with the observed decay intensities, but they do give us a rough idea of the origin of the decrease in intensity.

Once we go above the ground-state band, the α decay intensities become very small, of the order of $10^{-6}\%$ of the total decay intensity. This situation results from the poor match of initial and final wave functions—many of these excited states originate with vibrations or pair-breaking particle excitations, which are not at all similar to the paired, vibrationless 0^+ ground state of ^{242}Cm . You should note that there are some states for which there is no observed decay intensity at all. These include the 2^- states at 0.968 and 0.986 MeV, the 3^+ state at 1.070 MeV, and the 4^- state at 1.083 MeV. Alpha decay to these states is absolutely forbidden by the parity selection rule. For example, a $0 \rightarrow 3$ decay must have $\ell_\alpha = 3$, which must give a change in parity between initial and final states. Thus $0^+ \rightarrow 3^-$ is possible, but not $0^+ \rightarrow 3^+$. Similarly, $0 \rightarrow 2$ and $0 \rightarrow 4$

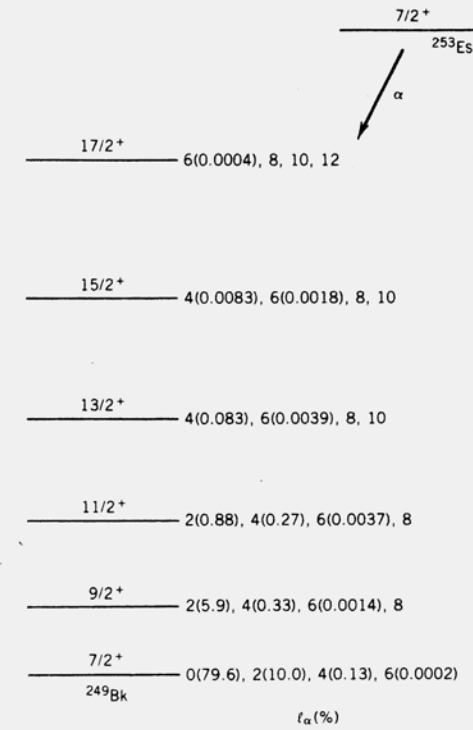


Figure 8.8 Intensities of various α -decay angular momentum components in the decay of ^{253}Es . For $\ell_\alpha = 8$ and higher, the intensities are not known but are presumably negligibly small. From the results of a study of spin-aligned α decays by A. J. Soinski et al., *Phys. Rev. C* **2**, 2379 (1970).

decays cannot change the parity, and so $0^+ \rightarrow 2^-$ and $0^+ \rightarrow 4^-$ are not permitted.

When neither the initial nor the final states have spin 0, the situation is not so simple and there are no absolutely forbidden decays. For example, the decay $2^- \rightarrow 2^+$ must have odd ℓ_α (because of the change in parity), and the angular momentum coupling rules require $0 \leq \ell_\alpha \leq 4$. Thus it is possible to have this decay with $\ell_\alpha = 1$ or 3. The next question that occurs is whether $\ell_\alpha = 1$ or $\ell_\alpha = 3$ is favored and by how much. Our previous discussion would lead us to guess that the $\ell_\alpha = 1$ intensity is roughly an order of magnitude greater than the $\ell_\alpha = 3$ intensity. However, measuring only the energy or the intensity of the decay gives us no information about how the total decay intensity is divided among the possible values of ℓ_α . To make the determination of the relative contributions of the different ℓ values, it is necessary to measure the angular distribution of the α particles. The emission of an $\ell = 1$ α particle is governed by a $Y_1(\theta, \phi)$, while an $\ell = 3$ α decay is emitted with a distribution according to $Y_3(\theta, \phi)$. If we determine the spatial distribution of these decays, we could in principle determine the relative amounts of the different ℓ values.

To do this experiment we must first align the spins of our α -radioactive nuclei, such as by aligning their magnetic dipole or electric quadrupole moments in a magnetic field or in a crystalline electric field gradient. Keeping the spins aligned requires that the nuclei must be cooled to a temperature at which the thermal motion is not sufficient to destroy the alignment; generally temperatures below 0.01 K are required (that is, less than 0.01 degree above the absolute zero of temperature!).

As an example of such an experiment, we consider the decay of ^{253}Es to states of the ground-state rotational band of ^{246}Bk . The possible ℓ values are indicated in Figure 8.8, and the results of measuring the α -particle angular distributions help us to determine the relative contribution of the different values of ℓ_α .

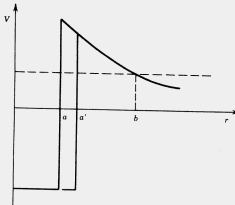


Figure 8.9 In a deformed nucleus, α particles escaping from the poles enter the Coulomb barrier at the larger separation a' , and must therefore penetrate a lower, thinner barrier. It is therefore more probable to observe emission from the poles than from the equator.

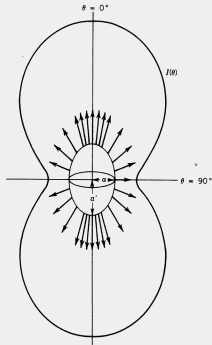


Figure 8.10 Intensity distribution of α particles emitted from the deformed nucleus at the center of the figure. The polar plot of intensity shows a pronounced angular distribution effect.

Since many α -emitting nuclei are deformed, these angular distribution measurements can also help us to answer another question: if we assume a stable prolate (elongated) nucleus, will more α 's be emitted from the poles or from the equator? Figure 8.9 suggests a possible answer to this question: at the larger radius of the poles, the α particle feels a weaker Coulomb potential and must therefore penetrate a thinner and lower barrier. We therefore expect that polar emission ought to be more likely than equatorial emission. Figure 8.10 shows the angular distribution of α emission relative to the symmetry axis. You can see that emission from the poles is 3–4 times more probable than emission from the equator, exactly as we expect on the basis of the potential.

8.6 α DECAY SPECTROSCOPY

The final topic in our discussion of α decay is this: What can we learn about the energy levels of nuclei by studying α decay?

Let's consider, for example, the 5.3-h decay of ^{251}Fm to levels of ^{247}Cf . (The levels of ^{247}Cf are also populated in the beta decay of ^{243}Es , but the half-life of that decay is so short, 4.7 min, that it is more difficult to use as a detailed probe of the level structure of ^{247}Cf .)

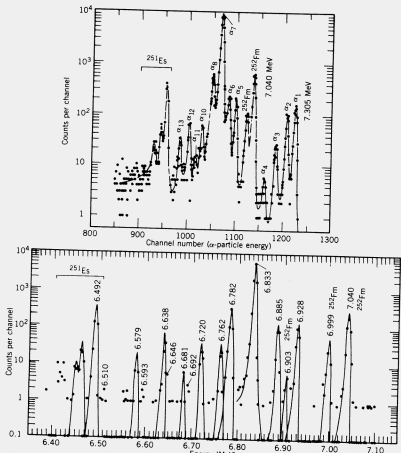


Figure 8.11 α spectrum from the decay of ^{251}Fm . The top portion shows the spectrum as observed with a Si detector. The bottom portion shows a portion of the same spectrum observed with a magnetic spectrometer, whose superior energy resolution enables observation of the 6.762-MeV decay, which would be missed in the upper spectrum. From Ahmad et al., *Phys. Rev. C* 8, 737 (1973).

Figure 8.11 shows the energy spectrum of α decays from the decay of ^{251}Fm . As you can see, there are 13 distinct groups of α particles; each group presumably represents the decay to a different excited state of ^{247}Cf . How can we use this information to construct the level scheme of ^{247}Cf ? Based on the α spectrum, we first must find the energy and intensity of each α group. The energy is found by comparing with decays of known energy (the impurity decays from the ^{252}Fm contaminant are helpful for this) and the intensity is found from the area of each peak. The result of this analysis is shown in Table 8.3, along with the uncertainties that come mostly from the counting statistics for each peak. (Notice that the

Table 8.3 α Decays from ^{251}Fm

α Group	α Energy (keV)	Decay Energy (keV)	Excited-State Energy (keV)	α Intensity (%)
α_1	7305 ± 3	7423	0	1.5 ± 0.1
α_2	7251 ± 3	7368	55	0.93 ± 0.08
α_3	7184 ± 3	7300	123	0.29 ± 0.03
α_4	7106 ± 5	7221	202	~ 0.05
α_5	6928 ± 2	7040	383	1.8 ± 0.1
α_6	6885 ± 2	6996	427	1.7 ± 0.1
α_7	6833 ± 2	6944	479	87.0 ± 0.9
α_8	6782 ± 2	6892	531	4.8 ± 0.2
α_9	6762 ± 3	6872	552	0.38 ± 0.06
α_{10}	6720 ± 3	6829	594	0.44 ± 0.04
α_{11}	6681 ± 4	6789	634	0.07 ± 0.03
α_{12}	6638 ± 3	6745	678	0.56 ± 0.06
α_{13}	6579 ± 3	6686	738	0.26 ± 0.04

strongest peaks have the smallest *relative* uncertainties.) To find the decay energies (that is, the relative energies of the nuclear states), we must use Equation 8.7, since the measured α energies are only the kinetic energies. These are also shown in Table 8.3.

The different ^{247}Cf excited states will quickly decay to the ground state by emitting γ -ray photons, so in constructing the decay scheme it is helpful to have the energies and intensities of the γ rays as well. Figure 8.12 shows the observed γ rays and Table 8.4 shows the deduced energies and intensities.

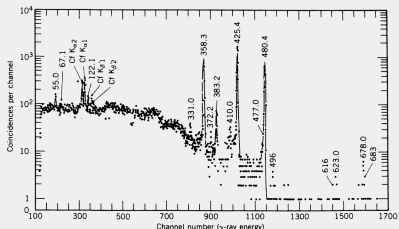


Table 8.4 γ Rays in ^{247}Cf following α decay of ^{251}Fm

Energy (keV)	Intensity (% of decays)	Energy (keV)	Intensity (% of decays)
55.0 ± 0.2	0.58 ± 0.08	425.4 ± 0.1	51 ± 4
67.1 ± 0.2	0.28 ± 0.05	477.0 ± 0.3	0.54 ± 0.08
122.1 ± 0.2	0.28 ± 0.05	480.4 ± 0.1	21 ± 2
331.0 ± 0.3	0.35 ± 0.07	496 ± 1	~ 0.08
358.3 ± 0.1	17 ± 1.5	616 ± 1	~ 0.05
372.2 ± 0.4	0.25 ± 0.05	623.0 ± 0.8	0.07 ± 0.02
382.2 ± 0.3	1.2 ± 0.13	678.0 ± 0.8	0.26 ± 0.06
410.0 ± 0.3	0.50 ± 0.07	683 ± 1	~ 0.04

Now the detective work comes. Let's assume (and here we must be very careful, as we see in the next example) that the highest energy α decay populates the ground state of ^{247}Cf . (In an even-even nucleus, this would be a very good assumption, because $0^+ \rightarrow 0^+$ α decays are very strong and not inhibited by any differences between the wave functions of the initial and final nuclear states. In an odd- A nucleus, the initial and final ground states may have very different characters so that the decay to the ground state may be very weak or even vanishing.) The decay just lower in energy differs from the ground-state decay by about 55 keV. Assuming this to populate the first excited state, we are pleased to find among the γ transitions one of energy 55 keV, which presumably represents the transition between the first excited state and the ground state. The next α decay populates a state at 123 ± 3 keV above the ground state, and we find among the γ rays one of energy 122.1 keV, which corresponds to a transition from the second excited state to the ground state. We also find a transition of energy 67.1 (= 122.1 - 55.0) keV, which results from transitions between the second and first excited states.

Let's guess that these three states (with assumed energies 0, 55.0 keV, 122.1 keV) form a rotational band whose states, we recall from the discussion of odd- A deformed nuclei in Section 5.3, have angular momenta $I = \Omega, \Omega + 1, \Omega + 2, \dots$, where Ω is the component of the angular momentum of the odd particle along the symmetry axis. The energy difference between the first excited state and ground state should then be

$$\Delta E_{21} = E_2 - E_1 = \frac{\hbar^2}{2J} [(\Omega + 1)(\Omega + 2) - \Omega(\Omega + 1)]$$

$$= \frac{\hbar^2}{2J} 2(\Omega + 1) \quad (8.19)$$

where we have used $E = (\hbar^2/2J)I(I + 1)$ for the energy of rotational states. Similarly, the difference between the ground state and second excited state is

$$\Delta E_{31} = E_3 - E_1 = \frac{\hbar^2}{2J} [(\Omega + 2)(\Omega + 3) - \Omega(\Omega + 1)]$$

$$= \frac{\hbar^2}{2J} 2(2\Omega + 3) \quad (8.20)$$

Combining these results with the experimental values, $\Delta E_{21} = 55.0$ keV and $\Delta E_{31} = 122.1$ keV, we conclude $\Omega = 3.5 \pm 0.2$ (I is $\frac{1}{2}$), $\Omega = \frac{5}{2}$) and $\hbar^2/2J = 6.11 \pm 0.1$ keV. These three states seem to form a rotational band with $I = \frac{1}{2}, \frac{3}{2}, \frac{5}{2}$. With our deduced values we can predict the energy of the $\frac{11}{2}$ state:

$$\Delta E_{41} = \frac{\hbar^2}{2J} \left[\frac{13}{2} \cdot \frac{15}{2} - \frac{7}{2} \cdot \frac{9}{2} \right] = 201.6 \text{ keV}$$

and the $\frac{13}{2}$ state

$$\Delta E_{51} = \frac{\hbar^2}{2J} \left[\frac{15}{2} \cdot \frac{17}{2} - \frac{7}{2} \cdot \frac{9}{2} \right] = 293.3 \text{ keV}$$

Apparently, the $\frac{11}{2}$ state is populated by the very weak α decay, but its γ decays may be too weak to be seen in the spectrum of Figure 8.12. The decay to the $\frac{13}{2}$ state is not observed.

The interpretation of the remaining states is aided by α - γ coincidence studies, in which we electronically select only those γ transitions that follow a given α decay within a certain short time interval (in this case 110 ns). Since this time is long compared to typical lifetimes of nuclear states, all γ rays that follow the α decay will be recorded, even those that follow indirectly (such as the case in which two γ 's are emitted in cascade, one following the other). The following coincidence relationships were observed:

Coincidence Gate γ Rays (keV)

α_5	383.2
α_6	372.2, 383.2
α_7	55.0, 67.1, 122.1, 358.3, 425.4, 480.4
α_8	331.0, 358.3, 410.0, 425.4, 477.0, 480.4
α_{12}	623.0, 678.0

The decay α_5 goes to a state at 383.2 keV, which then goes directly to the ground state by emitting a single γ ray. The decay α_6 populates a state at about 427 keV. There is no coincident γ ray of that energy, which indicates no direct transition to the ground state, but there is a transition of energy 372.2 keV which, when added to 55.0 keV, gives 427.2 keV, very close to the energy of the state. We therefore conclude that this state at 427.2 keV decays to the first excited state at 55.0 keV. There is also a coincident transition at 383.2 keV, and thus this state at 427.2 keV must decay to the previously established state at 383.2 keV, by emitting a γ ray of energy 427.2 - 383.2 = 44.0 keV; this γ ray is not observed. The decay α_7 to the state at 4^+ shows decays to the ground state and to the 55.0 and 122.1 keV states (425.4 + 55.0 = 480.4; 358.3 + 122.1 = 480.4). Similarly, the decay α_8 to a state of 532.0 keV shows direct transitions to the lower states (331.0 + 201.0 = 532.0; 410.0 + 122.1 = 532.1; 477.0 + 55.0 = 532.0) but not directly to the ground state. It also shows coincident transitions that originate from the 480.4-keV level, so there must be a transition of energy 51.6 keV (= 532.0 - 480.4). In a similar fashion we analyze the other α and γ decays, and Figure 8.13 shows the resulting decay scheme.

For the states above the $n = 4$ band, the assignments of spins and magnetic moments in $\Omega = \frac{1}{2}$ are as it was for the states of the

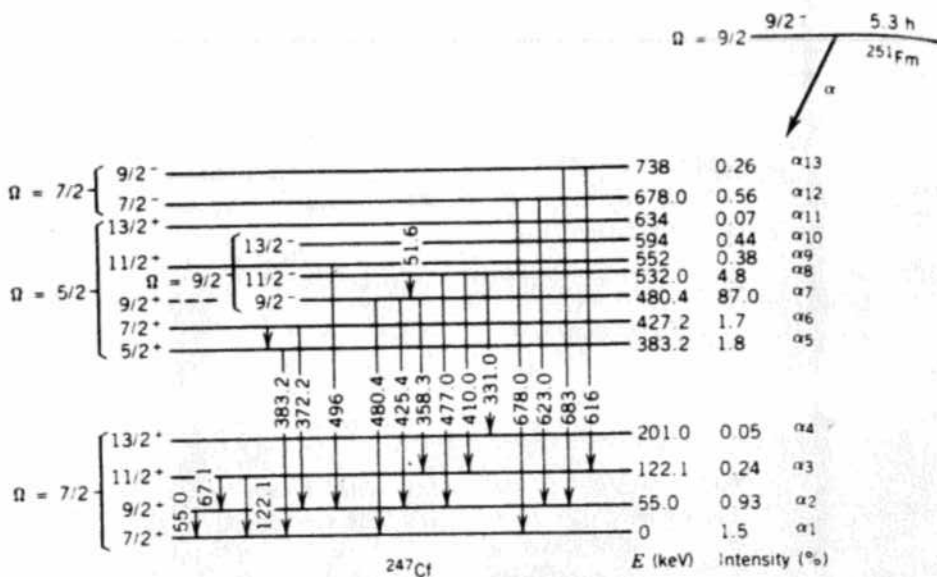


Figure 8.13 The decay scheme of ^{251}Fm to levels of ^{247}Cf deduced from α and γ spectroscopy. The spin assignments for the higher levels are deduced using γ -ray and internal conversion techniques described in Chapter 10.

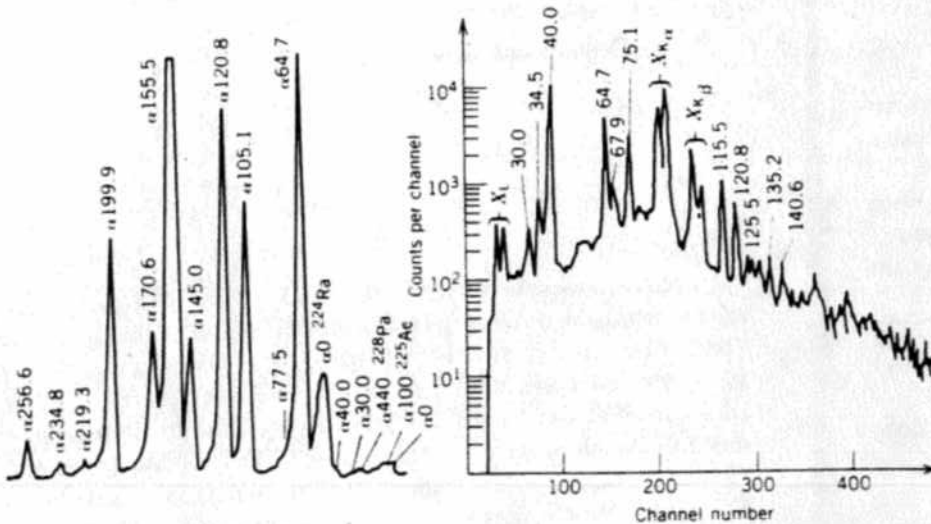


Figure 8.14 α (left) and γ (right) spectra from the decay of ^{229}Pa to ^{225}Ac . The α peaks are labeled according to the excited state populated in ^{225}Ac ; thus $\alpha 105.1$ indicates the decay leading to the excited state at 105.1 keV. Prominent peaks from impurities are also indicated. The γ spectrum is taken in coincidence with all α 's. From P. Aguer et al., *Nucl. Phys. A* **202**, 37 (1973).

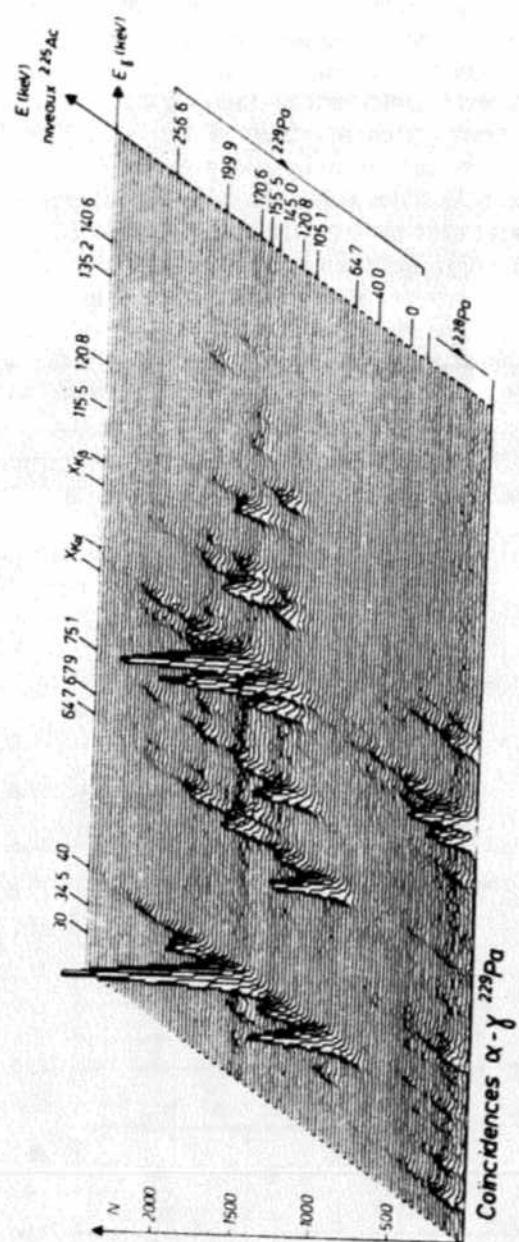


Figure 8.15 Three-dimensional (sometimes called two-parameter) representation of α - γ coincidences in the decay of ^{229}Pa . The horizontal axis shows γ -ray energies, labeled along the top. The oblique axis gives α -decay energies, labeled to indicate the ^{225}Ac state populated in the decay. The vertical axis gives the intensity of the coincidence relationship.

9/2⁻ 5.3 h
 ^{251}Fm

α_{13}
 α_{12}
 α_{11}
 α_{10}
 α_9
 α_8
 α_7
 α_6
 α_5

α_4
 α_3
 α_2
 α_1

Intensity (%)

deduced from α and γ
 deduced using γ -ray

135.8
 135.2
 140.6

3 400

^{229}Pa to ^{225}Ac . The α to ^{225}Ac ; thus $\alpha 105.1$ incident peaks from coincidence with all α 's

ground-state rotational band. To make these assignments, we need additional information from the γ decays; these measurements are discussed in Chapter 10.

Notice the strong α branch to the state at ~ 0.4 keV. This occurs because the wave functions of the initial and final states are identical—both come from the same $\Omega = \frac{3}{2}$ deformed single-particle state—and the result is that more than 93% of the decay intensity goes to states of that so-called “favored” band. The observed decay rates can be compared with values calculated for various deformed single-particle states using the Nilsson wave functions, and in general there is good agreement between the measured and calculated results, both for the favored and unfavored decays. It is such comparisons between theory and experiment that allow us to assign the single-particle states because the intrinsic Ω and Nilsson assignments are not directly measurable.

The data for this discussion were taken from I. Ahmad, J. Milsted, R. K. Sjöblom, J. Lerner, and P. R. Fields, *Phys. Rev. C* **8**, 737 (1973). Theoretical calculations of α transition amplitudes for states in even- A and odd- A deformed nuclei of the actinide region can be found in J. K. Poggenburg, H. J. Mang, and J. O. Rasmussen, *Phys. Rev.* **181**, 1697 (1969).

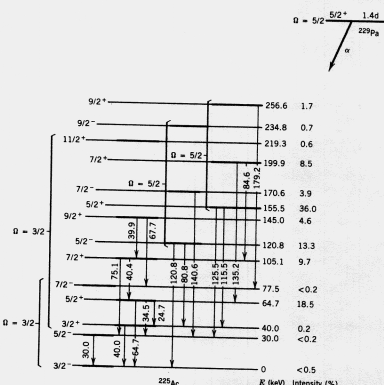


Fig. 8.16 Decay scheme of ^{229}Pa deduced from α and γ spectroscopy.

Another example of the study of nuclear spectra by through α decay is illustrated in Figures 8.14–8.16. Figure 8.14 shows the α and γ spectra from the decay $^{229}\text{Pa} \rightarrow ^{225}\text{Ac}$. You can see that the decay to the ground state (labeled a_0) can be very strong, the α - γ coincidence plot to elucidate the decay scheme, and a partially incomplete way to illustrate the coincidences is shown in Figure 8.15. A peak in this three-dimensional spectrum is a finite coincidence region between the α and the γ that label the axes. The information derived from the coincidence studies is used to make the decay scheme shown in Figure 8.16. Four rotational bands are identified in ^{225}Ac , positive and negative parity bands with $\Omega = \frac{1}{2}$ and $\frac{3}{2}$. The decaying ^{229}Pa is in the $\frac{3}{2}^+$ state, so in the favored decay to the $\frac{1}{2}^+$ band in the daughter has about 85% of the decay intensity. The decay to the $\frac{1}{2}^+$ ground-state rotational band is so strong by the nuclear wave function, resulting in the very weak (and possibly nonexistent) decay to the ground state. In this case it would lead to errors if we had assumed that the total energy observed a group ($a_{64.7}$, or $a_{44.0}$) if we looked carefully could lead to transitions to the ground state. The data for the ^{229}Pa decay come from P. Aguer, A. Peghaire, and C. F. Liang, *Nucl. Phys. A* **202**, 37 (1973).

A L L

Some what more extensive discussions of α decay can be found in Chapter 16 of R. D. Evans, *The Atomic Nucleus* (New York: McGraw-Hill, 1955), and in Chapter 13 of I. Kaplan, *Nuclear Physics* (Reading, MA: Addison-Wesley, 1955). For surveys of α -decay theory, see H. J. Mang, *Ann. Rev. Nucl. Sci.* **14**, 1 (1964), and J. O. Rasmussen, “Alpha Decay,” in *Alpha-, Beta- and Gamma-Ray Spectroscopy*, edited by K. Siegbahn (Amsterdam: North-Holland, 1965), Chapter XI. A discussion of the use of α decay for nuclear spectroscopy is that of F. S. Stephens, in *Nuclear Spectroscopy*, part A, edited by F. Ajzenberg-Selove (New York: Academic, 1959), Section I.E.2.

- Find the Q values of the following decays:
 - $^{247}\text{Bk} \rightarrow ^{243}\text{Am} + \alpha$; (b) $^{251}\text{Cf} \rightarrow ^{247}\text{Cm} + \alpha$; (c) $^{230}\text{Th} \rightarrow ^{226}\text{Ra} + \alpha$.
- For each decay given in Problem 1, calculate the kinetic energy and velocity of the emitted nucleus of the decay.
- From the known atomic masses, compute the Q values of the decays:
 - $^{242}\text{Pu} \rightarrow ^{238}\text{U} + \alpha$
 - $^{208}\text{Po} \rightarrow ^{204}\text{Pb} + \alpha$
 - $^{208}\text{Po} \rightarrow ^{196}\text{Pt} + ^{12}\text{C}$
 - $^{210}\text{Bi} \rightarrow ^{208}\text{Pb} + ^3\text{H}$
- In the decay of $^{242}\text{Cm} \rightarrow ^{238}\text{Pu}$, the maximum α energy is 6112.9 ± 0.1 keV. Given the mass of ^{238}Pu , find the mass of ^{242}Cm .
- The total α particle emission in the decay of ^{238}U to ^{234}Th is 1 ± 4 keV. From information known of ^{238}U , the mass of ^{234}Th .

Alpha Spectroscopy

Appendix D

Semiconductor Detectors

Source: "ORTEC® Introduction to Charged-Particle Detectors"

Introduction to Charged-Particle Detectors

Silicon Charged-Particle Detector Manufacturing

Table 1 summarizes the major physical properties of silicon. To produce silicon charged-particle detectors, ORTEC employs both ion-implantation and surface-barrier technologies. The two processes are complementary in that each technique is best for manufacturing certain types of detectors. Fig. 1 (A and B) shows simplified representations of the two manufacturing processes.

There are several advantages to using ion implantation:

- (a) A thinner and more rugged front contact; better energy resolution for some alpha spectroscopy applications
- (b) Lower electronic noise
- (c) Higher geometric efficiency for some alpha spectroscopy applications
- (d) Operation to 60°C and bakeout at 200°C.

The advantage of surface barrier technology is that it allows production of transmission detectors as thin as 10 µm or as thick as several mm (see Selection Chart).

ORTEC also manufactures deep, lithium-drifted silicon [Si(Li)] detectors for special applications.

Depletion Depth and Capacitance

Silicon detectors are reverse-biased diodes with parallel, planar electrodes and therefore have the capacitance of the corresponding parallel-plate capacitor. The electric field in the detector, however, is not constant but decreases linearly from the contact at which the p-n junction is made to the end of the depletion region (Fig. 2).

The nomograph in Fig. 3 shows the depth **W** of the depletion region as a function of the bias voltage applied to the detector and the resistivity of the silicon material. For a given value of bias, the depletion depth increases with increasing resistivity, and correspondingly, the slope of the electric field in Fig. 2 decreases with increasing material resistivity, that is, as the silicon material behaves more and more like an insulator. If, as shown in Fig. 2, **L** is the overall thickness of the silicon slice, the detector is totally depleted when **W** = **L**.

Table 1	
Atomic density, atoms/cm ³	4.96 X 10 ²²
Mass density, g/cm ³	2.33
Dielectric coefficient	12
Energy gap, eV	1.115
Average energy per electron-hole pair, eV/pair	3.62 at 300 K 3.76 at 80 K
Mobility, cm ² · V ⁻¹ · s ⁻¹	
Electron	1350 (2.1 X 10 ⁹ T ^{-2.5})
Hole	480 (2.3 X 10 ⁹ T ^{-2.7})

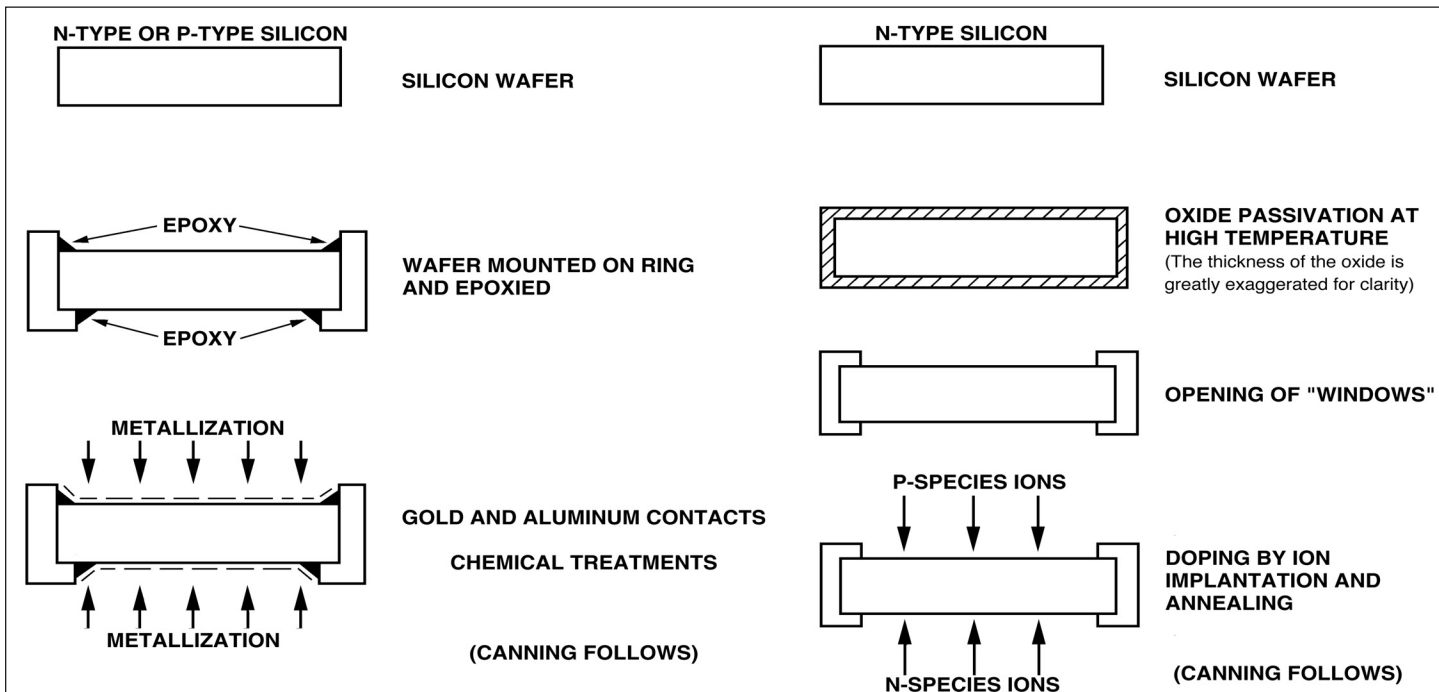


Fig. 1(A). Simplified Diagram of Surface Barrier Si Detector Manufacturing.

Fig. 1(B). Simplified Diagram of Ion-Implanted Si Detector Manufacturing.

Introduction to Charged-Particle Detectors

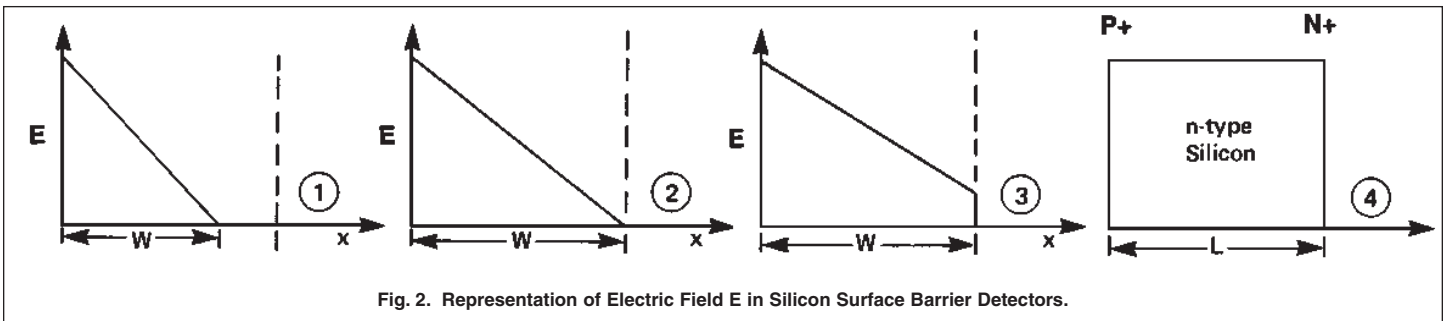


Fig. 2. Representation of Electric Field E in Silicon Surface Barrier Detectors.

The nomograph of Fig. 3 also shows the "specific capacitance" (capacitance per unit area) of silicon detectors for any given value of W . A detector's capacitance can be read directly from this nomograph once the active area has been determined.

The value of the capacitance is of interest because the effective electronic noise of preamplifiers used with silicon detectors increases with increasing capacitance values (Fig. 4). The electronic noise increase per unit capacitance increase is called the preamplifier's "slope."

Leakage Current

A silicon detector, just like any reverse-biased silicon diode, has a temperature dependent leakage current. At room temperature, ion-implanted detectors, such as the ULTRA Series, have a leakage current in the range of $\{D/100\} \times \{\sim 1-10 \text{ nA/cm}^2 \text{ active area}\}$, where D is the depletion thickness in microns; surface barrier detectors, on the other hand, have leakage current an order of magnitude higher, in the range of $\{D/100\} \times \{\sim 20 \text{ to } 100 \text{ nA/cm}^2\}$. As shown in Fig. 5, the leakage current is a strong function of the detector temperature and detector type.

The value of the leakage current is of interest, because, as shown in Fig. 5, the electronic noise increases with increasing leakage current.

Energy Resolution and Noise

A typical nuclear electronic chain is shown in Fig. 6.

The warranted energy resolution is measured in keV FWHM using a thin-window, 5.486-MeV ^{241}Am alpha particle point source placed at a distance from the detector equal to at least twice the detector diameter. The time constant in the main amplifier is also indicated: ORTEC uses 0.5 μsec pulse width at half the maximum pulse height for surface barrier detectors and 1 μsec for ULTRA detectors. The electronic noise of the detector is measured with the chain of Fig. 6, with an electronic pulser replacing the alpha source. This noise has historically been referred to as the "Beta resolution" because when the detector is used with very low specific ionization particles such as conversion electrons (Fig. 7), the energy resolution is approximately equal to the noise. The energy resolution, measured as described above, depends on a number of factors; the most important are:

- Electronic noise due to the detector leakage current and capacitance. This noise component can be minimized by

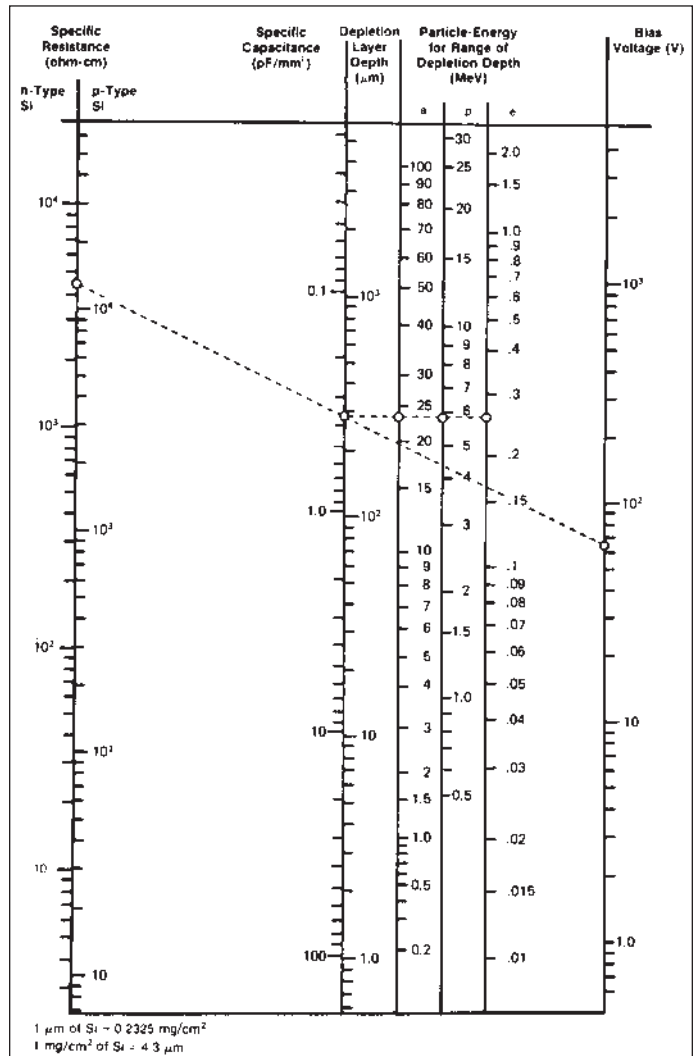


Fig. 3. Silicon Detector Parameters Nomograph. [Similar to Nomogram reported by J. L. Blankenship, *IEEE Trans. Nucl. Sci.* NS7 (2-3), 190-195 (1960).]

A straight edge intersecting the center vertical line at the required depletion depth will give combinations of resistivity and detector bias that may be used to achieve that depth. (Shown, for example, is the voltage that must be applied to a 13,000 $\Omega\text{-cm}$ p-type or 4500 $\Omega\text{-cm}$ n-type silicon detector to stop a 23-MeV alpha, a 6-MeV proton, or a 250-keV electron within the depletion depth.)

Introduction to Charged-Particle Detectors

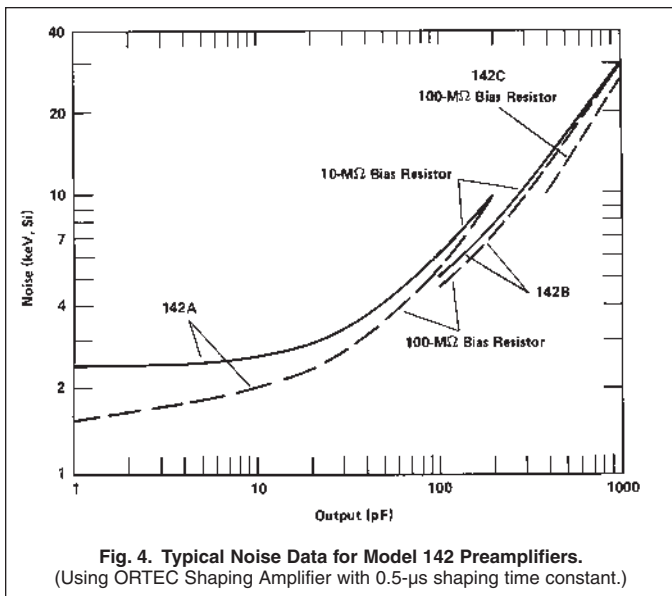


Fig. 4. Typical Noise Data for Model 142 Preamplifiers.
(Using ORTEC Shaping Amplifier with 0.5- μ s shaping time constant.)

choice of preamplifier and by optimum amplifier time constant selection. The time constant is preset at its optimum value in all ORTEC alpha spectrometers.

- b) Electronic noise due to the bias resistor. This noise component increases with decreasing values of the bias resistor. Typically, the value of the bias resistor is sufficiently high to make this component negligible. However, at elevated detector temperatures, it may become necessary to decrease the value of the bias resistor, with a concomitant noise increase.
- c) Energy loss and straggling in the detector entrance window. This factor is important when striving for high geometrical efficiency with the alpha source positioned as close as possible to the detector entrance contact. In this situation, alpha particles emitted perpendicular to the detector front contact pass through the entrance dead layer specified in the following summary table and, therefore, undergo the minimum energy loss; alpha particles that enter the front contact at an angle pass through a thicker dead layer, thereby losing more energy in the contact. The energy resolution is thus degraded.

Effects of Operating Temperature on Noise and Energy Resolution

ULTRA ion-implanted detectors, used primarily for alpha spectroscopy, are generally operated at room temperature. When optimum resolution is required, it is useful to reduce the detector noise by operation at low temperature. This is best accomplished by using surface barrier detectors instead of ULTRA detectors. The noise and energy resolution of surface barrier detectors can be substantially decreased by operating below room temperature, down to approximately -60°C. Below that temperature no further improvement is obtained because, with the leakage now \approx pA, the noise is dominated by the preamplifier noise and the detector capacitance, the latter, of course, not being a function of

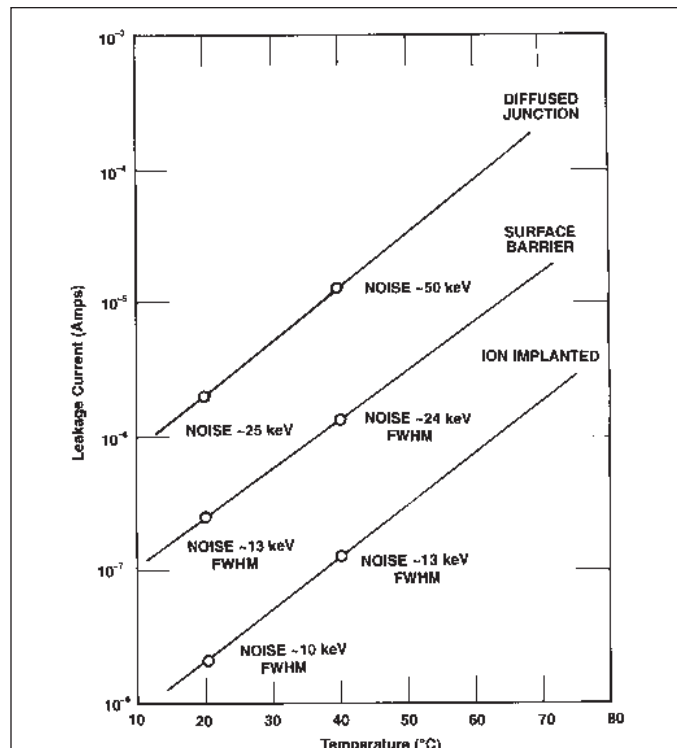


Fig. 5. Leakage Current and Noise vs. Temperature for 3 Types of Si Charged-Particle Detectors.

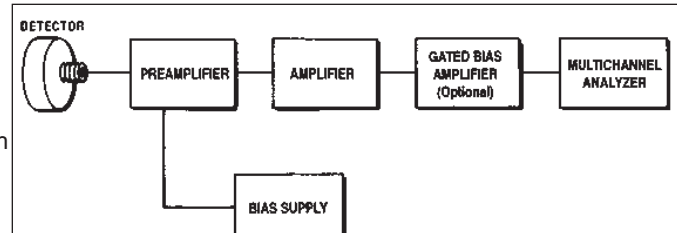


Fig. 6. Typical System for Charged-Particle Spectroscopy.

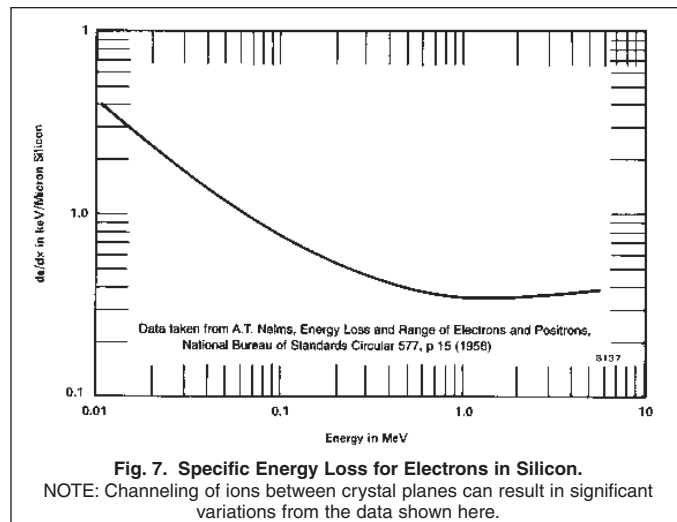


Fig. 7. Specific Energy Loss for Electrons in Silicon.
NOTE: Channeling of ions between crystal planes can result in significant variations from the data shown here.

Introduction to Charged-Particle Detectors

temperature. Figs. 8 and 9 show typical electronic noise and energy resolution measurements obtained with surface barrier detectors.

With ion-implanted ULTRA detectors, the noise is substantially lower at all temperatures, making them a clear choice at higher temperatures. The energy resolution **increase** that can be expected with ULTRAs at elevated temperature is approximately 15–20 keV FWHM at 60°C.

Selecting the Appropriate Si Detector for Your Application

Alpha Spectroscopy

The detectors of choice for alpha spectroscopy are ULTRAs with a depletion depth of ≥ 100 microns and ULTRA-AS detectors for ultra-low background applications. Many established installations are equipped with reliable Ruggedized (R-Series) Surface Barrier Detectors. As these require negative bias, the U Series are not a direct replacement in alpha spectrometer units. (All other ORTEC charged-particle detectors require positive bias.)

The reasons why the ULTRA and ULTRA-AS lines are widely used in alpha spectroscopy are the following:

- Alpha spectroscopists with low activity samples often position samples as close as possible to the front detector contact. As noted above, the thin (500 Å silicon equivalent) window results in optimal energy resolution.
- The front contact is cleanable. (This is also true of R-Series Surface Barrier Detectors, but not of other surface barrier detectors.)
- The type of edge passivation used with ULTRA Series Detectors permits positioning the sample as close as 1 mm from the detector entrance contact; the minimum distance with surface barrier detectors is 2.5 mm. As, in many cases, the efficiency of the detector depends strictly on geometrical factors, ULTRA detectors provide higher efficiency than surface barrier detectors.
- The low leakage current results in low noise, also contributing to good energy resolution.

An issue of particular importance in alpha spectroscopy is the need to perform **low-background** measurements. As health physics regulations become more stringent, it is becoming increasingly important to be able to analyze samples with extremely low activity. Measurements performed at ORTEC have confirmed that the ultimate limit to the low- background performance of silicon detectors, when manufactured and packaged with special materials and following strict cleaning procedures, is associated with the omnipresent **cosmic radiation**. This limit in the energy range from 3–8 MeV is 0.05 counts/hr/ 10^{-2} cc of active volume. This means that for a 450 mm² active area, 100-μm thick, low- background ULTRA-AS (AS denotes low background), a background counting rate of about 6 counts/day is expected. **To achieve such a low level, one must take exquisite care both concerning previous or present vacuum chamber contamination and in detector handling procedures.**

To minimize cosmic ray interactions, ULTRA-AS series are made as thin as possible, consistent with achieving good resolution. As natural alpha particles have a range not exceeding 30 microns in silicon, it would seem that a depletion depth not exceeding 30 microns should be sufficient. It would be were it not for the fact that such a high-capacitance detector would display excessive noise. A depletion depth close to 100 microns provides the best tradeoff.

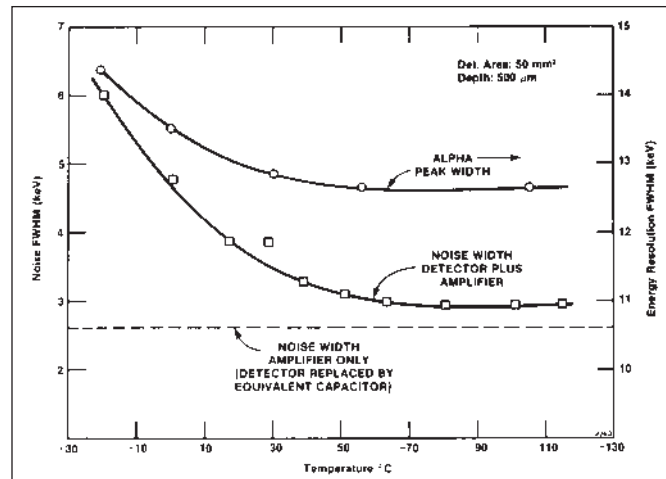


Fig. 8. Detector Noise and Alpha Energy Resolution as a Function of Temperature.

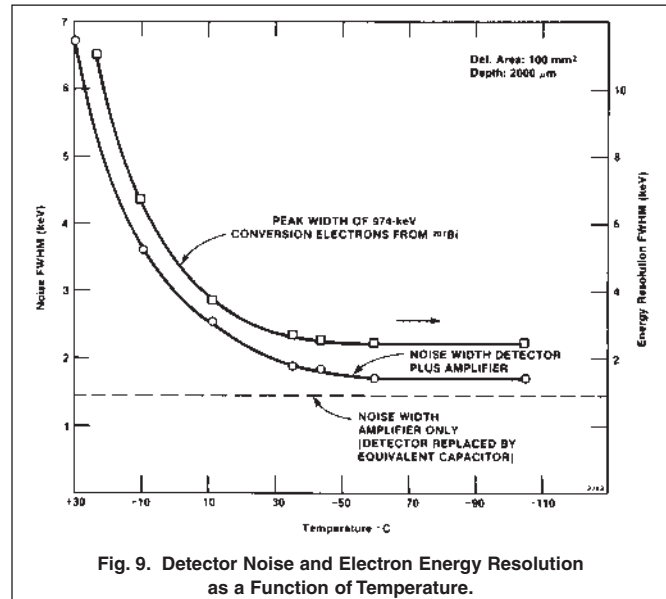


Fig. 9. Detector Noise and Electron Energy Resolution as a Function of Temperature.

Introduction to Charged-Particle Detectors

Some alpha spectroscopists employ an alpha recoil avoidance package to reduce the tendency for a gradual increase of background contamination on the detector surface. Information on this package is contained in the description of the ORTEC RCAP-2 system.

For rough spectroscopy and for simple counting applications (as in continuous air monitors), ORTEC offers the ruggedized ULTRA CAM line. ULTRA CAM detectors are light tight and moisture resistant.

Beta Spectroscopy and Counting

A key concern when selecting a silicon detector for room temperature beta spectroscopy or counting is the generation of a sufficiently large signal to well exceed the detector beta resolution. For example, 1 MeV electrons, which are minimum ionizing particles, deposit only 0.4 keV/micron of silicon (Fig. 7). The average energy loss in a 100- μm thick detector is 40 keV. As the threshold of the discriminator must be set 2.5 times above the beta resolution (noise), the beta resolution of the detector must be well below 15 keV FWHM to obtain meaningful data.

High quality beta spectroscopy cannot be obtained with room temperature silicon detectors. ORTEC offers a number of solutions:

- A complete Si(Li) detector-cryostat-preamplifier package, the BETA-X, for optimum energy resolution
- Thick, coolable silicon detectors (A- or L-Series).

Nuclear and Atomic Physics

The selection of appropriate detectors for nuclear and atomic physics is experiment dependent. Here are responses to frequently asked questions on this subject:

Q. Which detectors should be used for heavy-ion spectroscopy?

Because of the short, highly-ionized track of heavy ions, detectors with high electric field at the front contact (Fig. 2) are best. The F-Series Detectors have a warranted minimum electric field of 20,000 V/cm at the front contact.

Q. Which detectors and what techniques should be applied for low-energy ion and charged-particle spectroscopy?

For ions or particles in the energy range from 0 to 50 keV, one should cool both the detector and the first stage of the preamplifier. See "Detection Of Low Energy Heavy Particles With Silicon Barrier Detectors" by J.A. Ray and C.F. Barnett, IEEE Trans on Nuc. Sci. Vol NS-16, N1 (1969), pp. 82-86. An example of the results given in this paper is the spectrum shown in Fig. 10.

Q. Which detectors and what techniques should be applied for fast timing?

A silicon detector used for fast timing must have a high and uniform electric field throughout the depletion depth. Totally depleted detectors, such as an ULTRA or a high field partially depleted detector, capable of withstanding overbias should be used (Fig. 2). With particles in the MeV range and above, subnanosecond FWHM timing values are achievable (Ref: T.J. Paulus, et. al., IEEE NS-24, N1-1977).

Radiation Damage

Table 2 shows threshold doses for radiation damage with different types of charged particles.

The symptoms of radiation damage are: higher leakage current/noise followed by peak broadening and, sometimes, double peaking. In order to prolong the usable "life" of a detector in a radiation field causing damage, the detector must be kept cold (any cooling below room temperature helps; ideally the detector should be cooled to -60°C).

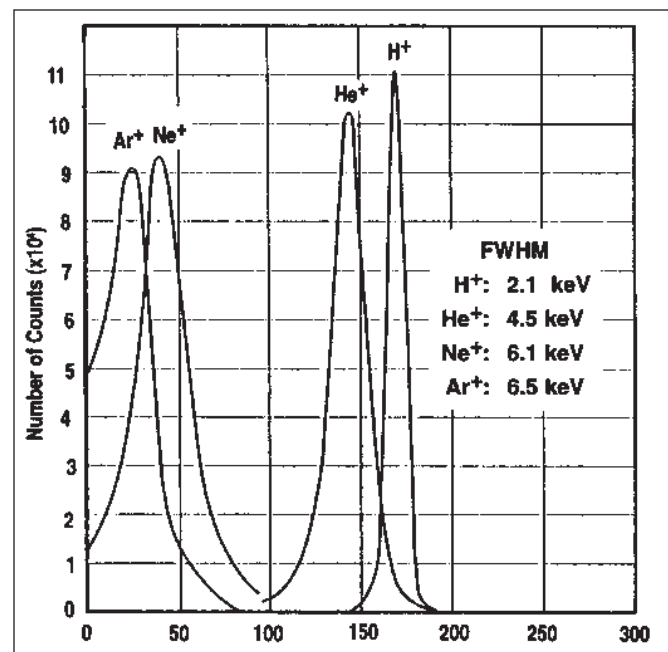


Fig. 10. The Pulse Height Spectrum of 40 keV H⁺, He⁺, Ne⁺, and Ar⁺ ions from a 7 mm² Detector (700 μm Depletion Depth, 20 k Ω -cm Resistivity).

Table 2. Effects of Radiation Damage in Silicon Detectors.				
Threshold Doses (particles/cm ²)				
Electrons	Fast Neutrons	Protons	Alpha Particles	Fission Fragments
10^{13}	10^{12}	10^{10}	10^9	10^8

Introduction to Charged-Particle Detectors

Parameters Affecting Performance Characteristics

Many parameters affect the performance of silicon charged-particle detectors. A description of the major parameters follows.

Area

The sensitive area is important because it affects both efficiency and energy resolution. When a low-intensity radiation source is used or when an accurate particle count is required (within the count-rate limits of the system), a large-area detector is desirable. However, since detector capacitance and electronic noise are proportional to the area, smaller detectors give much better resolution. Selecting the right detector size requires a compromise between efficiency and resolution.

Sensitive Depth

For energy spectrometry each output pulse must be generated with an amplitude proportional to the energy of the charged particle. Therefore, for these common applications the detector's sensitive depth must be sufficient to completely absorb all the particle energy (Fig. 3). As the sensitive depth increases, the detector capacitance C_D decreases, and this results in a decrease in preamplifier noise. However, the increase in sensitive depth also increases the sensitive volume of the detector, and this may increase the detector leakage-current-noise contribution. Minimum total system noise is obtained by matching the capacitance of the detector to the appropriate preamplifier.

In applications involving spectrometry of heavy charged particles, rather large electric fields are required to ensure complete charge collection and to ensure linearity and optimum resolution. Consequently, for heavy-ion or fission-fragment spectrometry the maximum sensitive depth is established by the need for large electric fields.

For high-resolution timing applications, in which the rise time of the information pulse must be very short, the charge transit distances have to be kept as small as possible and large electric fields maintained. In such cases, the sensitive depth may be restricted by the need for very precise timing information and occasionally by the need to discriminate against unwanted background.

Capacitance

The major effects of detector capacitance are its influence on the noise contribution from the preamplifier and its deterioration of the preamplifier rise time. In applications that require low total noise, it is necessary to minimize the capacitance C_D by restricting the active area and/or by optimizing the sensitive depth. Stray capacitance from cables, connectors, etc., must be added to the detector capacitance to establish the total capacitive load that determines the preamplifier contribution to the noise, and therefore must be minimized.

Electric-Field Strength

The minimum electric-field strength required for complete charge collection (i.e., optimum resolution and response linearity) depends on the mass (specific ionization density) of the charged particle being analyzed, with the more massive particles requiring higher field strengths. For charged particles (alpha particles or lighter), this minimum field is attained by meeting the required resolution specifications. For heavy-ion (fission-fragment) detectors, however, and for very thin totally depleted detectors, in which the resolution cannot be routinely tested, the minimum specified electric-field strength has been established by experimental data obtained during actual use in the field. In applications requiring very high-resolution timing, it is desirable to keep the average field strength as large as possible, consistent with optimum noise and sensitive depth.

Breakdown Voltage

For a given resistivity material the breakdown voltage of the diode establishes an upper limit on the electric-field strength and on the depletion depth. ORTEC does not use breakdown voltage as a basic specification, because it is redundant if the sensitive depth, noise, resolution, and/or field strength are specified.

Reverse-Leakage Current

A large reverse-leakage current results in detector noise and excessive voltage drop across the bias supply resistor (R_b).^{*} Since a quantitative relation between the detector leakage current and noise can be established only through a detailed knowledge of the origins of all current components, detector noise performance has been selected by ORTEC as the basic performance specification. Detectors whose leakage currents would produce excessive voltage drops across R_b are rejected by our quality-control standards. All ORTEC detectors are furnished with detailed data on their original leakage current so that this information may be used for troubleshooting and for estimates of the drop anticipated across R_b .

Silicon detectors made with ion-implantation and silicon-dioxide-passivated technologies have leakage current values substantially lower than surface barrier detectors of the same geometrical dimensions.

Introduction to Charged-Particle Detectors

Detector Noise

Noise sources in the detector and the preamplifier introduce a dispersion that broadens a pulse-height spectrum of mono-energetic particles. Noise is customarily specified in terms of FWHM (full width half maximum) broadening of a mono-energetic peak. The detector and the preamplifier are separate and independent sources of noise, and the total system noise is equal to the square root of the sum of the squares of the individual noise contributions. Noise specifications for ORTEC detectors include the total noise width for the detector and standard ORTEC electronics at a temperature of $21 \pm 1^\circ\text{C}$. These noise widths and actual resolutions therefore can be guaranteed only when the contribution from any other electronics does not exceed that from the appropriate ORTEC electronics.

Energy Resolution

The noise-broadening effect previously mentioned establishes a lower limit on the energy resolution (FWHM) of any given detector-preamplifier combination. However, factors such as statistical effects, imperfect charge collection, and variations in energy lost in the dead layer of the source and of the detector can cause additional broadening of the peak; their relative contribution is a strong function of the mass of the incident particle. For beta particles, the resolution is nearly always determined solely by the electronic noise broadening. For alpha particles, the ultimate resolution (with no significant contribution from noise) appears to be less than 10 keV. For very heavy ions such as ^{127}I , the typical resolution for nonchanneled particles is about 1 MeV.

Pulse Rise Time

The pulse rise time associated with any ionizing event is a complex function of the mass, energy, range, and orientation of the ionizing particle; the detector parameters (depletion depth, electric-field strength, diode series resistance, and sensitive area); and the characteristics of the associated electronics. Pulse rise times for typical ORTEC charged-particle detectors range from the order of one nanosecond to tens of nanoseconds. The charge collection time in silicon detectors at room temperature is ~ 100 ns/mm. In many experiments requiring nanosecond or subnanosecond time resolution, good energy resolution is also desired, usually resulting in a need for compromises in detector parameters. Consequently, this high-resolution-time requirement, together with all other relevant experimental information, should be specified at time of first inquiry.

Stacked Detectors

For some applications, such as $(\Delta E/\Delta x)(E)$ mass determinations and telescopic arrays, the energy range of the analyzed particles requires more depth than is provided by a single detector. Two or more detectors can then be combined so that the energy of the particle is totally absorbed in the detectors. The sum of the output pulses from the detectors will be proportional to the energy of the particle. For these applications the effective dead layer is the sum of the front and back dead layers (approximately equal to the electrode thickness) of all the detectors except the last one in the stack. For the last detector, only the front dead layer is considered. (Although all the detectors preceding the last one must be totally depleted, the last one need not be.) Quantitative, independent evaluation of this dead-layer thickness is supplied with each detector.

Parallel Connection of Two or More Detectors

In applications that require unusually large areas of sensitive depths, it is desirable to connect several detectors in parallel to the same preamplifier. In these circumstances, the total noise contribution to the energy resolution broadening can be determined by the following procedure:

The individual contributions of detector noise (total noise less preamplifier noise) are added by the mean-squares process:

$$N_{d,t}^2 = N_{d,1}^2 + N_{d,2}^2 + \dots + N_{d,i}^2 \quad (1)$$

where $N_{d,t}$ is the total noise contribution from the detectors and $N_{d,i}$ is the contribution of the i th detector.

The total capacitive load on the preamplifier is obtained by summing the detector capacitances and the stray capacitance:

$$\begin{aligned} C_t &= C_{d,i} + C_{d,2} + \dots + C_s \\ &= C_s + \sum_i C_{d,i} \end{aligned} \quad (2)$$

where C_t is the total load, $C_{d,i}$ is the capacitance of the i th detector, and C_s is the total stray capacitance, including that from cables, connectors, interconnections, etc. The value of C_t and the appropriate curve for preamplifier noise versus input capacitance are used to determine the preamplifier contribution to the noise. The total noise broadening is then obtained from

$$N_t^2 = N_{d,t}^2 + N_A^2 \quad (3)$$

where N_t is the total noise width and N_A is the preamplifier's contribution to the noise.

*Resistor, usually located in the preamplifier, has a value of $10 \text{ M}\Omega$.

Introduction to Charged-Particle Detectors

Charged-Particle Detector Multiplexing

Often in low-level counting applications, multiple spectrometers are employed to keep up with large numbers of low-level samples to be counted. Because these are low- or ultra-low-level applications, count rates are extremely low. For this reason, it is possible to employ a multiplexed system, where a gated multiplexer-router is used to send pulses from multiple detectors to separate memory segments in an MCA system. This can lead to substantial cost savings. The more advanced of these systems provide for independent start, stop, and preset of the multiplexed inputs.

Thickness Uniformity

Inadequate thickness uniformity of totally depleted ΔE detectors has undoubtedly been responsible for many disappointing experiments. A 10-MeV ${}^4\text{He}$ particle incident on a 50- μm -thick silicon detector will lose approximately 5.9 MeV in traversing the detector. The rate of energy loss (dE/dx) of the exiting particle, however, will be about 160 keV/ μm . This means that a detector thickness variation of 1 μm would cause an energy spread of 160 keV, which is many times greater than the detector resolution for particles that are completely absorbed in the detector. Considerations such as these show that precise control over the thickness uniformity of a device is highly desirable for many experiments. ORTEC uses an exclusive mechanical electrochemical wafer-polishing process that produces damage-free surfaces that are optically flat and parallel. By testing the wafers with optical interference techniques and by profiling the thickness of each wafer with an x-ray transmission technique, ORTEC ensures that each silicon wafer meets stringent thickness-uniformity specifications before being accepted as a planar totally depleted surface barrier detector (D Series). The measured mean detector thickness and uniformity are given on the Quality Assurance Data Sheet that accompanies each D Series detector.

Channeling and Crystal Orientation

The channeling of ions between crystal planes can produce significant differences in the rate of energy loss (and total range) between channeled and unchanneled ions. For very heavy ions this same effect can produce pronounced differences in the pulse-height linearity and energy resolution. Consequently, the silicon wafers for ORTEC totally-depleted and standard heavy-ion detectors are cut from the parent crystal at an angle that has been carefully selected to minimize channeling effects. Silicon charged-particle detectors that are cut at specific orientations are available on special order.

Test Data and General Information

Alpha Resolution

Alpha resolution is specified as the maximum peak width for a standard alpha source measured at one-half the peak height (FWHM) expressed in keV. The total system alpha resolution is measured and warranted for 5.486-MeV alphas from ${}^{241}\text{Am}$ with an ORTEC preamplifier chosen to be consistent with the detector capacitance and an ORTEC amplifier using equal differential and integral time constants as follows:

- 0.5 μs for A, B, C, F, L, and R Series;
- 1.0 μs for ULTRA, ULTRA-AS, and ULTRA CAM.

For totally depleted B Series detectors with \leq 500- μm thicknesses, the alpha resolution is measured through the exit (low-field strength) contact, and $>500\text{-}\mu\text{m}$ detectors measured with alpha particles through the front contact. The D and F Series are not warranted for alpha resolution but are warranted for system noise with suitable ORTEC electronics. Unless specified otherwise, resolution measurements are performed and warranted at $21 \pm 1^\circ\text{C}$.

Beta Resolution (System Noise)

The system noise width guaranteed maximum FWHM (which approximates beta resolution) is listed for each type of detector. Unless specified otherwise, measurements are performed and warranted at $21 \pm 1^\circ\text{C}$.

Electrons (beta particles) are, to a first approximation, sufficiently light to cause zero energy loss in the entrance window of silicon detectors. The beta energy resolution of silicon detectors is thus determined by the electronic noise of the detector and preamplifier; hence, the interchangeable "beta resolution/system noise" terminology.

Discriminator Threshold Setting

When silicon detectors are used as beta spectrometers, the threshold of the lower-level discriminator in the electronics must be set at 2.5 times the "beta resolution" to avoid spurious noise counts. Because the specific ionization of electrons is very low (e.g., 0.35 keV/ μm for minimum ionizing betas), it is often necessary to cool silicon detectors used as beta spectrometers. (Detectors with cryogenic epoxy must be special-ordered.) When this is done, the electronic noise caused by the detector leakage current is eliminated and the detector becomes equivalent to a pure capacitor. The electronic noise of the system can then be easily calculated from the noise vs. capacitance characteristics of the preamplifier.

Introduction to Charged-Particle Detectors

Heavy Charged Particles

Heavy charged particles lose energy by Coulomb interaction with the electrons and the nuclei of the absorbing materials. The collision of heavy charged particles with free and bound electrons results in the ionization or excitation of the absorbing atom, whereas the interaction with nuclei leads only to a Rutherford scattering between two types of nuclei. Thus the energy spent by the particle in electronic collisions results in the creation of electron-hole pairs, whereas the energy spent in nuclear collisions is lost to the detection process.

The concepts of specific ionization loss dE/dx and of range R can be used to summarize the interaction of heavy charged particles in semiconductor detectors when nuclear collisions are unimportant. The specific ionization loss measures the amount of energy lost by the particle per unit-length of its track; the range indicates how deeply the particle penetrates the absorbing material. Figure 11 shows the stopping power as a function of the energy, and Fig. 12 shows the range as a function of the energy in silicon and in germanium for alpha particles, protons, and deuterons.

Nuclear collisions can become an important part of the energy loss process, especially in the case of heavy ions and fission fragments. The theory describing this process is too complicated for a brief summary. We refer the reader to specialized literature such as the IEEE Transactions on Nuclear Science and the references footnoted here.^{1,2}

Finally, it should be mentioned that channeling effects (the steering of charged particles in open regions in the lattice) can reduce the specific ionization loss. Again, we refer the reader to the referenced literature for details on this particular phenomenon.^{1,2}

Electrons

The interaction of electrons with matter is similar to the interaction of heavy particles, with the following differences:

1. Nuclear collisions are not part of the interaction because of the very light electron mass.
2. At energies higher than a few MeV, radioactive processes (bremsstrahlung) must be considered in addition to the inelastic electron collision.
3. Again because of their light mass, electrons are so intensely scattered that their trajectory in the material is a jagged line; therefore, the concept of range as previously used cannot be applied. Rather, the concept of zero-transmission range is introduced. This is done by means of absorption experiments, which permit definition of the absorber thickness resulting in zero-electron transmission at a given energy. Figure 13 shows the zero-transmission range as a function of energy in silicon and germanium.

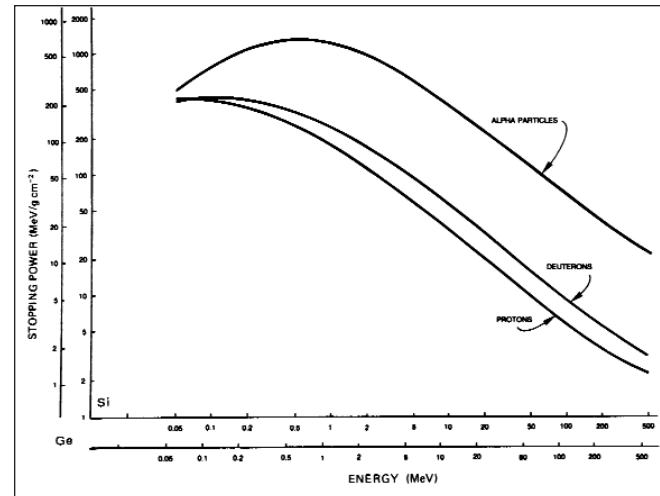


Fig. 11. Stopping Power vs. Energy for Photons, Deuterons and Alpha Particles in Si and Ge.

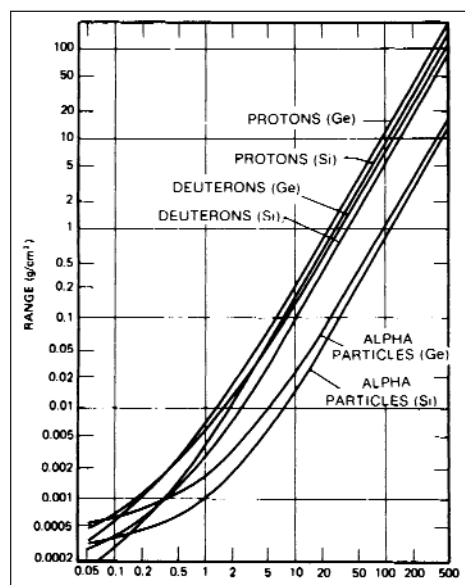


Fig. 12. Proton, Deuteron and Alpha Particle Ranges in Si and Ge.

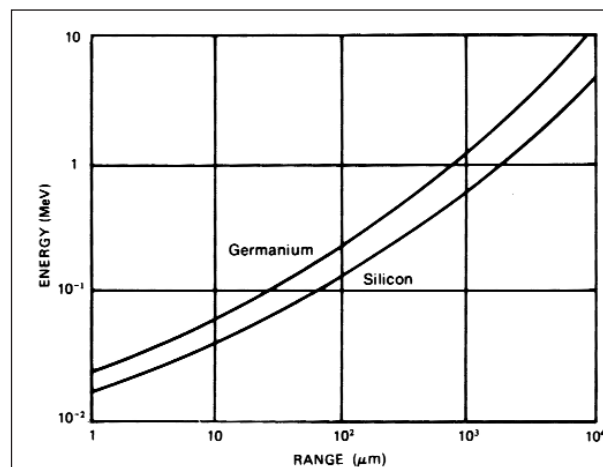


Fig. 13. Zero Transmission Range vs. Energy for Electrons in Si and Ge.

Introduction to Charged-Particle Detectors

ORTEC Charged-Particle Detector Data Summary and Selection Chart

Series	Chief Application	Starting Material	Range of Active Area (mm ²)	Range of Active Thickness (μm)	Warranted Operating Temperature Range*	Diode Structure	Nominal Structure** Stopping Power of Windows	
							Entrance	Exit
ULTRA†	High-resolution, high-efficiency alpha and beta spectroscopy	Si	25–3000	100–500	+50°C to –30°C	Implanted Boron — N-type Si Implanted As Partial Depletion	500 Å Si	
ULTRA AST†	Ultra-low background high-efficiency alpha spectroscopy	Si	300–1200	100	+50°C to –30°C	Implanted Boron — N-type Si Implanted As Partial Depletion	500 Å Si	
ULTRA CAMT†	Alpha and beta continuous air monitoring (counting in adverse environment)	Si	300–2000	100 (Deeper detector requires special order)	+50°C to –15°C	Implanted Boron — N-type Si Implanted As Partial Depletion	N/A	
A	High-Resolution charged-particle spectroscopy (Nuclear Physics and Chemistry-Space Physics)	Si	25–450	1000–2000	+25°C to –30°C	Gold — N-type Si Aluminum Partial Depletion	800 Å Si	
B	Particle identification, telescopes of detectors (Nuclear Physics and Chemistry-Space Physics)	Si	50–450	150–2000	+25°C to –30°C	Gold — N-type Si Aluminum Total Depletion	800 Å Si	2250 Å Si
C	Backscattering from a collimated source or beam target-angular correlation measurements (Nuclear Physics)	Si	50–450	100–1000	25°C to –30°C	Gold — N-type Si Aluminum Partial Depletion	800 Å Si	2250 Å Si
D	Time-of-flight measurements with heavy ions (Nuclear Physics)	Si	10–450	15–100	10°C to 25°C	Gold — N-type Si Aluminum Total Depletion Planar	800 Å Si	2250 Å Si
F	Heavy-ion spectroscopy (Nuclear Physics)	Si	100–900	≥60	+25°C to –30°C	Gold — N-type Si Aluminum Partial Depletion High Field Strength	800 Å Si	
L	Medium-energy proton (25 MeV) and other charged-particle energy spectroscopy	Si (Lithium compensated)	25–200	5000	+25°C to –196°C (LN ₂)	Gold — Lithium Compensated P-type Si Lithium (diffused)	2000 Å Si	
R	Charged-particle spectroscopy operable in air and ambient light	Si	50–2000	100–500	+25°C to –30°C	Aluminum — P-type Si Gold Partial Depletion	2300 Å Si	
Beta-X§	High-resolution beta spectroscopy	Si (Lithium compensated)	80	5000	–196°C (LN ₂)	Gold — Lithium Compensated — P-type Si Lithium (diffused)	2000 Å Si	

** Measured with 5.486-MeV natural alpha particles.

† ULTRA series detectors are manufactured by ion-implantation silicon-dioxide passivated technologies. Versions bakeable at 200°C available on special order.

§ The Beta-X detector is offered in a sealed cryostat.

¹ *Radiation Detection and Measurement* (2nd Edition) by Glenn F. Knoll, New York: John Wiley and Sons, 1989, and *Semiconductor Detectors*, edited by G. Bertolini and A. Coche, North Holland Publishing Co., 1968 (distributed in the U.S. by American Elsevier Publishing Co.), New York City.

² F.S. Goulding and R.H. Pehl, "Semiconductor Detectors," Section IIIA, *Nuclear Spectroscopy and Reactions*, J. Cerny, Ed. Academic Press (1974).

Specifications subject to change
051512

ORTEC®

www.ortec-online.com

Tel. (865) 482-4411 • Fax (865) 483-0396 • ortec.info@ametek.com
801 South Illinois Ave., Oak Ridge, TN 37831-0895 U.S.A.
For International Office Locations, Visit Our Website

AMETEK®
ADVANCED MEASUREMENT
TECHNOLOGY

Alpha Spectroscopy

Appendix E

Radiation Interaction: Energy Loss Measurement

Source: "Glenn F. Knoll, Radiation Detection and Measurement, Chap2 "

CHAPTER • 2

Radiation Interactions

The operation of any radiation detector basically depends on the manner in which the radiation to be detected interacts with the material of the detector itself. An understanding of the response of a specific type of detector must therefore be based on a familiarity with the fundamental mechanisms by which radiations interact and lose their energy in matter. Many general reference works are available concerning this broad topic; the classic text by Evans,¹ to mention only one, has served as a standard reference over several decades.

To organize the discussions that follow, it is convenient to arrange the four major categories of radiations introduced in Chapter 1 into the following matrix:

<i>Charged Particulate Radiations</i>	<i>Uncharged Radiations</i>
Heavy charged particles (characteristic distance $\approx 10^{-5}$ m)	\Leftarrow Neutrons (characteristic length $\approx 10^{-1}$ m)
Fast electrons (characteristic distance $\approx 10^{-3}$ m)	\Leftarrow X-rays and gamma rays (characteristic length $\approx 10^{-1}$ m)

The entries in the left column represent the charged particulate radiations that, because of the electric charge carried by the particle, continuously interact through the coulomb force with the electrons present in any medium through which they pass. The radiations in the right column are uncharged and therefore are not subject to the coulomb force. Instead, these radiations must first undergo a "catastrophic" interaction (often involving the nucleus of constituent atoms) that radically alters the properties of the incident radiation in a single encounter. In all cases of practical interest, the interaction results in the full or partial transfer of energy of the incident radiation to electrons or nuclei of the constituent atoms, or to charged particle products of nuclear reactions. If the interaction does not occur within the detector, these uncharged radiations (e.g., neutrons or gamma rays) can pass completely through the detector volume without revealing the slightest hint that they were ever there.

The horizontal arrows shown in the diagram illustrate the results of such catastrophic interactions. An X- or gamma ray, through the processes described in this chapter, can transfer all or part of its energy to electrons within the medium. The resulting *secondary electrons* bear a close similarity to the fast electron radiations (such as the beta particle) discussed in Chapter 1. Devices designed to detect gamma rays are tailored to promote such interactions and to fully stop the resulting secondary electrons so that their entire energy may contribute to the output signal. In contrast, neutrons may interact in such a way as to produce secondary heavy charged particles, which then serve as the basis of the detector signal.

Also listed in the diagram are order-of-magnitude numbers for the characteristic distance of penetration or average path length (range or mean free path) in solids for typical energy radiations in each category.

I. INTERACTION OF HEAVY CHARGED PARTICLES

A. Nature of the Interaction

Heavy charged particles, such as the alpha particle, interact with matter primarily through coulomb forces between their positive charge and the negative charge of the orbital electrons within the absorber atoms. Although interactions of the particle with nuclei (as in Rutherford scattering or alpha-particle-induced reactions) also are possible, such encounters occur only rarely and they are not normally significant in the response of radiation detectors. Instead, charged particle detectors must rely on the results of interactions with electrons for their response.

Upon entering any absorbing medium, the charged particle immediately interacts simultaneously with many electrons. In any one such encounter, the electron feels an impulse from the attractive coulomb force as the particle passes its vicinity. Depending on the proximity of the encounter, this impulse may be sufficient either to raise the electron to a higher-lying shell within the absorber atom (*excitation*) or to remove completely the electron from the atom (*ionization*). The energy that is transferred to the electron must come at the expense of the charged particle, and its velocity is therefore decreased as a result of the encounter. The maximum energy that can be transferred from a charged particle of mass m with kinetic energy E to an electron of mass m_0 in a single collision is $4Em_0/m$, or about 1/500 of the particle energy per nucleon. Because this is a small fraction of the total energy, the primary particle must lose its energy in many such interactions during its passage through an absorber. At any given time, the particle is interacting with many electrons, so the net effect is to decrease its velocity continuously until the particle is stopped.

Representative paths taken by heavy charged particles in their slowing down process are schematically represented in Fig. 2-1. Except at their very end, the tracks tend to be quite straight because the particle is not greatly deflected by any one encounter, and interactions occur in all directions simultaneously. Charged particles are therefore characterized by a definite *range* in a given absorber material. The range, to be defined more precisely below, represents a distance beyond which no particles will penetrate.

The products of these encounters in the absorber are either excited atoms or *ion pairs*. Each ion pair is made up of a free electron and the corresponding positive ion of an absorber atom from which an electron has been totally removed. The ion pairs have a natural tendency to recombine to form neutral atoms, but in some types of detectors, this

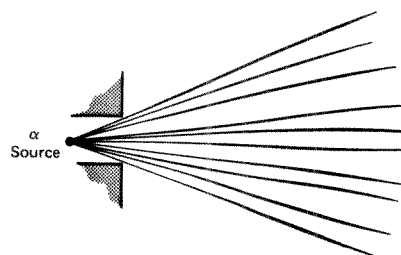


Figure 2-1 Representation of the tracks of alpha particles from a monoenergetic source.

recombination is suppressed so that the ion pairs may be used as the basis of the detector response.

In particularly close encounters, an electron may undergo a large enough impulse so that after having left its parent atom, it still may have sufficient kinetic energy to create further ions. These energetic electrons are sometimes called *delta rays* and represent an indirect means by which the charged particle energy is transferred to the absorbing medium. Under typical conditions, the majority of the energy loss of the charged particle occurs via these delta rays. The range of the delta rays is always very small compared with the range of the incident charged particle, and in most practical situations it is immaterial whether the energy is deposited directly by the primary particle itself or by the secondary delta rays.

B. Stopping Power

The *linear stopping power* S for charged particles in a given absorber is simply defined as the differential energy loss for that particle within the material divided by the corresponding differential path length:

$$S = -\frac{dE}{dx} \quad (2-1)$$

The value of $-dE/dx$ along a particle track is also called its *specific energy loss* or, more casually, its "rate" of energy loss.

For particles with a given charge state, S increases as the particle velocity is decreased. The classical expression that describes the specific energy loss is known as the *Bethe formula* and is written

$$-\frac{dE}{dx} = \frac{4\pi e^4 z^2}{m_0 v^2} N B \quad (2-2)$$

where

$$B = Z \left[\ln \frac{2m_0 v^2}{I} - \ln \left(1 - \frac{v^2}{c^2} \right) - \frac{v^2}{c^2} \right]$$

In these expressions, v and ze are the velocity and charge of the primary particle, N and Z are the number density and atomic number of the absorber atoms, m_0 is the electron

rest mass, and e is the electronic charge. The parameter I represents the average excitation and ionization potential of the absorber and is normally treated as an experimentally determined parameter for each element. For nonrelativistic charged particles ($v \ll c$), only the first term in B is significant. Equation (2-2) is generally valid for different types of charged particles provided their velocity remains large compared with the velocities of the orbital electrons in the absorbing atoms.

The expression for B in Eq. (2-2) varies slowly with particle energy. Thus, the general behavior of dE/dx can be inferred from the behavior of the multiplicative factor. For a given nonrelativistic particle, dE/dx therefore varies as $1/v^2$, or inversely with particle energy. This behavior can be heuristically explained by noting that because the charged particle spends a greater time in the vicinity of any given electron when its velocity is low, the impulse felt by the electron, and hence the energy transfer, is largest. When comparing different charged particles of the same velocity, the only factor that may change outside the logarithmic term in Eq. (2-2) is z^2 , which occurs in the numerator of the expression. Therefore, particles with the greatest charge will have the largest specific energy loss. Alpha particles, for example, will lose energy at a rate that is greater than protons of the same velocity, but less than that of more highly charged ions. In comparing different materials as absorbers, dE/dx depends primarily on the product NZ , which is outside the logarithmic term. High atomic number, high-density materials will consequently result in the greatest linear stopping power.

The Bethe formula begins to fail at low particle energies where charge exchange between the particle and absorber becomes important. The positively charged particle will then tend to pick up electrons from the absorber, which effectively reduce its charge and consequent linear energy loss. At the end of its track, the particle has accumulated z electrons and becomes a neutral atom.

C. Energy Loss Characteristics

1. THE BRAGG CURVE

A plot of the specific energy loss along the track of a charged particle such as that shown in Fig. 2-2 is known as a Bragg curve. The example is shown for an alpha particle of several MeV initial energy. For most of the track, the charge on the alpha particle is two electronic charges, and the specific energy loss increases roughly as $1/E$ as predicted by Eq. (2-2). Near the end of the track, the charge is reduced through electron pickup and the curve falls off. Plots are shown both for a single alpha particle track and for the average behavior of a parallel beam of alpha particles of the same initial energy. The two curves differ somewhat due to the effects of straggling, to be discussed below.

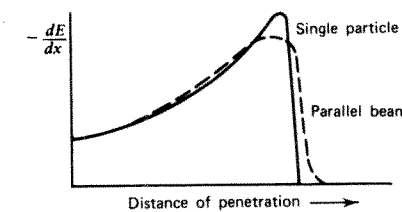


Figure 2-2 The specific energy loss along an alpha track.

RADIATION INTERACTIONS

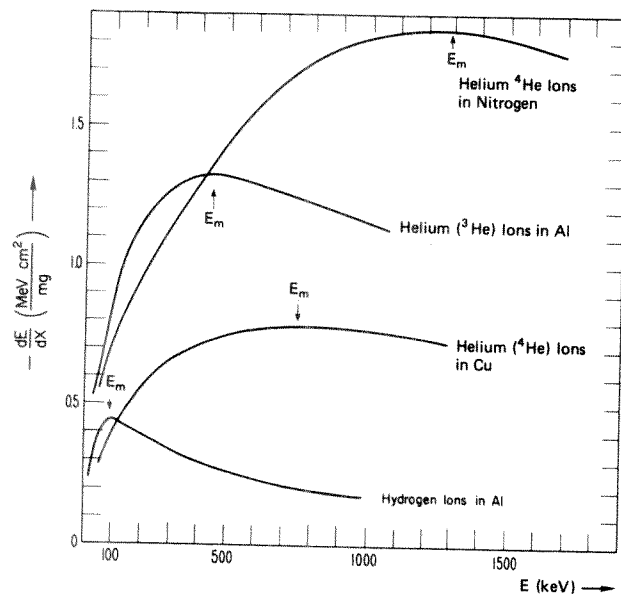


Figure 2-3 Specific energy loss as a function of energy for hydrogen and helium ions. E_m indicates the energy at which dE/dx is maximized. (From Wilken and Fritz.²)

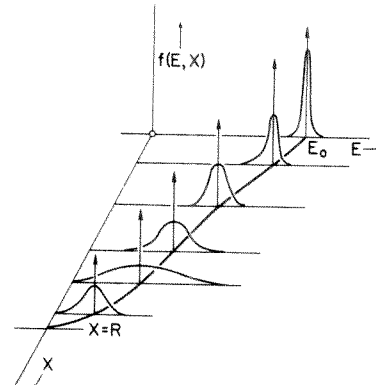


Figure 2-4 Plots of the energy distribution of a beam of initially monoenergetic charged particles at various penetration distances. E is the particle energy and X is the distance along the track. (From Wilken and Fritz.²)

INTERACTION OF HEAVY CHARGED PARTICLES

Related plots showing $-dE/dx$ versus particle energy for a number of different heavy charged particles are given in Fig. 2-3. These examples illustrate the energy at which charge pickup by the ion becomes significant. Charged particles with the greatest number of nuclear charges begin to pick up electrons early in their slowing down process. Note that in an aluminum absorber, singly charged hydrogen ions (protons) show strong effects of charge pickup below about 100 keV, but doubly charged ³He ions show equivalent effects at about 400 keV.

2. ENERGY STRAGGLING

Because the details of the microscopic interactions undergone by any specific particle vary somewhat randomly, its energy loss is a statistical or stochastic process. Therefore, a spread in energies always results after a beam of monoenergetic charged particles has passed through a given thickness of absorber. The width of this energy distribution is a measure of *energy straggling*, which varies with the distance along the particle track.

Figure 2-4 shows a schematic presentation of the energy distribution of a beam of initially monoenergetic particles at various points along its range. Over the first portion, the distribution becomes wider (and more skewed) with penetration distance, showing the increasing importance of energy straggling. Near the end of the range, the distribution narrows again because the mean particle energy has greatly been reduced.

D. Particle Range

1. DEFINITIONS OF RANGE

In order to quantify the definition of particle range, we refer to the conceptual experiment sketched in Fig. 2-5. Here a collimated source of monoenergetic alpha particles is counted by a detector after passing through an absorber of variable thickness. (We later contrast the behavior of other types of radiation when observed under similar conditions.) For alpha particles, the results are also plotted in Fig. 2-5. For small values of the absorber thickness, the only effect is to cause an energy loss of the alpha particles in the absorber as they pass through. Because the tracks through the absorber are quite straight, the total number that reach the detector remains the same. No attenuation in the number of alpha particles takes place until the absorber thickness approaches the length of the shortest track in the absorbing material. Increasing the thickness then stops more and more of the alpha particles, and the intensity of the detected beam drops rapidly to zero.

The range of the alpha particles in the absorber material can be determined from this curve in several ways. The *mean range* is defined as the absorber thickness that reduces the alpha particle count to exactly one-half of its value in the absence of the absorber.

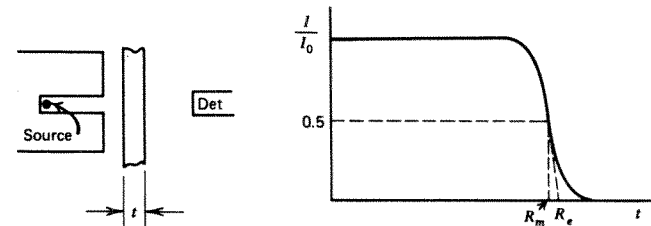


Figure 2-5 An alpha particle transmission experiment. I is the detected number of alpha particles through an absorber thickness, t , whereas I_0 is the number detected without the absorber. The mean range R_m and extrapolated range R_e are indicated.

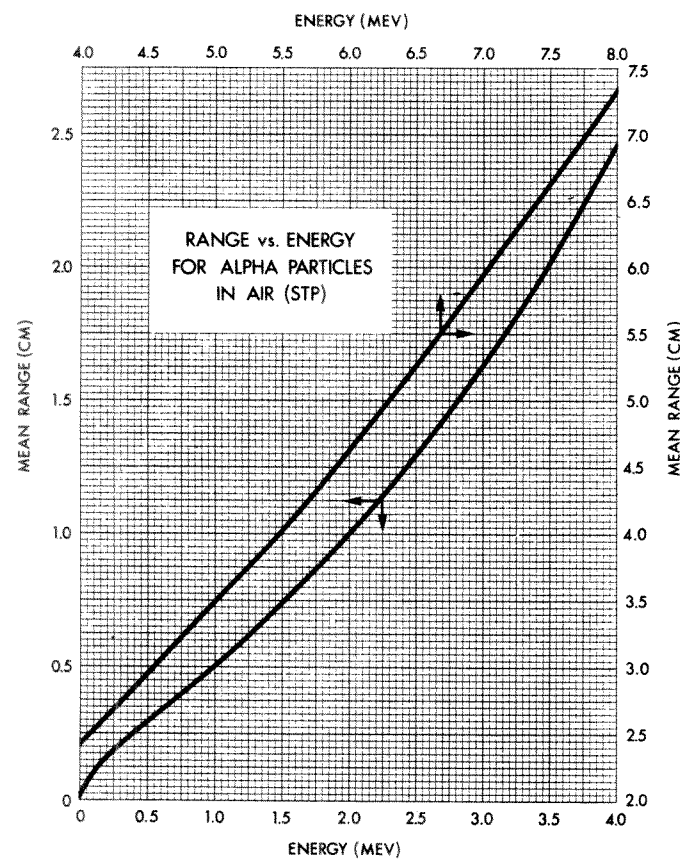


Figure 2-6 Range-energy plot for alpha particles in air at 15°C and 760 mm Hg pressure. (From *Radiological Health Handbook*, U.S. Department of Health, Education and Welfare, Washington, DC, 1970.)

This definition is most commonly used in tables of numerical range values. Another version that often appears in the literature is the *extrapolated range*, which is obtained by extrapolating the linear portion of the end of the transmission curve to zero.

The range of charged particles of a given energy is thus a fairly unique quantity in a specific absorber material. In the early days of radiation measurement, experiments of the type sketched in Fig. 2-5 were widely used to measure the energy of alpha particles indirectly by determining the absorber thickness equivalent to their mean range. With the availability of detectors that provide an output signal directly related to the alpha particle energy, such indirect measurements are no longer necessary.

Some graphs of the range of various charged particles in materials of interest in detectors are given in Figs. 2-6 through 2-8. As one obvious application of these curves, any detector that is to measure the full incident energy of a charged particle must have an active thickness that is greater than the range of that particle in the detector material.

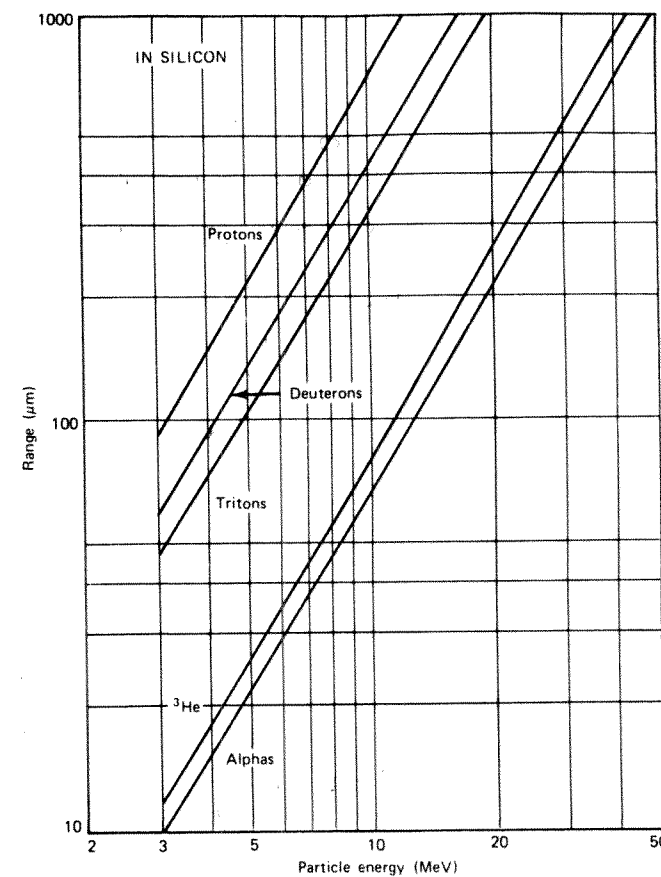


Figure 2-7 Range-energy curves calculated for different charged particles in silicon. The near-linear behavior of the log-log plot over the energy range shown suggests an empirical relation of the form $R = aE^b$, where the slope-related parameter b is not greatly different for the various particles. (From Skyrme.³)

2. RANGE STRAGGLING

Charged particles are also subject to *range straggling*, defined as the fluctuation in path length for individual particles of the same initial energy. The same stochastic factors that lead to energy straggling at a given penetration distance also result in slightly different total path lengths for each particle. For heavy charged particles such as protons or alphas, the straggling amounts to a few percent of the mean range. The degree of straggling is evidenced by the sharpness of the cutoff at the end of the average transmission curve plotted in Fig. 2-2. Differentiating this curve leads to a peak whose width is often taken as a quantitative measure of the importance of range straggling for the particles and absorber used in the measurement.

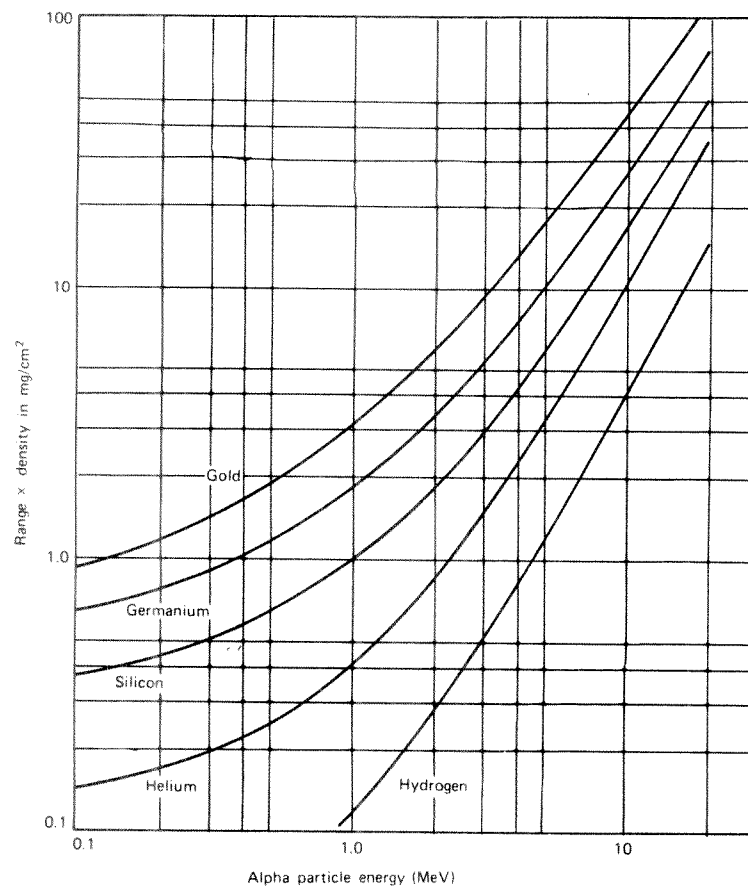


Figure 2-8 Range-energy curves calculated for alpha particles in different materials. Units of the range are given in mass thickness (see Section III.B.2) to minimize the differences in these curves. (Data from Williamson et al.⁴)

3. STOPPING TIME

The time required to stop a charged particle in an absorber can be deduced from its range and average velocity. For nonrelativistic particles of mass m and kinetic energy E , the velocity is

$$v = \sqrt{\frac{2E}{m}} = c\sqrt{\frac{2E}{mc^2}} = \left(3.00 \times 10^8 \frac{m}{s}\right) \sqrt{\frac{2E}{(931 \text{ MeV/amu})m_A}}$$

where m_A is the particle mass in atomic mass units. If we assume that the average particle velocity as it slows down is $\langle v \rangle = Kv$, where v is evaluated at the initial energy, then the

stopping time T can be calculated from the range R as

$$T = \frac{R}{\langle v \rangle} = \frac{R}{Kc} \sqrt{\frac{mc^2}{2E}} = \frac{R}{K \left(3.00 \times 10^8 \frac{m}{s}\right)} \sqrt{\frac{931 \text{ MeV/amu}}{2}} \sqrt{\frac{m_A}{E}}$$

If the particle were uniformly decelerated, then $\langle v \rangle$ would be given by $v/2$ and K would be $\frac{1}{2}$. However, charged particles generally lose energy at a greater rate near the end of their range, and K should be a somewhat higher fraction. By assuming $K = 0.60$, the stopping time can be estimated as

$$T \approx 1.2 \times 10^{-7} R \sqrt{\frac{m_A}{E}} \quad (2-3)$$

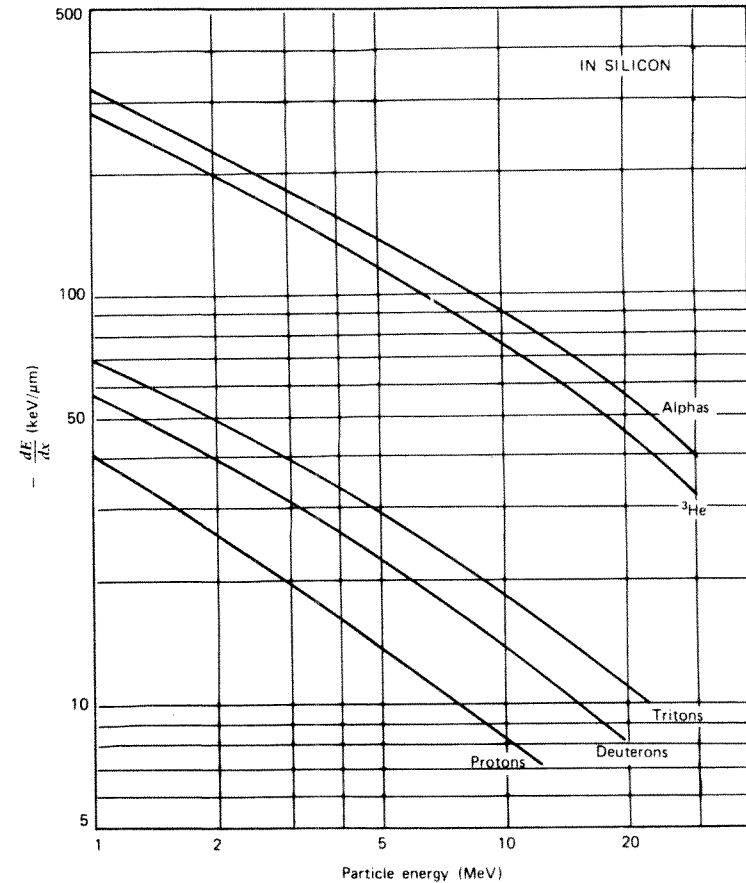


Figure 2-9 The specific energy loss calculated for different charged particles in silicon. (From Skyrme.³)

where T is in seconds, R in meters, m_A in amu, and E in MeV. This approximation is expected to be reasonably accurate for light charged particles (protons, alpha particles, etc.) over much of the energy range of interest here. It is not, however, to be used for relativistic particles such as fast electrons.

Using typical range values, stopping times calculated from Eq. (2-3) for charged particles are a few picoseconds in solids or liquids and a few nanoseconds in gases.

E. Energy Loss in Thin Absorbers

For thin absorbers (or detectors) that are penetrated by a given charged particle, the energy deposited within the absorber can be calculated from

$$\Delta E = \left(-\frac{dE}{dx} \right)_{\text{avg}} t \quad (2-4)$$

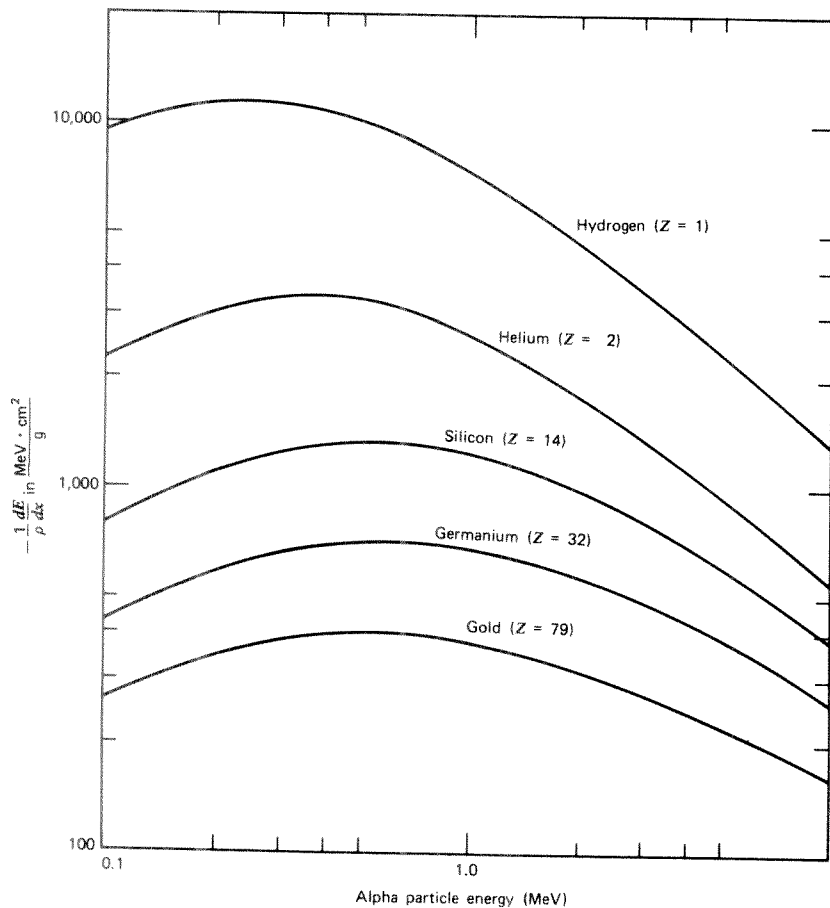


Figure 2-10 The specific energy loss calculated for alpha particles in different materials. Values are normalized by the density of the absorber material. (Data from Williamson et al.⁴)

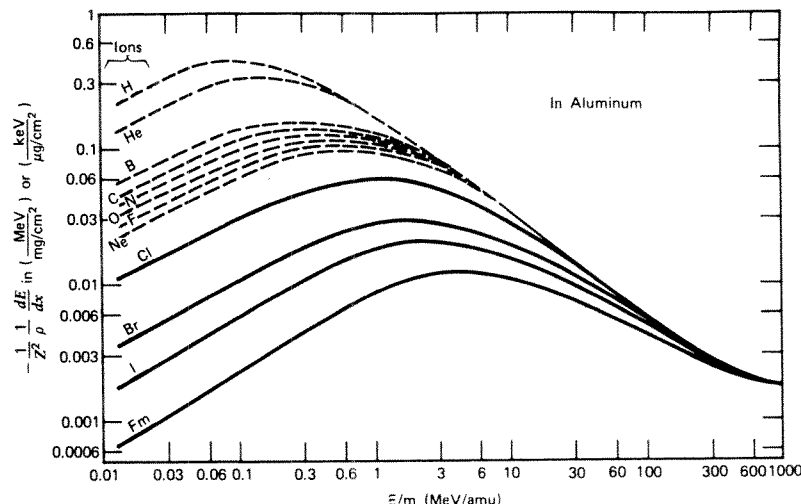
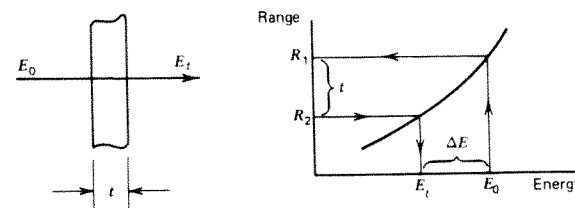


Figure 2-11 Plots showing the specific energy loss of various heavy ions in aluminum. The abscissa is the ion energy divided by its mass, and the ordinate is $-dE/dx$ divided by the density of aluminum and the square of the ion atomic number. Typical fission fragments (e.g., iodine) show a continuously decreasing $-dE/dx$ while slowing from their initial energy (~ 1 MeV/amu). (From Northcliffe and Schilling.⁷)

where t is the absorber thickness and $(-dE/dx)_{\text{avg}}$ is the linear stopping power averaged over the energy of the particle while in the absorber. If the energy loss is small, the stopping power does not change much and it can be approximated by its value at the incident particle energy. Tabular values for dE/dx for a number of different charged particles in a variety of absorbing media are given in Refs. 4–8. Some graphs for materials of interest in specific detectors are shown in Figs. 2-9 through 2-11.

For absorber thicknesses through which the energy loss is not small, it is not easy to obtain a properly weighted $(-dE/dx)_{\text{avg}}$ value directly from such data. In these cases, it is easier to obtain the deposited energy in a way that makes use of range-energy data of the type plotted in Figs. 2-6 through 2-8. The basis of the method is as follows: Let R_1 represent the full range of the incident particle with energy E_0 in the absorber material. By subtracting the physical thickness of the absorber t from R_1 , a value R_2 is obtained which represents the range of those alpha particles that emerge from the opposite surface of the absorber. By finding the energy corresponding to R_2 , the energy of the transmitted charged particles E_t is obtained. The deposited energy ΔE is then given simply by $E_0 - E_t$. These steps are illustrated below:



The procedure is based on the assumption that the charged particle tracks are perfectly linear in the absorber, and the method does not apply in situations where the particle can be significantly deflected (such as for fast electrons).

The combined effects of particle range and the decrease in dE/dx with increasing energy are illustrated in Fig. 2-12. Here the energy loss of protons in a thin detector is plotted versus the incident proton energy. For low energies, the proton range is less than the detector thickness. Therefore, as the energy is increased, the energy deposited in the detector (which is just equal to the incident energy) increases linearly. At a proton energy of 425 keV, the range is exactly equal to the detector thickness. For higher energies, only a portion of the incident energy is deposited, and the transmitted proton carries off the remainder. Under these conditions, the energy deposited in the detector is given by Eq. (2-4), or simply the product of the detector thickness and the average linear stopping power. Because the stopping power continuously decreases with increasing energy in this region (see Fig. 2-3), the deposited energy therefore *decreases* with further increases in the incident proton energy. The second curve in Fig. 2-12 plots the transmitted energy (E_t , on the diagram above) as recorded by a second thick detector.

F. Scaling Laws

Sometimes data are not available on the range or energy loss characteristics of precisely the same particle-absorber combination needed in a given experiment. Recourse must then be made to various approximations, most of which are derived based on the Bethe formula [Eq. (2-2)] and on the assumption that the stopping power per atom of compounds or mixtures is additive. This latter assumption, known as the Bragg-Kleeman

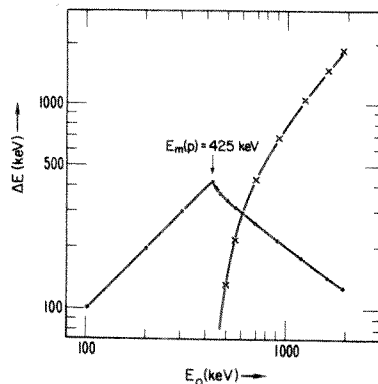


Figure 2-12 Energy loss of protons of initial energy E_0 in a silicon detector of $4.6 \mu\text{m}$ thickness (shown as dots). The transmitted energy for penetrating protons is also shown (as crosses). (From Wilken and Fritz.²)

rule, may be written

$$\frac{1}{N_c} \left(\frac{dE}{dx} \right)_c = \sum_i W_i \frac{1}{N_i} \left(\frac{dE}{dx} \right)_i \quad (2-5)$$

In this expression, N is the atomic density, dE/dx is the linear stopping power, and W_i represents the atom fraction of the i th component in the compound (subscript c). As an example of the application of Eq. (2-5), the linear stopping power of alpha particles in a metallic oxide could be obtained from separate data on the stopping power in both the pure metal and in oxygen. Some caution should be used in applying such results, however, since some measurements¹⁰⁻¹² for compounds have indicated a stopping power differing by as much as 10–20% from that calculated from Eq. (2-5).

It can be shown⁹ that the range of a charged particle in a compound material can also be estimated provided its range is known in all the constituent elements. In this derivation, it is necessary to assume that the shape of the dE/dx curve is independent of the stopping medium. Under these conditions, the range in the compound is given by

$$R_c = \frac{M_c}{\sum_i n_i (A_i / R_i)} \quad (2-6)$$

where R_i is the range in element i , n_i is the number of atoms of element i in the molecule, A_i is the atomic weight of element i , and M_c is the molecular weight of the compound.

If range data are not available for all the constituent elements, estimates can be made based on a semiempirical formula (commonly called the Bragg-Kleeman rule as well)

$$\frac{R_1}{R_0} \cong \frac{\rho_0 \sqrt{A_1}}{\rho_1 \sqrt{A_0}} \quad (2-7)$$

where ρ and A represent density and atomic weight, and subscripts 0 and 1 refer to different absorbing materials. The accuracy of this estimate diminishes when the two materials are of widely different atomic weights, so it is always best to use range data from a material that is as close as possible in A to the absorber of interest.

Range data can also be generalized to different charged particles within a given absorber material. By integration of Eq. (2-2), it can be shown that the range of a particle of mass m and charge z can be represented by

$$R(v) = \frac{m}{z^2} F(v) \quad (2-8)$$

where $F(v)$ represents a unique function of the particle initial velocity v . For particles of the same initial velocity, this factor will be identical and therefore we can write

$$R_a(v) = \frac{m_a z_b^2}{m_b z_a^2} R_b(v) \quad (2-9)$$

where the subscripts a and b refer to different charged particles. Thus, the range of a particle for which data are not available can be estimated by calculating its initial velocity, finding the range of any other particle of the same initial velocity in the same

material, and applying Eq. (2-9). It should be emphasized that these estimates are only approximate, because no account is taken of the change in charge state of the particle as it nears the end of its path. Correction factors necessary to compensate for this effect and predict the range more accurately are presented by Evans.¹

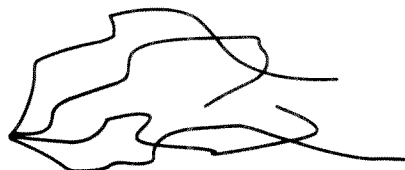
G. Behavior of Fission Fragments

The heavy fragments produced as a result of neutron-induced or spontaneous fission of heavy nuclei are energetic charged particles with properties somewhat different from those discussed up to this point. Because the fragments start out stripped of many electrons, their very large effective charge results in a specific energy loss greater than that encountered with any other radiations discussed in this text. Because the initial energy is also very high (see Fig. 1-4), however, the range of a typical fission fragment is approximately half that of a 5 MeV alpha particle.

An important feature of a fission fragment track is the fact that the specific energy loss ($-dE/dx$) decreases as the particle loses energy in the absorber. This behavior is in marked contrast to the lighter particles, such as alpha particles or protons, and is a result of the continuous decrease in the effective charge carried by the fragment as its velocity is reduced. The pickup of electrons begins immediately at the start of the track, and therefore the factor z in the numerator of Eq. (2-2) continuously drops. The resulting decrease in $-dE/dx$ is large enough to overcome the increase that normally accompanies a reduction in velocity. For particles with much lower initial charge state, such as the alpha particle, electron pickup does not become significant until near the end of the range.

II. INTERACTION OF FAST ELECTRONS

When compared with heavy charged particles, fast electrons lose energy at a lower rate and follow a much more tortuous path through absorbing materials. A series of tracks from a source of monoenergetic electrons might appear as in the sketch below:



Large deviations in the electron path are now possible because its mass is equal to that of the orbital electrons with which it is interacting, and a much larger fraction of its energy can be lost in a single encounter. In addition, electron–nuclear interactions, which can abruptly change the electron direction, sometimes occur.

A. Specific Energy Loss

An expression similar to that of Eq. (2-2) has also been derived by Bethe to describe the specific energy loss due to ionization and excitation (the “collisional losses”) for fast

electrons:

$$-\left(\frac{dE}{dx}\right)_c = \frac{2\pi e^4 NZ}{m_0 v^2} \left(\ln \frac{m_0 v^2 E}{2I^2(1-\beta^2)} - (\ln 2)(2\sqrt{1-\beta^2} - 1 + \beta^2) + (1-\beta^2) + \frac{1}{8}(1-\sqrt{1-\beta^2})^2 \right) \quad (2-10)$$

where the symbols have the same meaning as in Eq. (2-2), and $\beta \equiv v/c$.

Electrons also differ from heavy charged particles in that energy may be lost by radiative processes as well as by coulomb interactions. These radiative losses take the form of *bremssstrahlung* or electromagnetic radiation, which can emanate from any position along the electron track. From classical theory, any charge must radiate energy when accelerated, and the deflections of the electron in its interactions with the absorber correspond to such acceleration. The linear specific energy loss through this radiative process is

$$-\left(\frac{dE}{dx}\right)_r = \frac{NEZ(Z+1)e^4}{137m_0^2 c^4} \left(4 \ln \frac{2E}{m_0 c^2} - \frac{4}{3} \right) \quad (2-11)$$

The factors of E and Z^2 in the numerator of Eq. (2-11) show that radiative losses are most important for high electron energies and for absorber materials of large atomic number. For typical electron energies, the average bremsstrahlung photon energy is quite low (see Fig. 1-6) and is therefore normally reabsorbed fairly close to its point of origin. In some cases, however, the escape of bremsstrahlung can influence the response of small detectors.

The total linear stopping power for electrons is the sum of the collisional and radiative losses:

$$\frac{dE}{dx} = \left(\frac{dE}{dx}\right)_c + \left(\frac{dE}{dx}\right)_r \quad (2-12)$$

The ratio of the specific energy losses is given approximately by

$$\frac{(dE/dx)_r}{(dE/dx)_c} \approx \frac{EZ}{700} \quad (2-13)$$

where E is in units of MeV. For the electrons of interest here (such as beta particles or secondary electrons from gamma-ray interactions), typical energies are less than a few MeV. Therefore, radiative losses are always a small fraction of the energy losses due to ionization and excitation and are significant only in absorber materials of high atomic number.

B. Electron Range and Transmission Curves

I. ABSORPTION OF MONOENERGETIC ELECTRONS

An attenuation experiment of the type discussed earlier for alpha particles is sketched in Fig. 2-13 for a source of monoenergetic fast electrons. Even small values of the absorber thickness lead to the loss of some electrons from the detected beam because scattering of

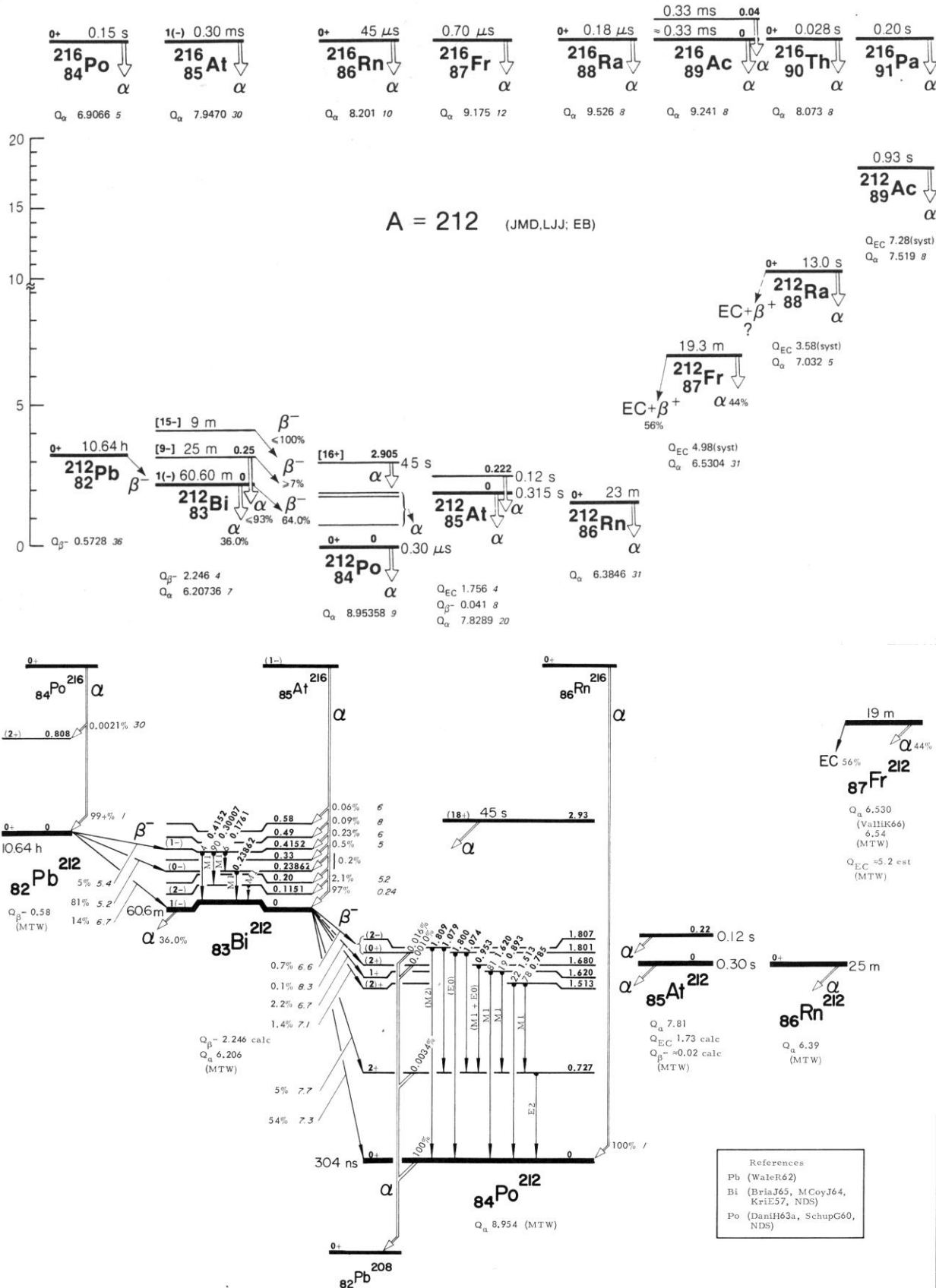
Alpha Spectroscopy

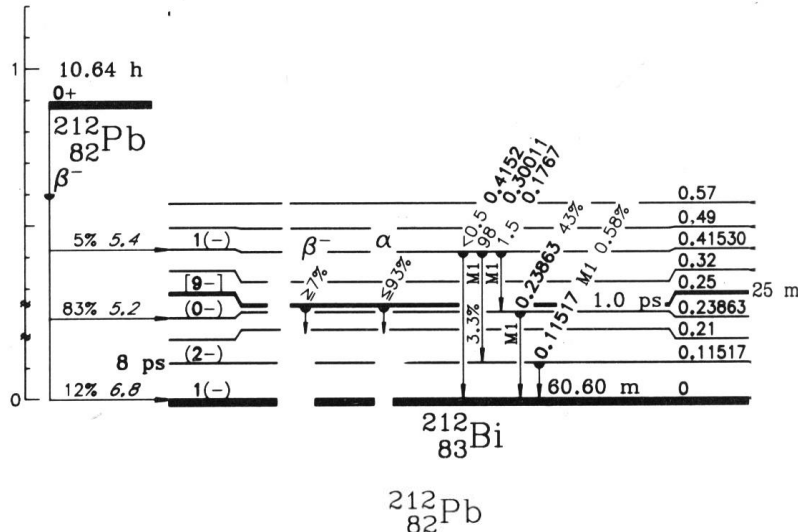
Appendix F

Level Schemes

Source: “Table of isotopes, C. M. LEDERER et al.”

“





Δ : -7.5626 {ANDT 19 175(77)}

\ddagger : β^- {PRSL 139A 659(33)}

genet: parent ^{212}Bi , not parent $^{212}\text{m}^1\text{Bi}$, from level scheme {PC78 Baisden, ND B8 165(72)}

$t_{1/2}$: 10.64312 h {JPPa 16 115(55), AnPs 12v10 783(55)}; others: {VLnM 10n8 97n3(55), PPSL 66A 608(53), Nwls 39 575(52), RMP 3 427(31)}

Class: A; Ident: chem, genet {RMP 3 427(31)}

Prod: descendant ^{228}Th {BK64 Hyde2}

β : 0.568629 (12%), 0.330725 mag {PRSL 195A 287(48)}

others: {IzF 22 198(58), IzF 12 673(50), Dokl 68 257(49), PPSL 61 466(48), PRSL 139A 659(33)}

γ : 0.2386265 mag conv {CJP 43 171(65), ND B8 165(72)}

0.1151738 mag conv {ArkF 25 87(63)}

0.1151789 mag conv {CJP 41 2202(63)}

(norm: $\gamma_{0.239}$ (γ 43%), JMD, LJJ), (intensities relative to γ_{100} for ^{208}TI in equilibrium) $\text{Bi K}_\alpha X$ (γ , 71.6%), $\text{Bi K}_\beta X$ (γ , 20.1%), 0.115163 (γ , 1.685, e_{L1+2}/γ 1.0712), 0.176675 (γ , 0.14518, e_K/γ 2.15), $\gamma_{0.239}$ (γ , 1253, e_{L1+2}/γ assumed 0.128), 0.300115 (γ , 9.53, e_K/γ 0.385), 0.4152 (γ , <0.05, e_K/γ >0.2) Ge(Li), mag conv {ND B8 165(72), PC72 Gunnink, ZETF 32 682(57), IzF 21 954(57), JMD, LJJ}

$\gamma_{0.239}$ (L_1/L_2 9.4810, $L_1/L_2/L_3$ 131.737/13.95/1) mag conv {ZP 203 480(67)}

$\gamma_{0.115}$ ($L_1/L_2/L_3$ 100/10.43/0.8810), $\gamma_{0.239}$ (L_1/L_2 9.6218, L_1/L_3 1359) mag conv {ZETF 35 348(58), NP 9 498(59)}

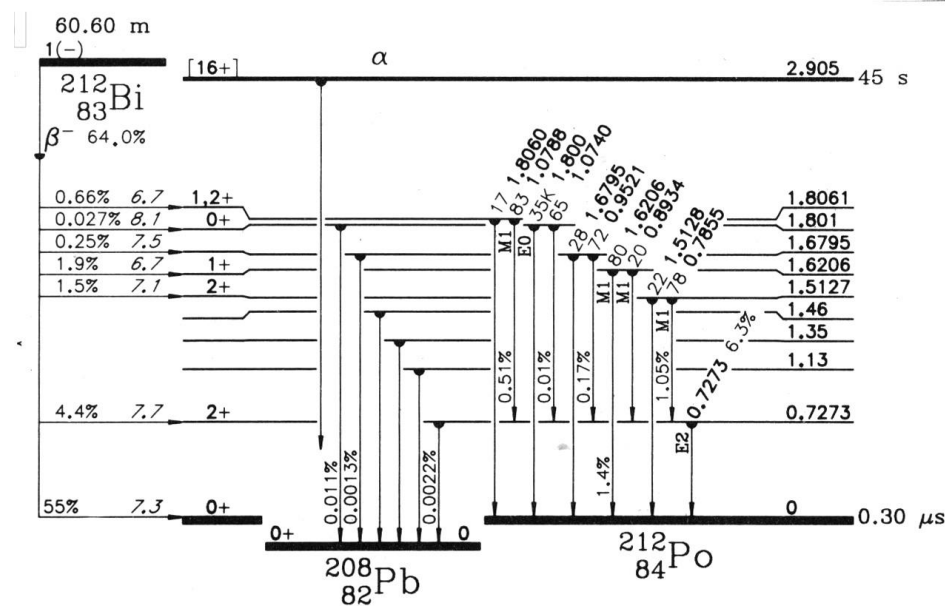
$\gamma_{0.239}$ (K/L_3 91021, L/M 4.416, $M/N+O+\dots$ 3.32) mag conv {Fzko 1 171(69)}

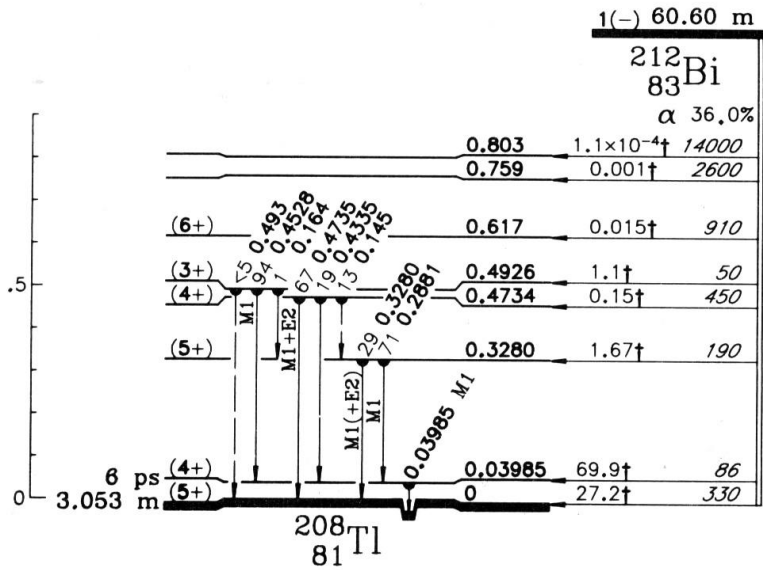
0.23859015 (K/L_1 5.9621, K/L_2 60.371), 0.30007021 mag conv {NIM 82 29(70), NIM 35 171(65), ZP 188 252(65)}

0.11514 (K 2.12%, $K/L_1/L_2/L_3$ 4.5/1/0.121/<0.02), 0.17667 (K 0.087%, K/L_1 5.1), 0.23860 (K 28.1%, $K/L_1/L_2/L_3$ 6.0/1/0.1163/0.00664, M_1/M_2 8.52), 0.30012 (K 1.06%, K/L 5.94, $L/M+N+\dots$ 3.4), 0.4152 (K 0.003%) mag conv {NP 4 579(57), IzF 20 367(56), IzF 20 363(56)}

(intensity relative to γ_{125} for $\gamma_{0.239}$) $\gamma_{0.115}$ (e_K/γ 4.84), $\gamma_{0.177}$ (e_K/γ 1.53), $\gamma_{0.415}$ (γ , 0.416), other γ rays observed scint, scint-scint $\gamma\gamma$ coinc {NuCo 10v21 430(61)}

$\gamma_{0.239}$ (K 31.36%) mag-conv {PRSL 195A 287(48)}





^{212}Bi

$\Delta: -8.1356$ {ANDT 19 175(77)}

β^- : 64.00%, α 36.00% {PPSL 86 423(65)}; β^- 64.19%, α 35.81% {NP 30 599(62), NIM 7 350(60)}; β^- 64.04%, α 35.96% {PR 120 189(60)}; others: {PPSL 79 10(62), CR 253 98(61), Nuovo Cimento 20 450(61), Nuovo Cimento 9 734(58), PPSL 72 300(58), PR 104 1629(56), PPSL 66A 608(53), PR 54 413(38)}

$t_{1/2}: 60.60043\text{ m}$ {INC 19 375(61)}; 60.5 m {RMP 3 427(31)}

Class: A; Ident: chem, genet {RMP 3 427(31)}

Prod: descendant ^{228}Th {Bk64 Hyde2}

α : $\alpha_0 6.09008737$ ($\dagger 27.2$), $\alpha_{40} 6.05098530$ ($\dagger 69.9$), $\alpha_{328} 5.7693$ ($\dagger 1.67$), $\alpha_{473} 5.6263$ ($\dagger 0.15$), $\alpha_{493} 5.6073$ ($\dagger 1.08$), $\alpha_{617} 5.4863$ ($\dagger 0.016$) mag {CR 269B 652(69), Metr 7 65(71), ANDT 12 479(73), CR 233 790(51)}

$\alpha_0 6.090$ ($\dagger 27.1$), $\alpha_{40} 6.051$ ($\dagger 69.7$), $\alpha_{328} 5.768$ ($\dagger 1.78$), $\alpha_{473} 5.626$ ($\dagger 0.165$), $\alpha_{493} 5.607$ ($\dagger 1.19$), $\alpha_{617} 5.481$ ($\dagger 0.014$), $\alpha_{759} 5.345$ ($\dagger 0.001$), $\alpha_{803} 5.3022$ ($\dagger 1.1 \times 10^{-4}$) mag {NP 16 246(60)}

$\alpha_0 6.090$ ($\dagger 26.82$), $\alpha_{40} 6.050$ ($\dagger 70.22$), $\alpha_{328} 5.762$ ($\dagger 1.672$), $\alpha_{473} + \alpha_{493}$ ($\dagger 1.222$), $\alpha_{617} 5.481$ ($\dagger \approx 0.03$) semicond, ion ch {NP 30 599(62)}

others: {HPAC 34 240(61), CR 250 3156(60), CR 245 676(57), IzF 20 1451(56), PRSL 216A 219(53), PR 54 18(38), PRSL 145A 235(34)}

β^- : 2.250525 mag {PRSL 195A 287(48)}

2.256 mag, mag-scint $\beta\gamma$ coinc {PPSL 61 466(48)}

2.27 ($\dagger 63$), 1.55 ($\dagger 10$), 0.93 ($\dagger 7.5$), 0.675 ($\dagger 6$), 0.454 ($\dagger 8.5$), 0.0855 ($\dagger 5$) mag, mag-scint $\beta\alpha$ coinc {PR 107 531(57)}

others: {PR 74 1196(48), PRSL 139A 659(33)}

γ with α : 0.03985 / mag conv {CJP 43 171(65)}

(intensities relative to $\dagger 100$ for $\gamma_{2,615}$ (with ^{208}Tl in equilibrium)) 0.039875 ($\dagger 3.063$), $0.125?$ ($\dagger \gamma < 0.09$), 0.14402 ($\dagger \gamma 0.02811$), 0.1640 ($\dagger \gamma 0.0139$), 0.2880077 ($\dagger \gamma 0.953$), 0.29512 ($\dagger \gamma 0.06717$), 0.3279610 ($\dagger \gamma 0.393$), 0.43355 ($\dagger \gamma 0.041$), 0.4528310 ($\dagger \gamma 1.043$), 0.47352 ($\dagger \gamma 0.133$), $\gamma_{0.493}$ ($\dagger \gamma < 0.05$) Ge(Li) {ND B8 165(72), PC72 Gunnink}

(intensities relative to $\dagger 100$ for $\gamma_{2,615}$ (with ^{208}Tl in equilibrium)) $\gamma_{0.288}$ ($\dagger 0.95$, $e/\gamma 0.537$, K/L/M 5.55/1/0.226), $\gamma_{0.328}$ ($\dagger 0.38$, $e/\gamma 0.354$, K/L 6.012), $\gamma_{0.434}$ ($\dagger 0.057$), $\gamma_{0.453}$ ($\dagger 0.972$, $e/\gamma 0.183$, K/L 4.36), $\gamma_{0.473}$ ($\dagger 0.141$, $e/\gamma 0.148$, K/L 2.215), $\gamma_{0.493}$ ($\dagger \gamma < 0.01$) Ge(Li), Ge(Li)-semicond $\gamma\alpha$ coinc, semicond-semicond $\gamma\alpha$ coinc {Nuovo Cimento 10v 49A 125(67), JMD, LJU}

$\gamma_{0.040}$ ($L_1/L_2/L_3/M_1/M_2/M_3/N_{1+2}/O_{1+2} 100025/1065/8.233/26215/305/6.225/76.542/104$) mag conv {ArkF 25 87(63), ArkF 28 397(65)}

$\gamma_{0.040}$ ($e/\gamma 22.5546$), $\gamma_{0.328}$ ($e_K/\gamma 0.313$), other γ rays observed scint-semicond $\gamma\alpha$ coinc {ZP 197 328(66)}

0.03985 ($L_1/L_2/L_3 100050/925/82$), 0.14494 ($\dagger_K 0.046$), 0.2882 ($\dagger_K 0.37$, K/L 5.1), 0.2941 ($\dagger_L 0.008$), 0.3280 ($\dagger_K 0.11$, K/L 7.8), 0.4338 ($\dagger_K 0.0064$), 0.45298 ($\dagger_K 0.12$, K/L 4.7), 0.4730 ($\dagger_K 0.019$), 0.4932 ($\dagger_K 0.010$) mag conv {ZETF 32 682(57), IzF 21 954(57), JMD, LJU}

(intensities relative to $\dagger 100$ for $\gamma_{2,615}$ (with ^{208}Tl in equilibrium)) no $\gamma_{0.145}$ ($\dagger \gamma < 0.006$), no $\gamma_{0.617}$ ($\dagger \gamma < 0.004$) scint-ion ch $\gamma\alpha$ coinc {NP 30 599(62)}

γ with β^- : (intensities relative to $\dagger 100$ for $\gamma_{2,615}$ (with ^{208}Tl in equilibrium))

(norm: $\gamma_{0.727}$ ($\gamma 6.32\%$)) 0.727277 ($\dagger \gamma 18.54$, $e_K/\gamma 0.0143$, K/L 5.518, L/M 3.620), 0.785467 ($\dagger \gamma 3.087$, $e_K/\gamma 0.0367$, K/L 7.8), 0.893351 ($\dagger \gamma 1.023$, $e_K/\gamma 0.0368$, K/L 4), 0.9521010 ($\dagger \gamma 0.493$, $e_K/\gamma 0.045$), 1.07405 ($\dagger \gamma 0.04422$, $e_K/\gamma < 0.3$), 1.0788010 ($\dagger \gamma 1.494$, $e_K/\gamma 0.0193$), no $\gamma_{1.25}$ ($\dagger \gamma < 0.04$), 1.5127510 ($\dagger \gamma 0.877$, $e_K/\gamma 0.022$), 1.6206210 ($\dagger \gamma 4.2015$, $e_K/\gamma 0.006717$), 1.67955 ($\dagger \gamma 0.193$), 1.8002 ($\dagger \gamma 0.0245$, $e_K/\gamma > 0.24$), 1.80605 ($\dagger \gamma 0.316$, $e_K/\gamma 0.0267$) Ge(Li), mag conv {ND B8 165(72), PC72 Gunnink, ZP 176 30(63), IzF 21 954(57), JMD, LJU}

0.727087 , 0.785378 , 0.893439 , 1.0786210 Ge(Li) {NIM 69 353(69)}

1.513110 ($\dagger \gamma 0.9915$), 1.62088 ($\dagger \gamma 4.8520$), 1.679515 ($\dagger \gamma 0.237$), no $\gamma_{1.801}$ ($\dagger \gamma < 0.01$), 1.806010 ($\dagger \gamma 0.4110$), other γ rays observed Ge(Li) {CR 267B 1362(68), CR 267B 1366(68)}

0.727229 ($K/L/M 4.4/1/0.2$) mag conv {IzF 20 877(56)}

$0.600?$, $\gamma_{0.893}$ ($\dagger \gamma 1.066$), ≈ 1.25 ($\dagger \gamma \leq 0.35$), $\gamma_{1.513}$ ($\dagger \gamma 0.737$), $\gamma_{1.806}$ ($\dagger \gamma 0.234$), other γ rays observed scint-ion ch $\gamma\alpha$ coinc {NP 30 599(62)}

$^{212}_{\text{Po}}$

Δ : -10.3815 {ANDT 19 175(77)}

α : α {CR 233 790(51)}

$t_{1/2}$: 0.2962 μs delay coinc {PR C12 318(75)}; 0.3044 μs delay coinc {PPSL 62A 253(49)}; 0.3055 μs delay coinc {INP 45 49(63)}; 0.3048 μs delay coinc {IIso 23 527(72)}; others: {PPSL 79 10(62), JPJa 8 110(53), PR 75 100(49), CJR 26A 255(48), PCam 44 440(48), HPAc 16 259(43), Nat 144 152(39)}

Class: A; Ident: genet {RMP 3 427(31)}

Prod: descendant ^{228}Tn {Bk64 Hyde2}

α : 8.78437 γ mag {Cf71 Tedton 1, ANDT 12 479(73)}

8.78485 γ mag {RMxF 20 17(71)}

$\mu\text{-range } \alpha$: (alphas from excited states of ^{212}Po following ^{212}Bi decay
(intensities per 100 ^{212}Bi β^- decays))

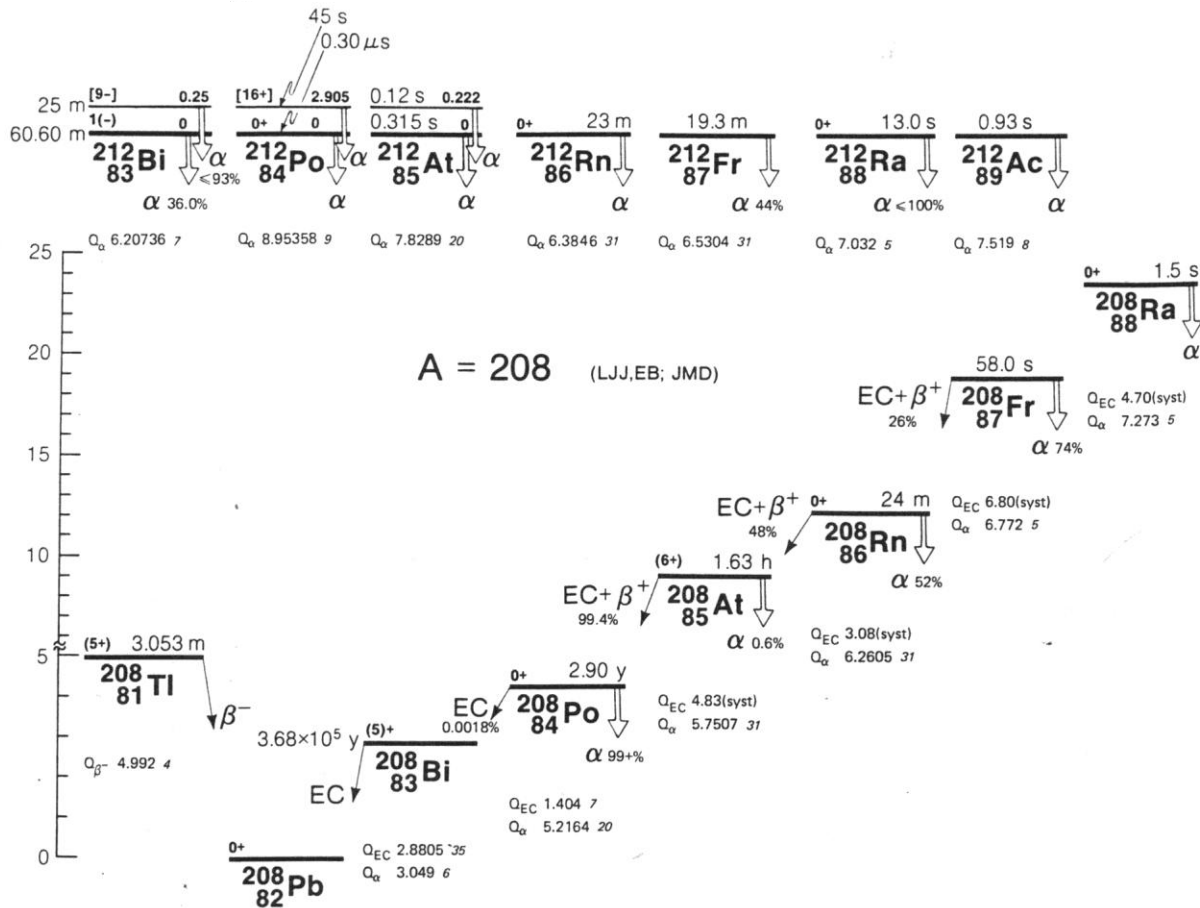
9.495 γ (± 0.0035), 10.422 γ (± 0.0020), 10.543 γ (± 0.017) mag
{JBlv n25 254(53), ND B8 165(72)}

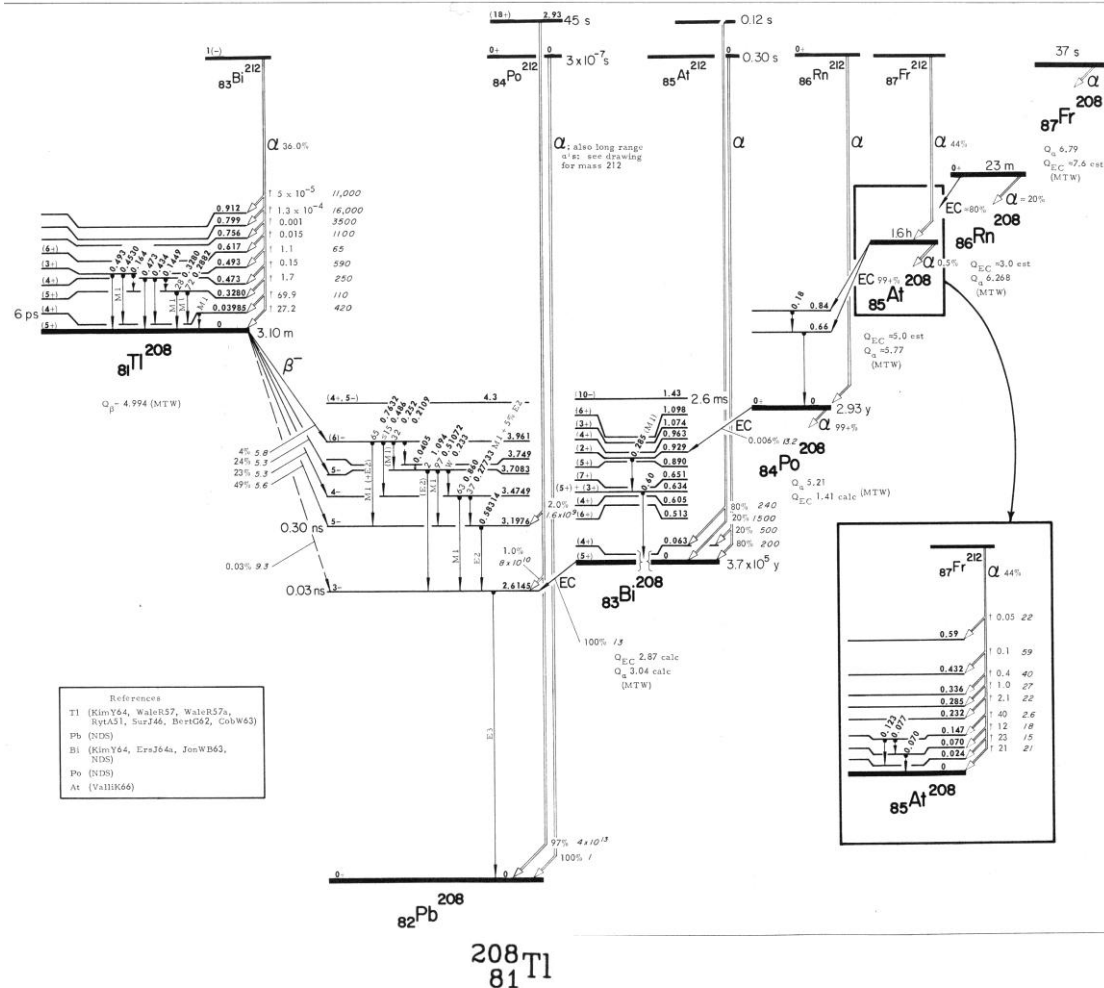
9.498 γ (± 0.0034), 10.431 γ (± 0.0010), 10.549 γ (± 0.016)
mag, semicond {CR 260 3037(65)}

(alphas from excited states of ^{212}Po following $^{212m1}\text{Bi}$ decay
(intensities relative to ± 100 for $^{212m1}\text{Bi} \alpha_{40}$))

9.89050 (± 1), 10.10550 (± 6), 10.22050 (± 6) semicond
{PC78 Bairden}

α : others: {LBL-1666 4(73), NIM 99 179(72), Metr 7 65(71),
NP 30 599(62), HPAc 34 240(61), CR 250 3156(60),
JPPa 16 732(55), CR 238 1215(54), JPPa 15 583(54),
RMP 26 1(54), JBlv n25 254(53), PRSL 216A 219(53),
CR 233 790(51)}





$\Delta = -16.7686$ {ANDT 19 175(77)}

β^- {ZP 199 25(67)}

$t_{1/2}$: 3.052733m {IRRL 8 75(71)}; 3.0556m {KDVM 36n4(67)}; others:
 {RaAc 14 72(70), AuC10 85(57), RMP 3 427(31)}

Class: A; Ident: chem, genet {RMP 3 427(31)}

Prod: descendant ^{228}Th {Bk64 Hyde2}

β: **2.38** ($\approx 0.03\%$), **1.80** (48.82%), **1.52** (22.77%), **1.29** (23.9%), **1.04** (4.6%) *mag-secnt* **βγ** coinc
PRSC 48 12A(54) PR 120 189(60) LU FB?

1.796 (52%), 1.521 (22%), 1.274 (21%), 1.04? (<0.6%),
 0.64? (4.51%) mag, mag-sciat & coinc {ZP 199 25(67)}

others: {NuOC s10v3 377(56), PPSL 61 466(48),
 no $\beta_{4.99}$ (<0.2%) method not given {PPSL 66A 808(53)}

PRSL 147A 572(34)}

γ : (norm: $\gamma_{2.615}$ (γ 99.79%), from level scheme) $0.21140^{+0.15}_{-0.17}$,
 $(\gamma_0 0.172, e_K/\gamma 0.97)$, $0.23336^{+0.15}_{-0.13}$ ($\gamma_0 0.313, e_K/\gamma 0.46$),

0.2526110 ($\dagger, 0.805, e_K/\gamma 0.51, K/L_1 2.8, 0.27743$ ($\dagger, -6.83,$
 $e_K/\gamma 0.38, K/L_1/L_2/L_3 615.30/100/12.56/1.93$), **0.4859515**
 $(\dagger, 2.552, 4.232, 2.542703, 4.232)$)

(\dagger , 0.0505, e_K/γ 0.21), 0.51072320 (\dagger , 21.69, e_K/γ 0.0844, $K/L_1/L_2 = 100/17.3/14/2.16$), 0.58313923 (\dagger , 86.3, e_K/γ assumed 0.015, $L_1/L_2 = 0$), 0.58867436 (\dagger , 86.3, e_K/γ assumed 0.015, $L_1/L_2 = 0$).

$$e_k/y \text{ assumed } 0.015, \quad L_{1+2}/L_3 = 9, \quad 0.58867 \quad (\dagger, 0.042), \\ 0.65013 \quad (\dagger, 0.0365), \quad 0.70523 \quad (\dagger, 0.0224), \quad 0.72204 \quad (\dagger, 0.0194) \\ (\dagger, 0.20314), \quad 0.74872 \quad (\dagger, 0.0434), \quad 0.76313 \quad (\dagger, 1.649)$$

($t_{\nu} = 203.74$), 0.74572 , ($t_{\nu} = 345.7$), 0.765158 , ($t_{\nu} = 649.7$), 0.82627 , $K/L = 5.1.2$), 0.82122 ($t_{\nu} = 0.0404$), 0.860378 , ($t_{\nu} = 12.04$, $e_K/\gamma = 0.0243$, $K/L = 5.0.2$), 0.88332 ($t_{\nu} = 0.0313$).

0.92762 ($\dagger, 0.12511$), **0.98272** ($\dagger, 0.19715$), **1.09392** ($\dagger, 0.374$), **1.12574** ($\dagger, 0.0052$), **1.16083** ($\dagger, 0.0113$), **1.18523**

1.28283 (± 0.0525), 1.38115 (± 0.0073),
 1.64757 (± 0.0021), 1.74407 (± 0.0021), 2.61447 (± 100 ,

e_K/γ 0.00202, K/L 5.5) Ge(Li), mag conv {NP A240 87(75), CR 277B 467(73), NP 63 353(65), ZETF 33 1144(57), ZF 17-16-16(57)}

ZP 176 30(63), IzF 20 877(56), CJP 43 171(65),
CJP 39 468(61), NIM 56 189(67), NIM 69 353(69), LJJ, EB}

Alpha Spectroscopy

Appendix G

Cooking with Alpha Rays

Source: <http://www.ugrad.physics.mcgill.ca/resources/alpha/cooking.pdf> by Mark Orchard-Webb

Cooking with Alpha Rays

Mark Orchard-Webb
orchard@physics.mcgill.ca

February 14, 2000

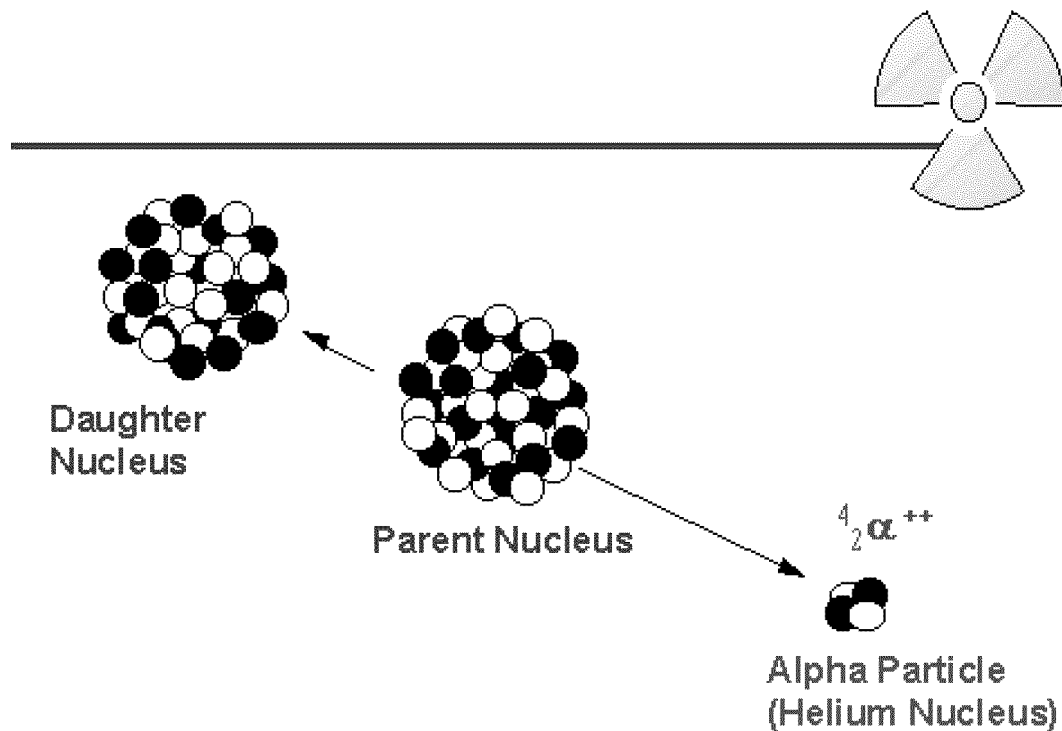


Figure 1: Friend or Foe

1 Hello Victims

What will follow will be a hastily thrown together walk through of how one might use some of the available tools to analyse some data related to, but not limited to the Alpha Decay experiment. We will use Unix, I assume you have accounts, and know how to transfer data. DOS on pre i386 machines can no longer be supported. I am no longer updating the software, I can't compile it anymore.

DISCLAIMER: Do not, on any account, take what is written here as an official guide to the experiment. My mission is to show you how to use the software. It is merely by convenience that I discuss the experiment.

2 How Come All The Files Are 8704 Bytes Long?

The files are binary, we will need software to read them effectively.

3 Looking at a Sample File

```
[bofh@odin Alpha_Decay]$ ls data
f1.spm   f148.spm  f197.spm  f245.spm  f294.spm  f342.spm  f391.spm  f50.spm
f10.spm  f149.spm  f198.spm  f246.spm  f295.spm  f343.spm  f392.spm  f51.spm
f100.spm f15.spm   f199.spm  f247.spm  f296.spm  f344.spm  f393.spm  f52.spm
f101.spm f150.spm  f2.spm    f248.spm  f297.spm  f345.spm  f394.spm  f53.spm
...
f144.spm f193.spm  f241.spm  f290.spm  f339.spm  f388.spm  f47.spm   f96.spm
f145.spm f194.spm  f242.spm  f291.spm  f34.spm   f389.spm  f48.spm   f97.spm
f146.spm f195.spm  f243.spm  f292.spm  f340.spm  f39.spm   f49.spm   f98.spm
f147.spm f196.spm  f244.spm  f293.spm  f341.spm  f390.spm  f5.spm   f99.spm
[bofh@odin Alpha_Decay]$
```

So the data is in a subdirectory data.

```
[bofh@odin Alpha_Decay]$ spmread
bash: readspm: command not found
```

I did that deliberately! You need to add an element to your path ... I have made an aliased script to handle this chore! Come tell me when you realize why it must be an alias, not just an executable script, I'll be very happy!

```
[bofh@odin Alpha_Decay]$ addpath labs
[bofh@odin Alpha_Decay]$ spmread
Usage spmread [-alz] [-e elapsed-time] [-l lower] [-u upper]
-a : convert to activity
-i : just give information about spectrum
-z : remove zero count columns
defaults:
    lower = 0
    upper = max_channel
[bofh@odin Alpha_Decay]$
```

Ah, much better. So let's try

```
[bofh@odin Alpha_Decay]$ spmread -z data/f100.spm
26      2      1.41421
27      6      2.44949
28     10      3.16228
29     10      3.16228
30     25      5
```

```

31      11      3.31662
32      20      4.47214
33      15      3.87298
...
1971    10      3.16228
1972     7      2.64575
1973     4      2
1974     4      2
1975     1      1
1976     4      2
1977     1      1
1978     2      1.41421
1980     1      1
1990     1      1
2003     1      1
2021     1      1
[bofh@odin Alpha_Decay]$

```

Fascinating! Three columns of data, something one might be inclined to feed into gnuplot.

```

[bofh@odin Alpha_Decay]$ spmread -z data/f100.spm > f100.dat
[bofh@odin Alpha_Decay]$ emacs f100.gnu &
[3] 26629
[bofh@odin Alpha_Decay]$

```

Oops, how long was this file recorded for? Check the infomation mode of spmread

```

[bofh@odin Alpha_Decay]$ spmread -i data/f100.spm
File was saved as "f100.spm" on Sep 21 1999 at 02:39:48 am
2048 channels
300 seconds elapsed time
Acquisition started: 21/09/1999 at 02:34:48.12 (Sep 21, 1999 at 02:34:48 am)
Acquisition stopped: 21/09/1999 at 02:39:48.06 (Sep 21, 1999 at 02:39:57 am)
ID string: "f100.spm"
PCA version: 2.11
Real elapsed time : 299 seconds
[bofh@odin Alpha_Decay]$

```

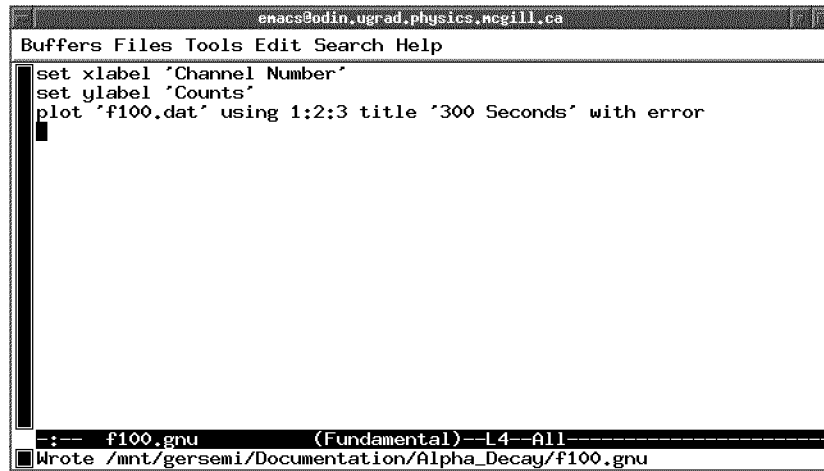


Figure 2: Emacs at work

Ok, lets have a look at this masterpiece.

```
[bofh@odin Alpha_Decay]$ gnuview f100.gnu  
[bofh@odin Alpha_Decay]$
```

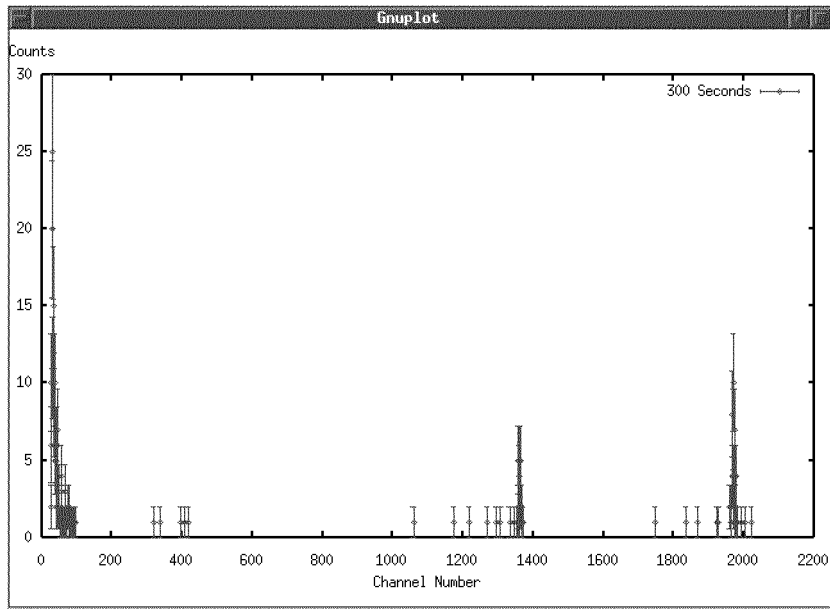


Figure 3: Gnuplot at work

Exquisite! But lets look more closely to the range 1200 — 1400. We could use gnuplot's range limiting command, but why make him do extra work, lets use sppread's range limiting ability.

```
[bofh@odin Alpha_Decay]$ spmread -z -l 1200 -u 1400 data/f100.spm > f100.dat  
[bofh@odin Alpha_Decay]$ gnuview f100.gnu
```

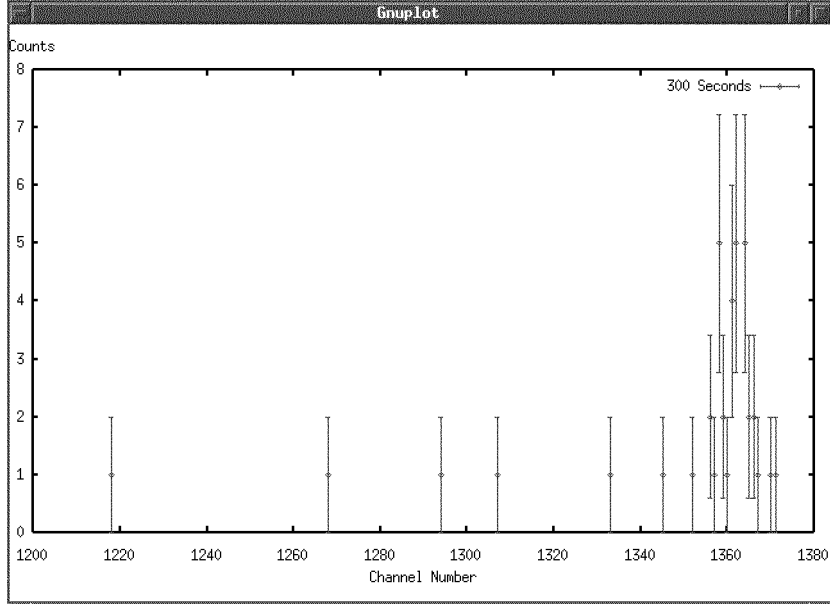


Figure 4: Gnuplot Wars

Yikes! That data is a bit sparse! Perhaps we could sum up all the data files into one. Indeed, we shall use `spmsum`.

```
[bofh@odin Alpha_Decay]$ spmsum -z -l 1200 -u 1400 data/f > sum.dat
Processing data/f1.spm
Processing data/f2.spm
Processing data/f3.spm
...
Processing data/f429.spm
Processing data/f430.spm
Processing data/f431.spm
Processing data/f432.spm
Processing data/f433.spm
[bofh@odin Alpha_Decay]$ cp f100.gnu sum.gnu
```

A quick tinker with `sum.gnu` to fix up the names and times

```
set xlabel 'Channel Number'
set ylabel 'Counts'
plot 'sum.dat' using 1:2:3 title '129900 Seconds' with error
```

And a quick glance

```
[bofh@odin Alpha_Decay]$ gnuview sum.gnu
```

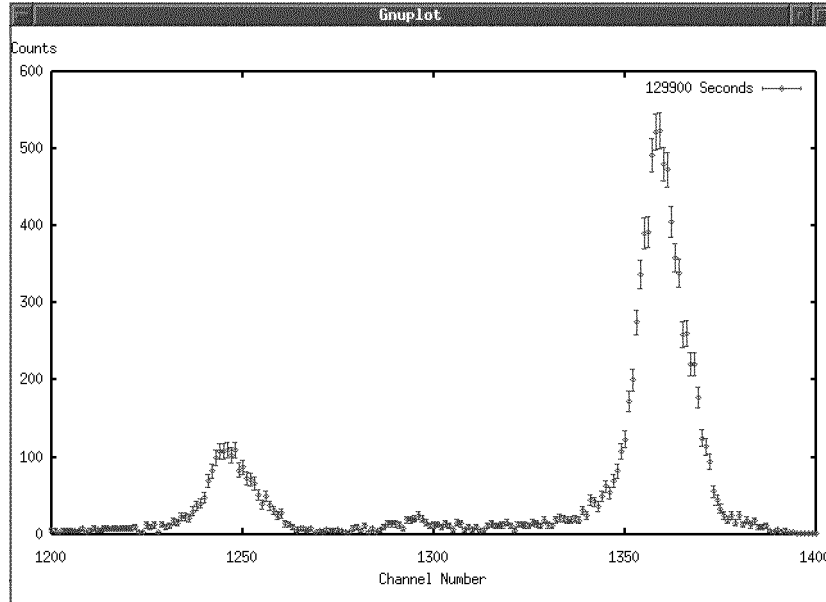


Figure 5: Gnuplot Strikes Back

That is truly marvelous, look you can even see the two main peaks, the 6.05MeV, and the 6.08MeV. Wait a moment, they look kind of far apart to be those peaks! May be there has been a shift in some vital parameter during the experiment! Is there a tool which can show me a time evolution of a peak? As of September 21, 1999 there is yes, `spmtrkpk` (mnemonic Spectrum Track Peak)

```
[bofh@odin Alpha_Decay]$ spmtrkpk -l 1200 -u 1400 data/f > peak.dat
Processing data/f1.spm
Processing data/f2.spm
Processing data/f3.spm
```

```
...
Processing data/f429.spm
Processing data/f430.spm
Processing data/f431.spm
Processing data/f432.spm
Processing data/f433.spm
[bofh@odin Alpha_Decay]$ cp f100.gnu peak.gnu
```

Patch the script

```
set xlabel 'Time (s)'
set ylabel 'Peak Centroid (channels)'
plot 'peak.dat' using 1:2:3 title 'Damaged Goods' with error
```

Lets get it over with ...

```
[bofh@odin Alpha_Decay]$ gnuview peak.gnu
```

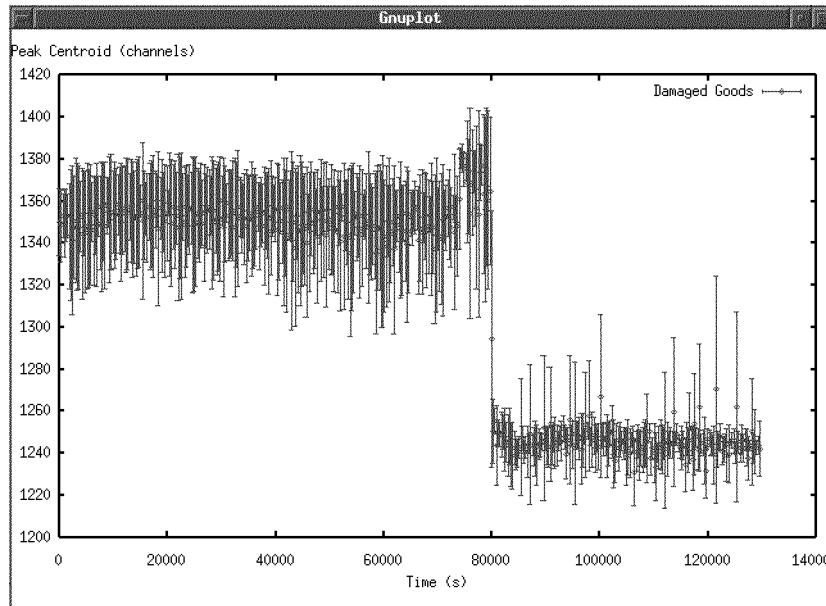


Figure 6: Don't Kill The Gnuplot Messenger

What could have happened at 80 kiloseconds? What catastrophe! Well ... How come the only group who didn't do nasty things to their detector isn't having these problems? Well, these are philosophical questions, what about looking at a time evolution of the area under the curve? This time we use spmintpk (Spectrum Integrate Peak)

```
[bofh@odin Alpha_Decay]$ spmintpk -a -l 1200 -u 1400 data/f > act.dat
Processing data/f1.spm
Processing data/f2.spm
Processing data/f3.spm
...
Processing data/f429.spm
Processing data/f430.spm
Processing data/f431.spm
Processing data/f432.spm
Processing data/f433.spm
[bofh@odin Alpha_Decay]$ cp f100.gnu act.gnu
```

This stuff is getting pretty intuitive now I hope! Patch the script

```
set xlabel 'Time (s)'  
set ylabel 'Activity (counts / s)'  
plot 'act.dat' using 1:2:3 title 'Damaged Goods' with error
```

Lets get it over with ...

```
[bofh@odin Alpha_Decay]$ gnuview act.gnu
```

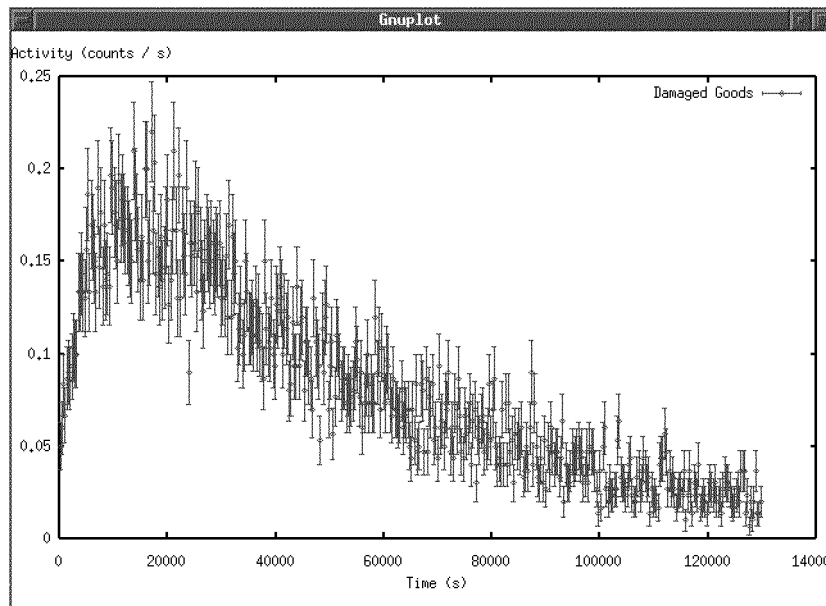


Figure 7: Final Gnuplot

Well, that isn't so bad after all, considering!

4 Data Aerobics

Now we come to the tricky part, comparing the nice abstract data to the harsh realities of fact. Let us first address the calibration relationship, we have

$$E(\text{ch}) = m * \text{ch} + b \quad (1)$$

Let us write a quick awk script to take care of this, in this example called `calib.awk`

```
BEGIN {  
    m = 4.394e-3; # MeV / ch  
    b = 0.511;      # MeV  
}  
  
{  
    print m * $1 + b, $2, $3;  
}
```

Ok, lets create a raw data file which contains the summed data, then let us run this data through the calibration filter.

```
[bofh@odin Alpha_Decay]$ spmsum data/f > sum-raw.dat  
[bofh@odin Alpha_Decay]$ cat sum-raw.dat | awk -f calib.awk > sum-calib.dat
```

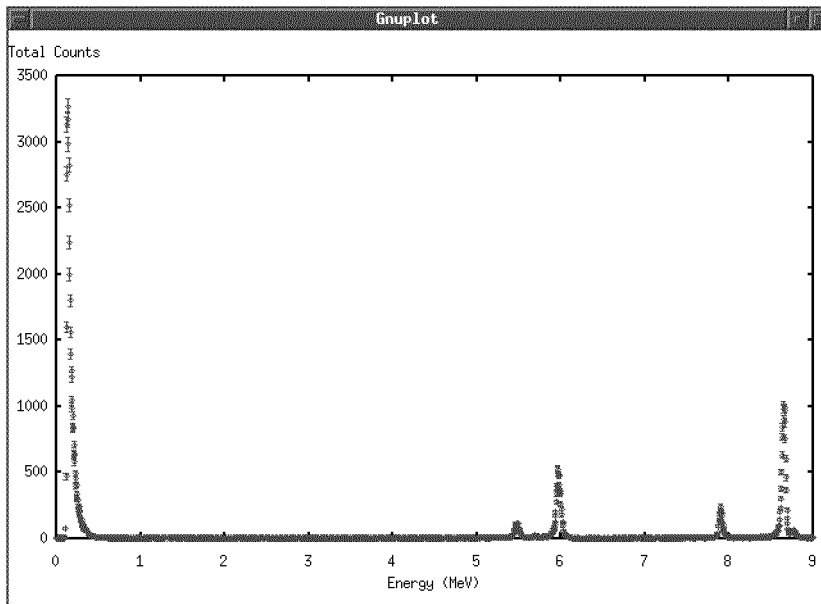


Figure 8: The Long Awaited Graph

Lets look at the rightmost peak, over the range 8.5 MeV to 9 MeV, we can use awk again to extract this range.

```
[bofh@odin Alpha_Decay]$ cat sum-calib.dat | awk '($1 > 8.5) && ($1 < 9)' { print $0 } > apeak.dat
[bofh@odin Alpha_Decay]$
```

Don't worry, you may, one day, feel perfectly happy typing commands the length of your arm.

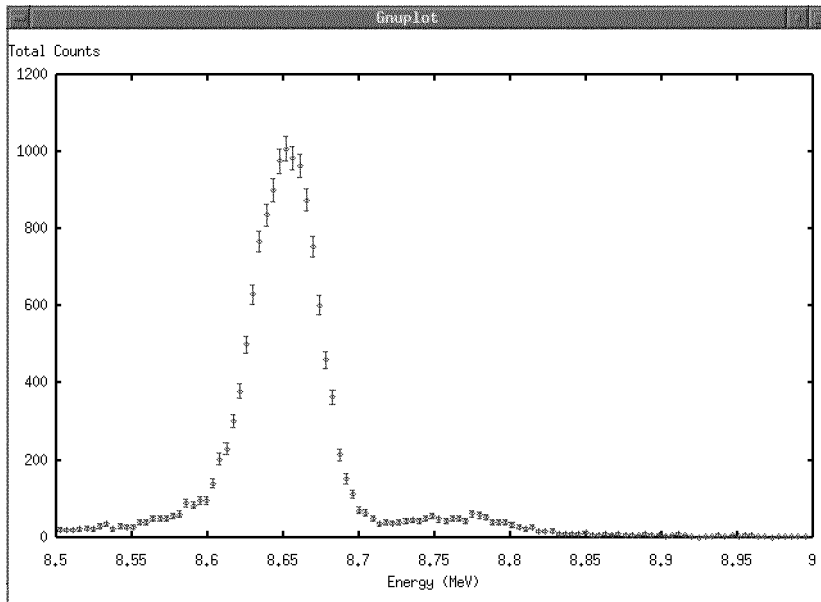


Figure 9: A Closer Look

Ok, lets adjust those limits to 8.6 - 8.7 MeV, you can bring back that awk command with the [Up] and [Down] arrows!

```
[bofh@odin Alpha_Decay]$ cat sum-calib.dat | awk '($1 > 8.6) && ($1 < 8.7)) { print $0 }' > apeak.dat
[bofh@odin Alpha_Decay]$
```

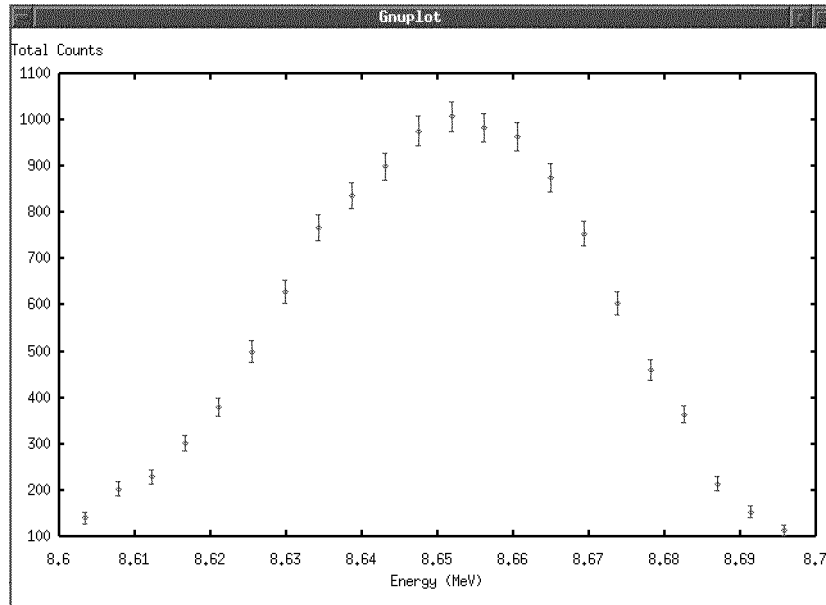


Figure 10: Mount Breaukindata

We now invoke the name of greatly feared beast ...

```
[bofh@odin Alpha_Decay]$ moosefit
```

The screen takes on a sinister appearance and glares back at you. Boldly press the [Return] key to drop a menu, observe this instruction is given at the bottom of the screen ...



Figure 11: The MooseFit Console

Select Datafile, if your arrow keys give you trouble, [ctrl]-[P] and [ctrl]-[N] will work as expected, and hit Enter.

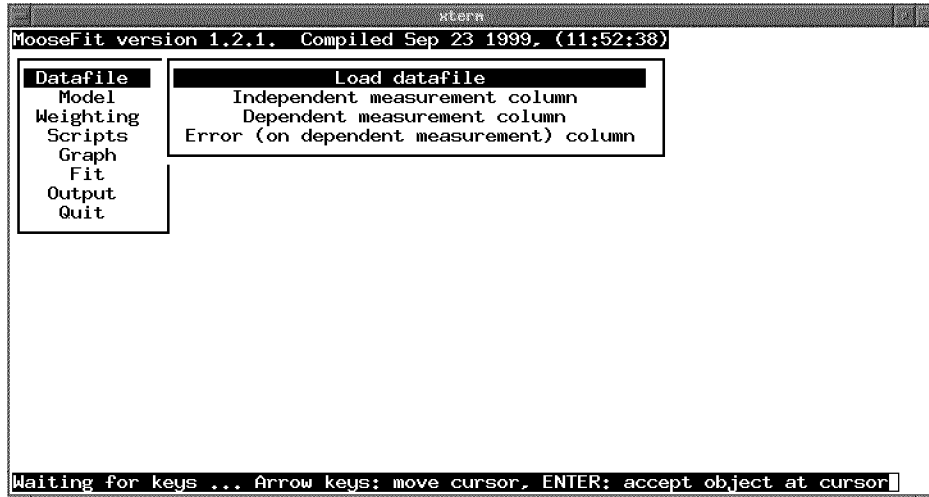


Figure 12: Menu Madness

Select Load Datafile, press [Enter]. Move the cursor to the desired datafile and press [Enter].



Figure 13: File Selection

Press [Escape] a few times to back out of the menus, you can now see a summary of the fitting environment.

```

extern
MooseFit version 1.2.1. Compiled Sep 23 1999, (11:52:38)
No function selected
Datafile:
/mnt/gersemi/Documentation/Alpha_Decay/apeak.dat
consisting of 22 rows of 3 columns.
Independent measurement: column 1
Dependent measurement: column 2
Error on dependent measurement: column 3
Points are equally weighted
parameters:

RETURN - fall down menus (All other keys will be discretely ignored)■

```

Figure 14: The Stats So Far

Go to the menu, and select Graph, this will pop up a gnuplot of the data.

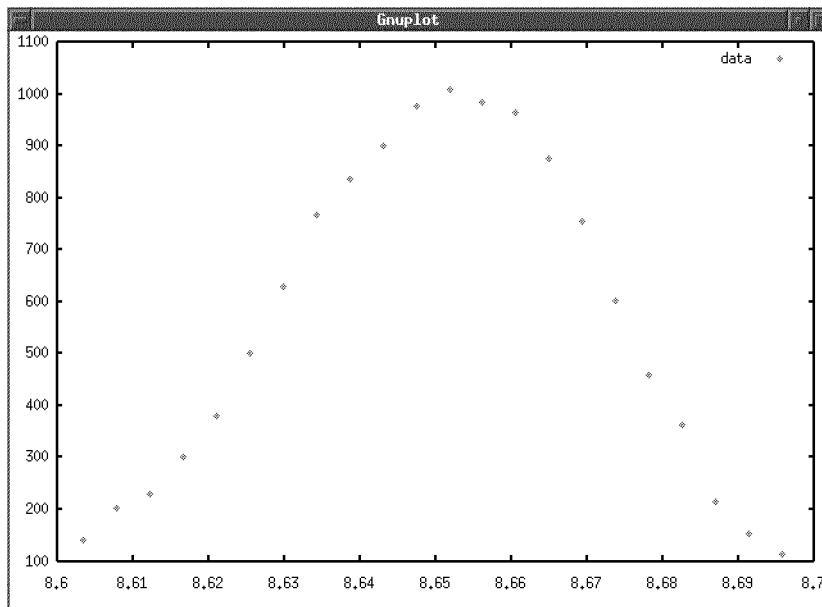


Figure 15: That Again!

But the error-bars are missing, select Weighting, and from the submenu select Instrumental, then reselect Graph. This should be much better. Now we need to generate a fitting function, select Model, Modify modelling equation, and then Create new function. Type in the equation desired,

```

MooseFit version 1.2.1. Compiled Sep 23 1999, (11:52:38)
Datafile Model Modify modelling equation
Weighting Independent variable selection
y = A * exp (-0.5 * ((x - mu) / sigma) ^ 2)

x = 0
Reduced chi-squared = NaN

Destroying floating window

```

Figure 16: Specifying the function

In this case, y is the dependent variable, and x is the independent variable, but moosefit has no way of knowing which of the variables A , x , μ or σ is the independent variable, and which are parameters. Thus you could select x as the from the Independent variable selection menu entry. Then, there is the small matter of the Parameter settings, you **must** choose values which are **close** to the best-fit values, how close will be a matter of experience! Looking at the graph, I say $\mu = 8.65$, $\sigma = 0.02$, and $A = 1000$.

```

MooseFit version 1.2.1. Compiled Sep 23 1999, (11:52:38)
Datafile Model Modify modelling equation
Weighting Scripts Independent variable selection
Graph Fit Documentation/Alpha_Decay/apeak.dat
Output Quit Parameter settings
Dependent measurement: column 2 Error on dependent measurement: column 2
as measurement: column 2 A = 1000
22 rows of 3 columns mu = 8.65
sigma = 0.02
Points are instrumentally weighted (using column 3)
parameters:
A = 1000
mu = 8.65
sigma = 0.02
Reduced chi-squared = 11.6217

Waiting for keys ... Arrow keys: move cursor, ENTER: accept object at cursor

```

Figure 17: Specifying the parameters

Returning to the root menu, and reselecting Graph the fit function is now super imposed.

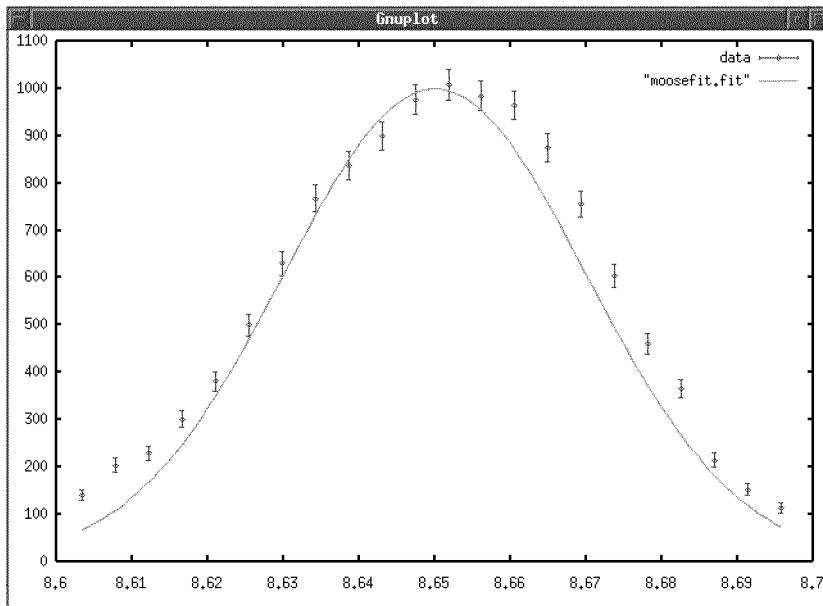


Figure 18: Not a bad guess

I feel this is good enough, so now, and only now, do I move on to the actual Fit selection. But better safe than sorry, before fitting, I shall save a script which can recreate this environment. Got to the Scripts menu, select Save current settings to a script file, and enter a filename.

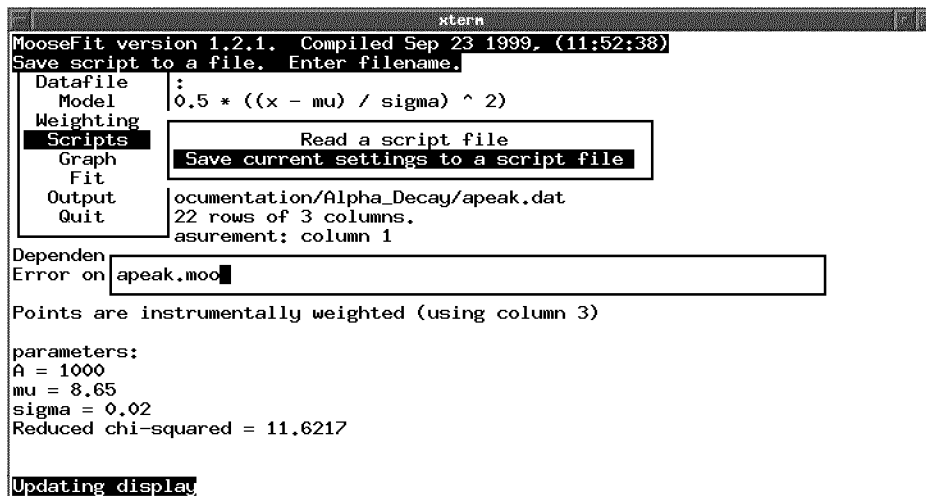


Figure 19: Just In Case

Ok, now I hit Fit, there is a flurry of activity in the graph, and then it stops ... hopefully it stops, the non terminating fit is most annoying.

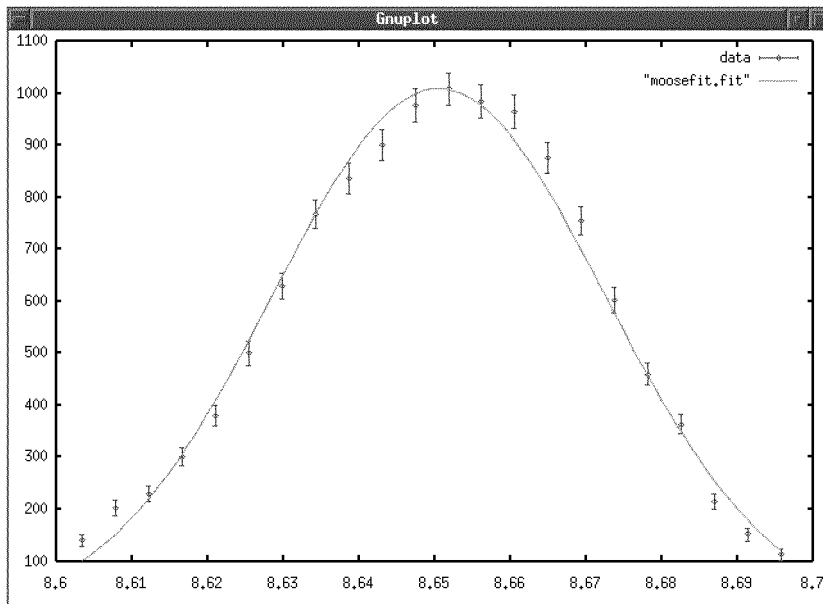


Figure 20: Best Fit

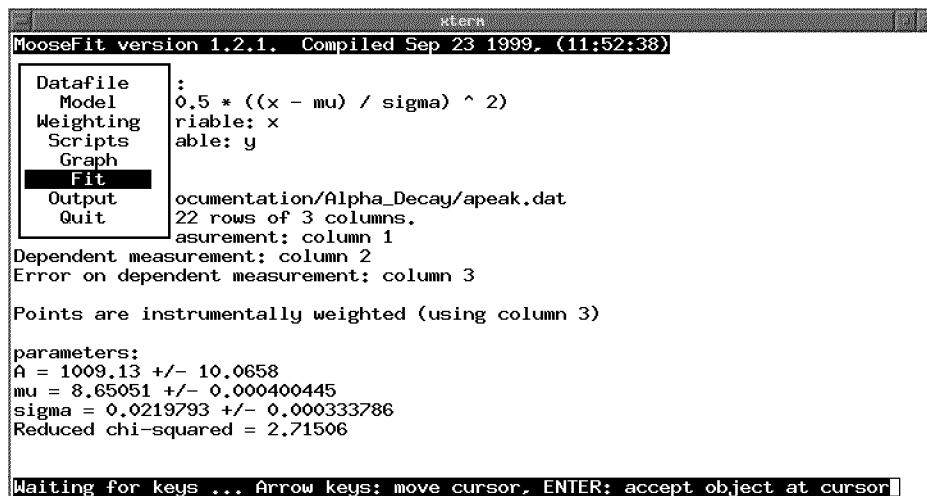


Figure 21: The Parameters

Now the fit is complete, the parameters are shown with error. It is probably a good idea to save this information for posterity. Under the Output menu there are three options, Save fit parameters to file saves the parameter table, as seen, to a file; Create datafile with both data and fit dumps the data table to a file, Create gnuplot script answers the question ... how can I print the graph.

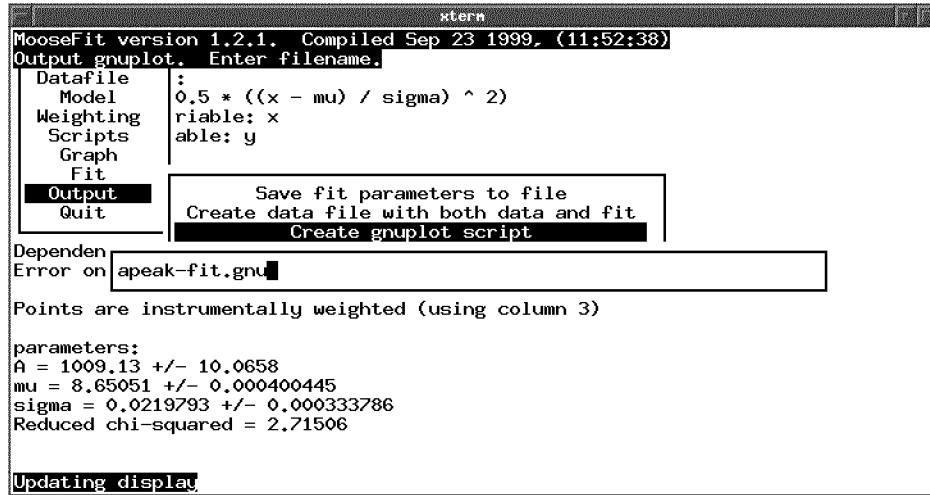


Figure 22: Saving the graph

Examining the resultant file,

```
y(x) = A * exp (-0.5 * ((x - mu) / sigma) ** 2)

A = 1009.13
mu = 8.65051
sigma = 0.0219793
plot y(x) title 'A * exp (-0.5 * ((x - mu) / sigma) ^ 2)', \
'/mnt/gersemi/Documentation/Alpha_Decay/apeak.dat' using 1:2:3 title 'data' with error
```

we see this can be easily edited to contain the appropriate text labels, and treated in the usual manner.

```
[bofh@odin Alpha_Decay]$ gnuview apeak-fit.gnu
[bofh@odin Alpha_Decay]$ gnuprint apeak-fit.gnu
```

Also, looking at the script we saved earlier,

```
function y = A * exp (-0.5 * ((x - mu) / sigma) ^ 2)
independent x
A = 1000.000000
mu = 8.650000
sigma = 0.020000
data "/mnt/gersemi/Documentation/Alpha_Decay/apeak.dat"
```

We can see that is is pretty self explanatory, he says, walking away, with a florish of hand waving, it is obvious that ...

One hint I would give is that you can delete the data line, thus you can load the function and parameters without the data, and use the menu to load a different data file.

The following moosefit script can be found in /mnt/gersemi/Documentation/Alpha_Decay/activity.moo

```
function a = n0 * 11 * 12 * (exp (-11 * t) - exp (-12 * t)) / (12 - 11) + 12 * n
2 * exp (-12 * t)
independent t
11 = 1.82915e-05
12 = 0.000191253
n0 = 116706
n2 = 5044.53
```

Which should seem familiar to you ... it can be used like this

```
[bofh@odin Alpha_Decay]$ moosefit activity.moo
```

```
xterm
MooseFit version 1.2.1. Compiled Sep 23 1999, (11:52:38)

Model function:
a = n0 * 11 * 12 * (exp (-11 * t) - exp (-12 * t)) / (12 - 11) + 12 * n
Independent variable: t
Dependent variable: a

No datafile loaded

Points are equally weighted

parameters:
11 = 1.82915e-05
12 = 0.000191253
n = 0
n0 = 116706

RETURN - fall down menus (All other keys will be discretely ignored)
```

Figure 23: No Datafile Loaded

Load up the activity versus time data

```
xterm
MooseFit version 1.2.1. Compiled Sep 23 1999, (11:52:38)
Select data file to be loaded.
File Selection mode: ENTER: accept file, ESC: abort, SPACE: switch to ...
 cwd: /mnt/gersemi/Documentation/Alpha_Decay
Weighting | Dependent measurement column
Scripts | Error (on dependent measurement) column
Graph
Fit #guide.ltx# gnuplot.gif moosefit.err moosefit8.gif
Output act.dat gnuplot2.gif moosefit.fit moosefit9.gif
Quit act.gnu gnuplot3.gif moosefit.tmp peak.dat
activity.moo gnuplot4.gif moosefit1.gif peak.gnu
parameter alpha.gif gnuplot5.gif moosefit10.gif sum-calib.dat
11 = 1.82 apeak-fit.gnu gnuplot6.gif moosefit11.gif sum-calib.gnu
12 = 0.00 apeak.dat gnuplot7.gif moosefit12.gif sum-calib.gnu
n = 0 apeak.gnu gnuplot8.gif moosefit13.gif sum-raw.dat
n0 = 1167 calib.awk guide.aux moosefit2.gif sum.dat
emacs.gif guide.dvi moosefit3.gif sum.gnu
f100.dat guide.log moosefit4.gif sum.gnu"
f100.gnu guide.ltx moosefit5.gif webtex.defs
f100.gnu~ guide.ltx" moosefit6.gif webtex.inc
f100.gnu~ int.dat moosefit7.gif

Waiting for keys ... Arrow keys: move cursor, ENTER: accept object at cursor
```

Figure 24: Locked and Load

Don't forget to choose instrumental weighting, or the error bars are meaningless. And with out further ado ... you are on your own!

